Università degli Studi di Padova

University of Padova

Department of Information Engineering

Ph.D. School in Information Engineering

Information Science and Technology

XXVIII series

Ph.D. Thesis

Reconfigurable Antennas and their Applications

Muhammad Saeed Khan

School Director

Chair.mo Prof. Matteo Bertocco

Supervisor

Antonio-Daniele Capobianco

Curriculum Coordinator

Prof. Carlo Ferrari

NOVEMBER 2015

ACKNOWLEDGMENTS

All the praise and thanks to almighty ALLAH who bestowed with countless blessings. There are numerous factors after every breakthrough in ones life. I would like to take this opportunity to thank each and every one of them.

I would like to express my sincere thanks to Dr. Antonio-Daniele Capobianco for providing immense guidance and supervision throughout my PhD studies and research at University of padova. Humanity is the first and foremost ingredient for a teacher and I found him a best teacher. I learnt appreciation and acknowledgement for the students, besides other teaching techniques from him. I learnt patience and dedication as a researcher from him. I would also like to thank Dr. Benjamin Braaten who supervised me with full dedication, keen devotion and immense commitment during my stay at North Dakota State university. I appreciate his moral support during times of my family problem. I am really grateful to Cariparo foundation for providing me financial support during my stay at University of Padova. I would also like to thank Dr. Farhan Shafique and Dr. Bilal Ijaz who encouraged me for research.

I appreciate the prayers, hard work, support and encouragement of my family. Finally i would like to thank all my fellows at University of Padova and North Dakota State University for their collaboration and support during research.

Finally, I would like to thank all of my relatives, friends and well-wishers for keeping me in your prayers and wishes all the time.

DEDICATION

To my family and teachers.

ABSTRACT

One of the biggest challenge in modern communication systems is to provide a single antenna for different applications. Existing antenna systems are limited to some applications. So it is important to design a single reconfigurable antenna for multiple applications.

Five different reconfigurable printed antennas for different applications are designed during the study of this thesis. In the first design an antenna for frequency reconfigurable applications is designed. The electrical length of the conductor is changed using PIN diodes and the resonance of antenna is shifted from 4.27 GHz to 3.56 GHz. Good agreement between simulated and measured results is observed. In the second and third designs, Ultra wideband (UWB) Multiple-Input Multiple-Output (MIMO) antennas with on-demand Wireless Local Area Network (WLAN) rejection are designed. The second design consists of two elements UWB-MIMO antenna and stubs are connected to the ground plane using PIN diodes. These stubs act as a stop-band filter and reject the band at 5.5 GHz center frequency. This design has a compact size of $23 \times 39.8\ mm^2$. The third design has almost same features as of second design but it has four elements. These elements are placed orthogonally to each other. The total size of this proposed design is $50 \times 39.8\ mm^2$. The ground plane is common and a band-stop design is placed between the ground planes. This band-stop design is connected with the ground plane using PIN diodes. When diodes are biased, the current is travelled to the nearly placed band-stop design and a notch is obtained around 5.5 GHz. In fourth design a reconfigurable array with a sensing circuit is

designed. The array consists of four individual reconfigurable patches which are attached to the different conformal surfaces. These patches are reconfigured from 3.15 GHz to 2.43 GHz using PIN diodes. The correct phase at each element is provided using phase shifters. The sensing circuit is designed in such a way that only input voltage is changed to provide the correct phase on the switching frequency. The patterns of the array are recovered on both switching frequencies when array is attached to wedge or cylindrical surface. In the last design a series-fed array is designed. Composite Right/Left Handed Transmission Line (CRLH-TLs) are used instead of traditional meanderline microstrip lines to connect the array elements. These CRLH-TLs provided the zero phase at each connecting element, which resulted in broad side radiation patterns. To reconfigure the antenna to another frequency a small patch and second CRLH-TL is connected between array elements.

SOMMARIO

Una delle sfide pi grandi nei moderni sistemi di telecomunicazioni realizzare una singola antenna idonea allimpiego in differenti ambiti. I sistemi di antenna esistenti infatti sono limitati solo a poche funzionalit. Risulta quindi importante progettare una singola antenna, riconfigurabile per una molteplicit di utilizzi.

In questo lavoro di tesi vengono presentate cinque diverse antenne stampate e riconfigurabili. Per primo verr presentata il design di una antenna riconfigurabile in frequenza; la lunghezza elettrica del radiatore viene cambiata usando dei diodi PIN spostando la frequenza di risonanza da 4.27 GHz a 3.56 GHz. Viene rilevato un buon accordo tra risultati sperimentali e quelli simulati. Nel secondo e nel terzo design vengono implementate antenne UWB-MIMO con capacit di rigettare a comando la banda di funzionamento WLAN. Nel dettaglio, il secondo design dantenna consiste di due radiatori UWB-MIMO impiegati assieme a degli stub che sono connessi al piano di massa tramite diodi PIN. Gli stubs si comportano come filtri elimina-banda che inibiscono la radiazione intorno ai 5.5 GHz. Il design realizzato risulta molto compatto misurando solo 23x39.8 mm2. Il terzo design di antenna ha quasi le stesse caratteristiche del precedente ma formato da quattro elementi: questi sono posizionati ortogonalmente luno allaltro. Lingombro complessivo risulta di 50x39.8 mm2. Il piano di massa condiviso ed una struttura elimina-banda posta tra i radiatori. Tale struttura connessa con il piano di massa tramite dei diodi PIN. Quando i diodi sono polarizzati la corrente la attraversa portando alla formazione di un notch nellintorno dei 5.5GHz. Nel quarto design viene presentata una schiera di antenne riconfigurabile comandata da un sensore. La schiera formata da quattro antenne patch riconfigurabili che sono posizionate su diverse superfici conformi. Le antenne patch sono rese riconfigurabili con luso di diodi PIN per operare a 3.15 Ghz o 2.43 GHz. La fase di cui necessita ciascun radiatore per compensare la deformazione

della superficie viene fornita da dei variatori di fase. Tali variatori di fase sono realizzati in modo tale che necessitano solo di una tensione di pilotaggio in ingresso; il diagramma di radiazione della schiera viene ricomposto ad entrambe le frequenze di funzionamento quando la superficie inizialmente piana viene piegata ad angolo o circolarmente. Nellultimo design viene presentata una schiera di antenne alimentate in serie tramite linee CRLH che vengono impiegate al posto di linee a microstriscia tradizionali. Questo permette di fornire uno shift di fase nullo a ciascun elemento radiante della schiera in modo da ottenere una modo di radiazione trasversale. Per riconfigurare la schiera ad operare ad una frequenza diversa una piccola patch ed una seconda linea di trasmissione CRLH viene connessa tra gli elementi radianti.

TABLE OF CONTENTS

LIST OF TABLES

LIST OF FIGURES

CHAPTER 1. INTRODUCTION

1.1. Setting the definition of the problem

The most critical and important part of any communication system is antenna. During the last 50 years, nine different types of antennas have proliferated in communication systems. These varieties include microstrip antennas, helical antennas, loop antennas, dipoles/monopoles, slot/horn antennas, log periodic antennas, dielectric antennas, reflector antennas and frequency independent antennas. Each category is suitable for a particular application due to its inherent benefits. These basic antennas are changed to adapt the properties of a new system. However, these basic antennas impose restrictions on the performance of overall system that arises due to fixed antenna characteristics. To eliminate or overcome such restrictions, antennas are made reconfigurable so that their behaviour can adjust the changing environmental conditions and system requirements. A significant number of antennas having the properties of switching between two frequency bands [1]-[5] and permanently rejecting WLAN signals of the UWB-MIMO [7]-[15] have been proposed. The rejection of the WLAN signals is required when a UWB communications system is strongly affected by WLAN signals.

1.2. Motivation

Providing an on-demand rejection is useful for the UWB-MIMO communication systems, where UWB signals are strongly affected by the WLAN signals. The WLAN signals can be tuned only when the application requires the particular frequency. If the band is permanently rejected than the WLAN applications needs separate communication system or antennas which can increase the cost and space, available for the communication systems.

For a SELFLEX (Self adapting flexible) array, the pattern can be re-constructed for different applications by using the reconfigurable antennas and applying correct

phase for each application. Rather than using a separate array, PIN diodes and chokes can be used to tune the frequency of the antenna array.

Metamaterials can be used to reduce the size of an overall array. If two different metamaterials are used for two different frequencies and correct phase is applied to the series connecting elements than the broad side pattern of the array can be achieved.

1.3. Objective

The objectives of this thesis are:

1. Design a compact frequency reconfigurable antenna which can be tuned to two different frequencies.

2. Design a compact UWB-MIMO, two elements and four elements antenna array with On-demand rejection capabilities.

3. Design a reconfigurable conformal array which can re-construct its pattern when the proper phase is applied.

4. A series-fed frequency reconfigurable metamaterial based antenna array which can achieve the broad side radiation pattern when tuned to its particular frequency.

1.4. Thesis outline

A brief introduction, principle motivation and objectives are presented in this chapter.

In chapter 2, the background of frequency reconfigurable antennas, UWB-MIMO antennas with WLAN rejection, conformal antennas and metamaterial based antennas is discussed.

In chapter 3, reconfigurable switch is discussed in detail. The configuration of the PIN diode in simulation and the steps involved in the experiments are discussed.

In chapter 4, five different antennas are discussed which are reconfigured using the PIN diodes. The reconfigurability is applied first time to some applications.

Finally, chapter 5, concludes the whole thesis and suggests some future directions.

CHAPTER 2. BACKGROUND AND LITERATURE REVIEW

Printed antennas are mostly used in modern wireless and satellite communication systems due to their light weight, low cost, small size and improved directivity. After the invention of printed antenna technology in the 1950s, a lot of research has been carried out for printed antennas. Due to rapid growth of modern wireless technologies, the researchers are focusing on reconfigurable printed antennas. In the following section, the definition of the reconfigurability is discussed along with the groups. In the later sections different applications of reconfigurability along with some designs are discussed.

In antenna, reconfigurability is the capacity to change the fundamental operating characteristics of a radiator through electrical, mechanical or other means. Reconfigurable antennas can be placed in four groups based on the properties of the reconfiguration. These are shown in Figure 1.

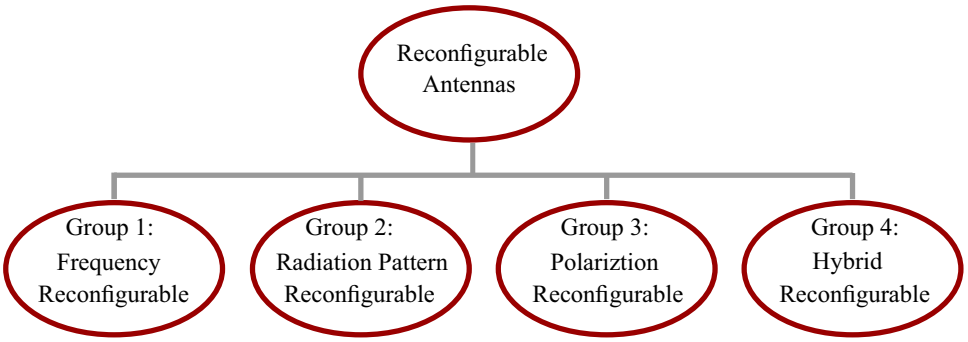

Figure 1: Different categories of reconfigurable antennas.

1. ***Group 1: Frequency reconfigurable antennas***

   Antennas under this group can alter their frequency. These type of antennas can be switched to multiple frequency bands and are very useful for cognitive radio applications.

2. ***Group 1: Radiation pattern reconfigurable antennas***

   Antennas under this group can alter their pattern on a fixed frequency. These antennas alter their pattern to allow radiation in a certain direction e.g. mobile antennas.

3. ***Group 1: Polarization reconfigurable antennas***

   Antennas under this group are capable of switching between different polarization modes. This feature of switching polarization is used to reduce the polarization mismatch losses in portable devices

4. ***Group 1: Hybrid reconfigurable antennas***

   Antenna under this group can be tuned to several antenna parameters, for instance frequency and radiation pattern. The most common use of this application is combination of beam scanning and frequency agile to improve spectral efficiencies.

2.1. Frequency Reconfigurability

An antenna can be tuned to a different frequency by changing its electrical length. In these type of antennas conductor is modified to change the electrical length of the antenna by using switches, PIN diodes or varactor diodes. The first patent design on reconfigurable antenna was reported back in 1983 by Schaubert [6]. After reviewing the extensive literature, some of the frequency reconfigurable designs are discussed below.

In [4], a frequency reconfigurable antenna for three different applications was presented. The bands were reconfigured using two switches. If switch 1 was deactivated (off), while switch 2 was activated (on), the two frequency bands with center frequencies of 2.44 and 5.5 GHz were achieved. The bandwidth of these bands was 0.31 and 1.83 GHz, respectively. When both switches (switch 1 and switch 2) were

deactivated (off), a single impedance bandwidth from 2.30 to 2.64 was achieved. When both switched are activated (on), the three frequencies bands with center frequencies of 2.41, 3.36 and 5.62 GHz were achieved. The bandwidth of these frequency bands was 0.23, 0.62 and 1.35 GHz. The lay out the antenna proposed in [4] is shown in Figure 2. As shown in Figure 2, that conductor L_3 was used to connect the antenna with a circular ring. This conductor acted as a switch 1 in

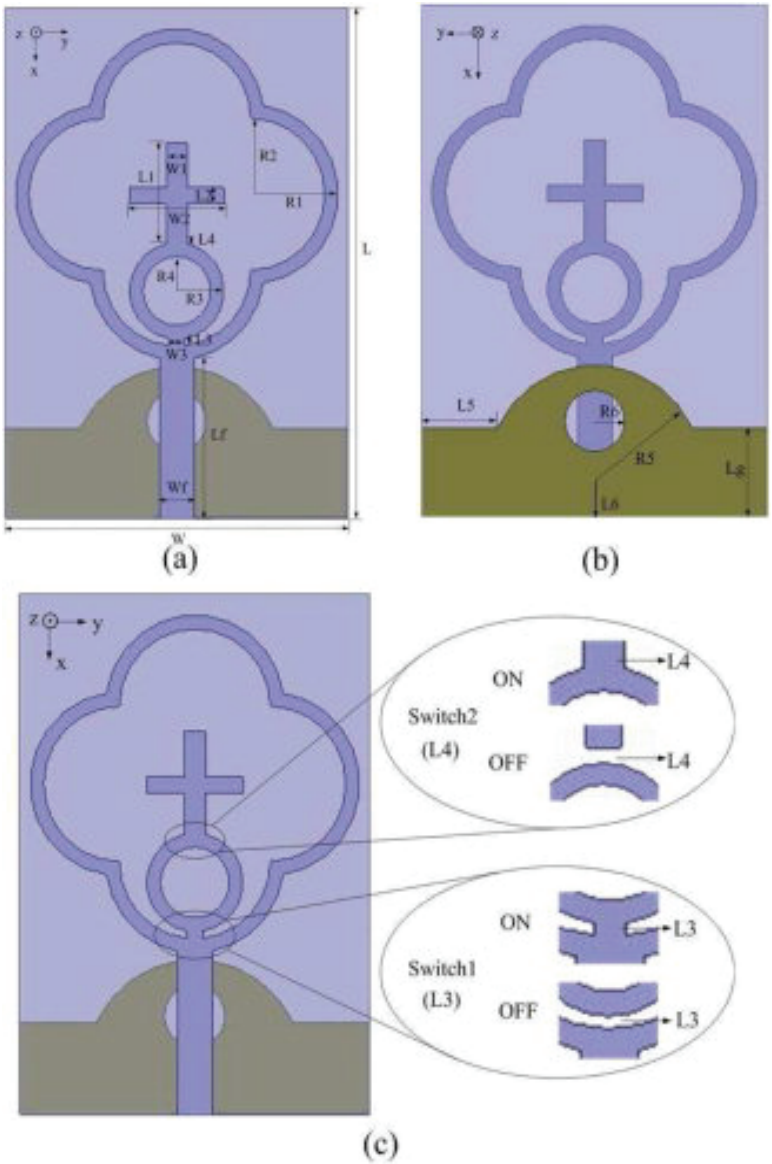

Figure 2: Geometry of the antenna proposed in [4]. (a) Top view (b) bottom view and (c) reconfigurable mechanism.

simulation and changed the electrical length of the antenna. In a similar fashion, another conductor L_4 was used to connect the inverted T-shaped stub to the circular ring. The conductor L_4 acted as a switch 2. Although the proposed design in [4], had good impedance matching and far-filed characteristics but in simulation and experimental results, only conductor was used and the losses due to PIN diodes were not included.

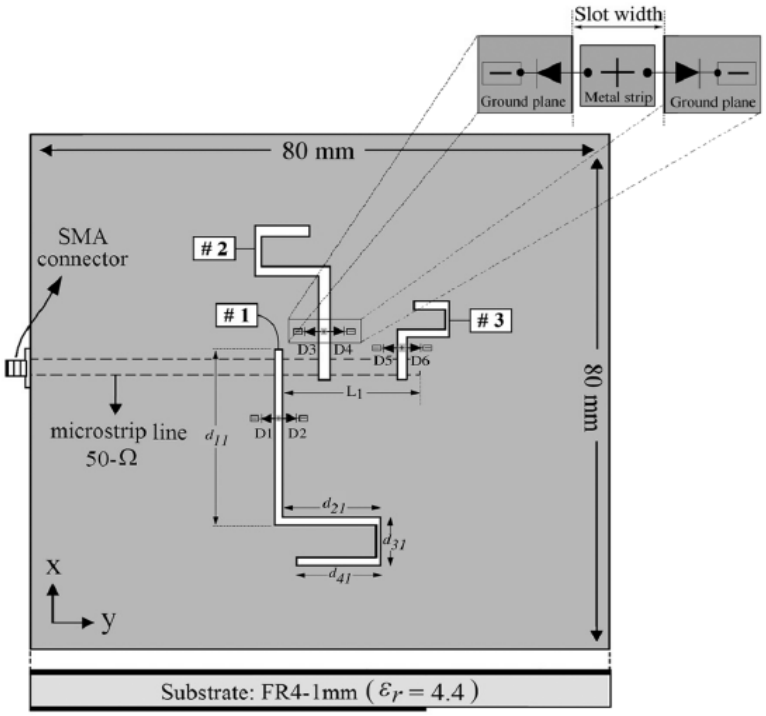

Figure 3: Geometry of the multifrequency triple slot antenna proposed in [16].

Another design in [16], proposed a slot reconfigurable antenna. The antenna can be tuned to three different frequencies. Seven different states were achieved using PIN diodes. These PIN diodes were mounted on the back side of the substrate between the ground plane and three metal strips inside the slots. The layout of the proposed antenna in [16], is depicted in Figure 3. For state 1, diodes D_3, D_4, D_5 and D_6 were biased and D_1 and D_2 were unbiased. During this state resonance frequency around 2.4 GHz was achieved. When diodes D_3 and D_4 were unbiased and all other diodes

were biased for state 2. The resonance was shifted to 3.5 GHz. For state 3, diodes D_5 and D_6 were unbiased and remaining diodes were biased to shift the frequency around 5.6 GHz. When all other diodes were unbiased and only two diodes D_5 and D_6 were biased for state 4, two frequency bands around 2.4 and 3.5 GHz were achieved, respectively. Similarly for state 5, only diodes D_3 and D_4 were biased to achieve the dual frequency operation around 2.4 and 5.6 GHz, respectively. For state 6, the lower band was shifted to 3.5 GHz and upper band was not shifted from 5.6 GHz by biasing the D_1 and D_2 diodes only. When all diodes were unbiased for state 7, a triple band operation was achieved around 2.4, 3.5 and 5.6 GHz, respectively. In all the states, the electrical length was changed which resulted in the change of resonance frequency. The proposed design in [16] is too large for small portable wireless devices also the measured results are shifted from the simulated results.

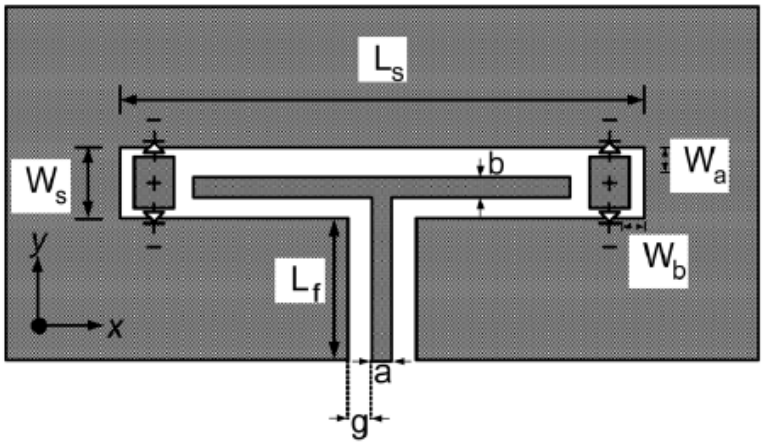

Figure 4: Configuration of the reconfigurable slot antenna proposed in [17].

Another reconfigurable design was proposed in [17]. The schematic of the proposed design in depicted in Figure 4. The proposed antenna was coplanar single folded slot antenna. The length of the slot was changed using a low cost PIN diode. To get the resonance at 5.25 GHz, the length L_s was kept 21.22 mm. Metallic strips were placed in the slot and connected to the ground plane through PIN diodes. The

diodes altered the slots perimeter by connecting or disconnecting the metal strip to the ground plane. When diodes were biased, the metallic strips were connected to the ground plane, which resulted in the reduction of the slot parameter. This reduction in the slot shifted the resonance of the antenna to 5.775 GHz. In the experimental setup, the PIN diodes were biased using the bias lines that were connected to the metallic strips. To unbias the diodes, these bias lines were not connected to the antenna.

2.2. Ultrawide band Multiple-Input Multiple-Output Antennas or Band Notched UWB-MIMO Antennas

2.2.1. Two Elements UWB-MIMO antennas

Ultra-wideband (UWB) Multiple-Input-Multiple-Output (MIMO) antennas are considered to be an integral part of high speed wireless technologies of the near future; for example Wireless Personal Area Networks (WPANs). This is because antenna diversity, such as spatial diversity, pattern diversity or polarization diversity are well established techniques proven to enhance the performance of MIMO systems. However, in many UWB applications, unwanted interference from Wireless Local Area Networks (WLANs) operating in the 5.8 GHz band can interfere with weak WLAN signals, or strong WLAN signals may disturb the nearby UWB-MIMO receivers [18]-[22]. To minimize this interference, over the last decade researchers and designers have used band-reject UWB or UWB-MIMO antennas [22]-[24], [7]-[15].

The design proposed in [8], achieved the band notched function for IEEE 802.11a operating in 5.15-5.825 GHz band. Two $\lambda/4$ slits were inserted in the radiators to achieve this function. The configuration of the proposed UWB-MIMO antenna presented in [8], is shown in Figure 5. The radiators were fed by tapered microstrip lines in order to achieve the wide band matching. A rectangular stub was introduced in the middle of the ground plane to reduce the mutual coupling between two feeding lines. Two semi-circular slots were also used under the radiators to adjust the

impedance bandwidth of the antenna. Moreover, two rectangular stubs were used to control the length of the stub and also improve the bandwidth. Each $\lambda/4$ slit shorts the antenna at the relevant frequency so it can be viewed as a $\lambda/4$ resonator. These slits concentrate the current on the slit edges to achieve the band-notched function. The length of this slot was achieved by eqn. (2.1), [8].

$$L = sl + sw = \frac{\lambda}{4} = \frac{c}{4f_o \cdot \sqrt{\frac{(\epsilon_r+1)}{2}}} \tag{2.1}$$

By changing the sl and sw, the total length of the slits can be changed and the notch

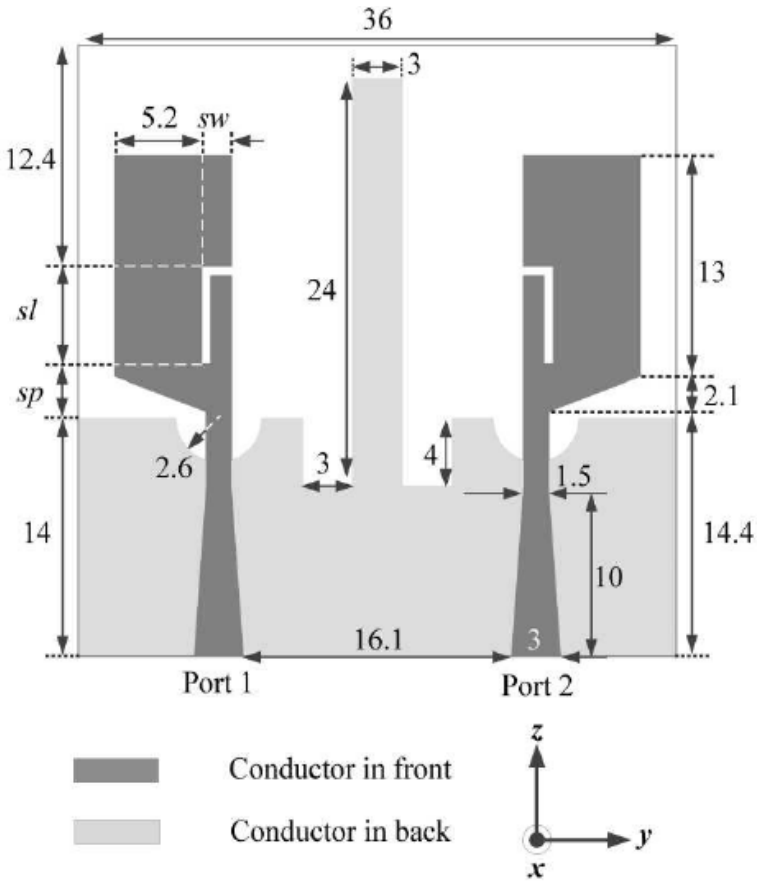

Figure 5: Configuration of the UWB-MIMO antenna presented in [8].

band can be shifted. Good agreement between simulated and measured results was obtained. But the antenna rejects the WLAN band permanently and can be used for

those application where WLAN is not required nearby.

Another design proposed in [10], has printed folded monopole antenna coupled with a parasitic inverted-L element. An open stub was inserted in the antenna to reject the WLAN (5.15-5.85 GHz) band as shown in Figure 6.

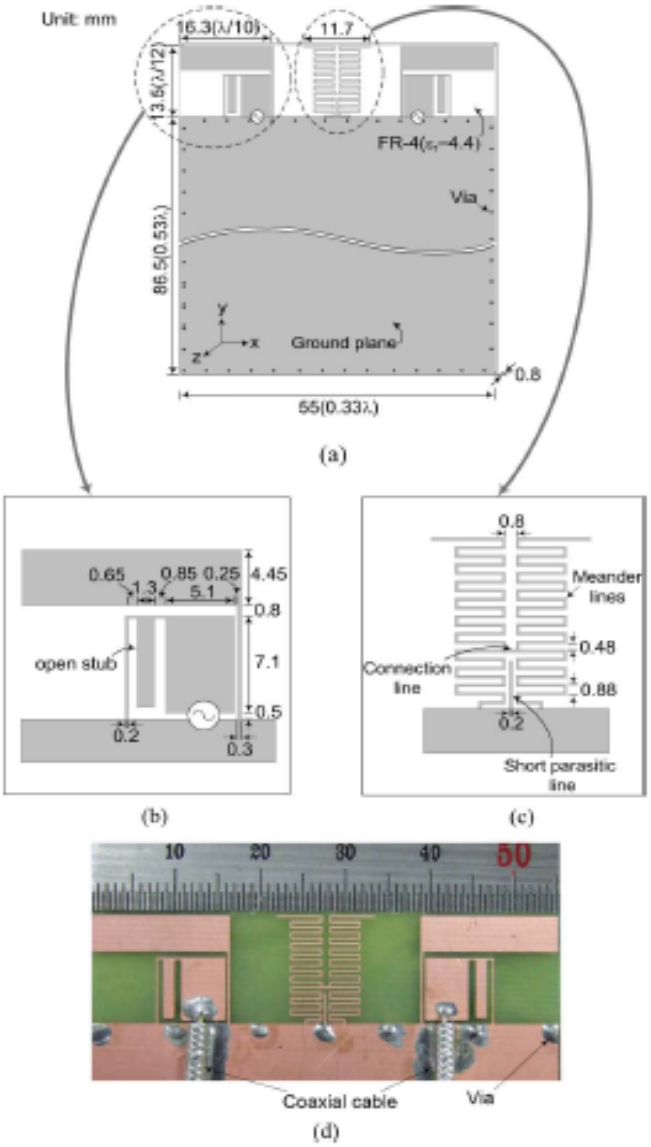

Figure 6: Configuration of the UWB-MIMO antenna presented in [10]. (a) Front view of the antenna (b) radiator on the left-hand side (c) meander lines structure for reducing mutual coupling and (d) printed layout of the antenna.

To achieve the WCDMA band and whole UWB band, the length of the inverted-

L element was adjusted. Also the gap between inverted-L element and folded monopole was adjusted to achieve the good impedance matching over the complete bandwidth. The length of the open stub was kept 17 mm which is approximately 0.5λ of 5.5 GHz. The parasitic meander lines were added to the middle part of the substrate to reduce the mutual coupling between antenna element. As shown in Figure 6(c), these lines were made by joining symmetric meander lines with connection lines. A short parasitic line was also the part of the meander line structure. The total length of meander line structure was kept around 39 mm so that it can act as quarter-wavelength reflector. This meanderline structure improved the isolation from 1.82-1.89 GHz. This was due to the quarter-wavelength reflector which blocked the current on the ground plane between antenna elements. With these features of the open stub and meander line structure, although low envelope correlation, high isolation and efficiency of more than 91% was obtained over the complete bandwidth except the rejected band. But the band was permanently rejected.

In [7], a dual notch band ultra-wideband (UWB) multiple-input multiple-output (MIMO) with isolation of more than 20 dB was proposed. Each element was designed using a U shaped radiator and a rectangular metal strip. The U-shaped radiator was printed on the front side of the substrate with an open slot. The rectangular strip was printed on the back side of the substrate as shown in Figure 7. The ground plane consisted of two protruded ground parts, which were also connected by using a small metal strip. Due to overlapping of the radiator and metal strip, a strong capacitive coupling occurred. This coupling caused destructive interference for the excited surface currents, making large reflection for the frequencies about 5.5 GHz, and the band notched characteristics were achieved. By decreasing the width of w_S, the notch can be shifted towards higher frequencies. To reject the band from 3.3 to 3.7 GHz, two symmetric 0.25λ slots were etched into the radiator. These slots acted

like a LC resonator. At 3.5 GHz, the currents concentrated around the slots did not radiate and a notch is obtained. This notch was controlled by the values of $(s_{l1} + s_{l2})$. Although the design proposed in [7], can reject two bands but the reconfigurability was not applied so this design can be applied to those applications where 3.3 to 3.7 GHz bandwidth and WLAN are not required.

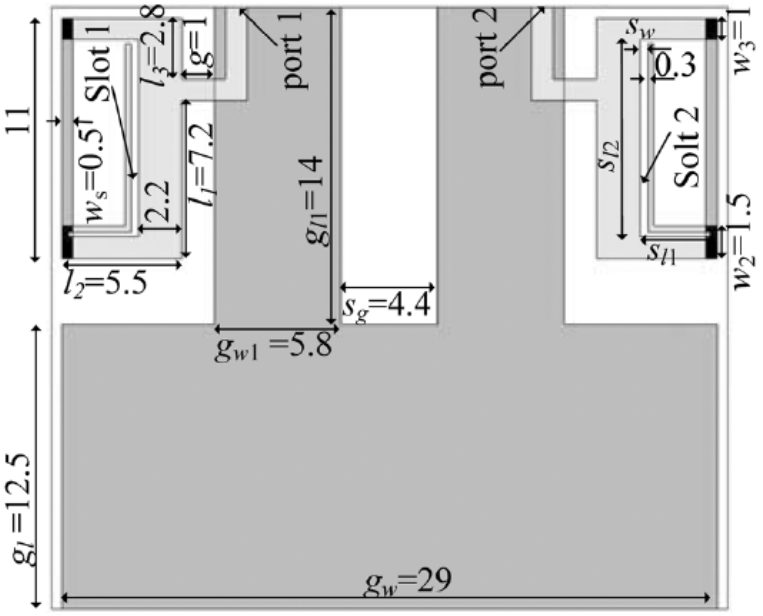

Figure 7: Layout of the UWB-MIMO antenna presented in [7].

2.2.2. Four Elements UWB-MIMO antennas

In [25], a single radiator was shared by two antenna elements. A T-shaped slot was etched in the radiator, also a stub was extending on the ground plane as shown in Figure 8. The proposed antenna had a pentagonal radiator, which was fed by two tapered microstrip lines in order to achieve the wide band matching. These microstrip were placed perpendicularly to each other so that the polarization diversity could be achieved. A stub on the ground plane was extended to reduce the mutual coupling between elements. This stub acted as reflector which absorbed the electromagnetic energy and decreased the current on the other element. Also T-shaped slot was used to

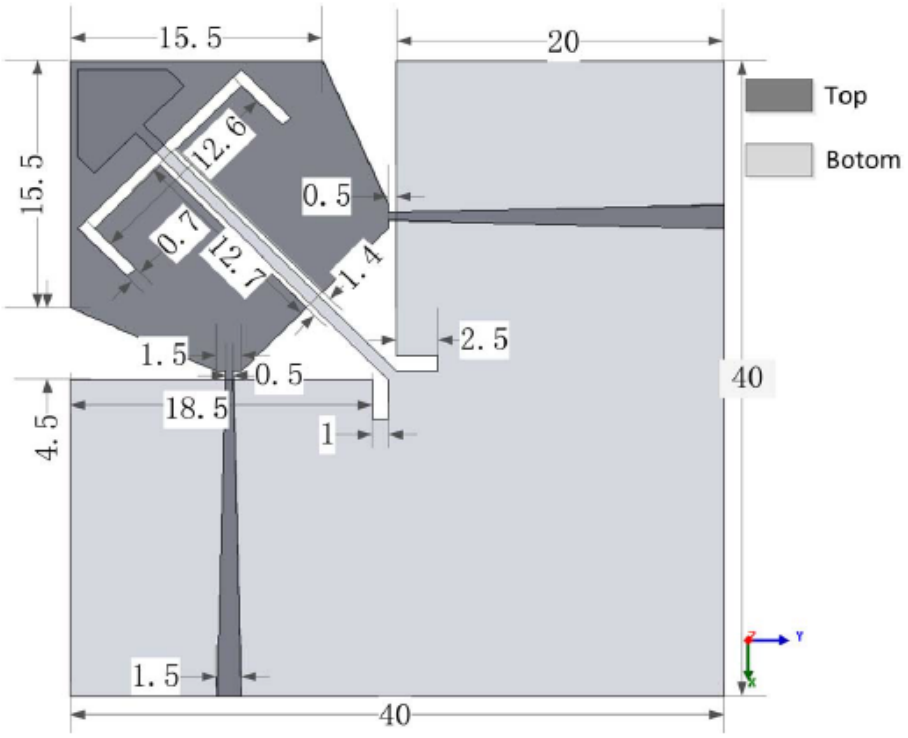

Figure 8: Geometry of the two elements UWB-MIMO antenna presented in [25].

decrease the coupling between antenna elements. This T-shaped slot concentrated the current on its edges and can also be viewed as a quarter-wavelength slot resonator at 3 GHz. When it resonated, the current did not travel to the other part of the antenna which improved the isolation between antenna elements. Two small slots were also etched in the ground plane which reduced the amount of the current travelling to the other part of the ground plane. Similarly the proposed design was modified to the four elements as shown in Figure 9. The four elements were kept symmetrical by two diagonal lines and the feeding structures were perpendicular to each other. In this design four elements UWB-MIMO antenna was proposed but antenna was not made to obtain band notched characteristics.

In [11], a compact 4×4 UWB-MIMO antenna was proposed. An electromagnetic bandgap (EBG) structure was employed to reject the WLAN band. The layout of

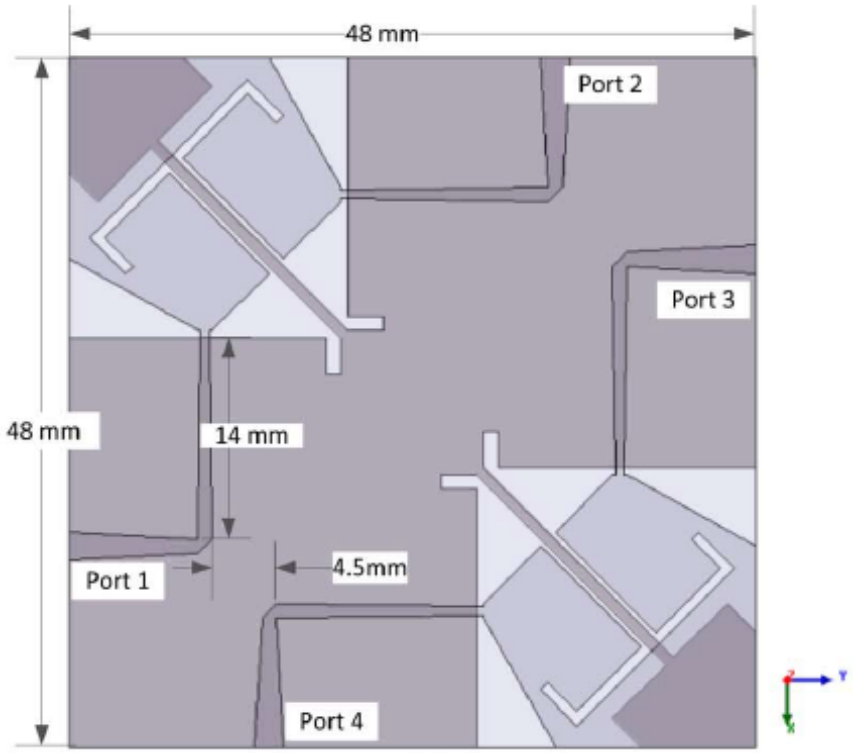

Figure 9: Geometry of the four elements UWB-MIMO antenna presented in [25].

the single element with mashroom-like EBG structure is shown in Figure 10.

To convert this single design to 4 element UWB-MIMO, a microstrip multimode resonator (MMR) stub structure was inserted on the top side as shown in Figure 11. As a starting point a circular monopole UWB antenna was designed from 3.1 to 10.6 GHz. Later on EBG structures were integrated such that the microstrip line was placed in between EBG structures. This EBG structure acted as a stopband filter. As shown in Figure 10(c), there was a capacitance produced between EBG structures and microstip line and also inductance was introduced due to the current flow through via. If the distance between EBG structure and microstrip line was increased than the bandwidth of notch band was decreased. The capacitance also influenced the bandwidth of notch band. If the capacitance was increased than the bandwidth of notch band was also increased. So optimum dimensions were chosen to achieve the band notched characteristics from 5 to 6 GHz.

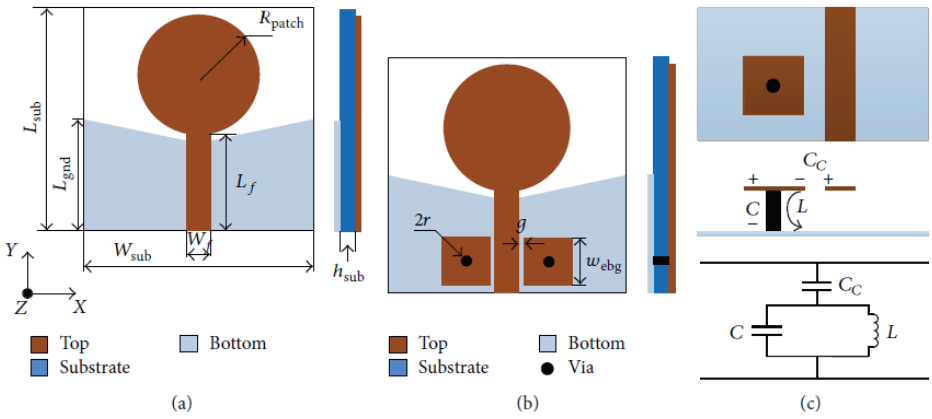

Figure 10: Geometry of the single element UWB antenna presented in [11]. (a) Layout without EBG structure (b) layout with EBG structure and (c) equivalent circuit.

When these elements are rotated and placed to get a 4 elements UWB-MIMO antenna than high coupling between nearly placed elements was observed. So a stub structure consisted of MMR was adopted. These stubs were connected through a square patch and placed in between the antenna elements. The length of a single MMR was adjusted near to quarter wavelength.

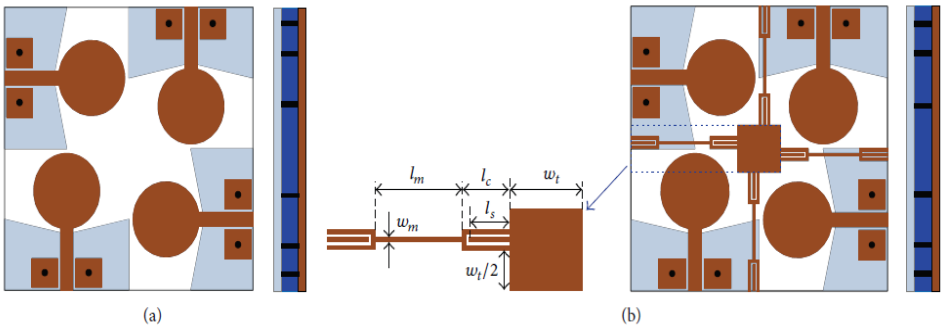

Figure 11: Geometry of the four elements UWB antenna presented in [11]. (a) Layout of initial design and (b) final UWB-MIMO antenna with MMR stub structure.

According to the principle of MMR, the stub structure produced a stopband filter, therefore it suppressed the copolarization elements at the center frequency for which it was designed. Overall good agreement between simulated and measured results was observed also the far-field characteristics of this proposed design made it

suitable for UWB-MIMO applications but this design was not made reconfigurable to adopt its characteristics for different scenarios.

In [12], a triple band notched antenna was presented. Two identical monopoles were placed perpendicularly to each other as shown in Figure 12.

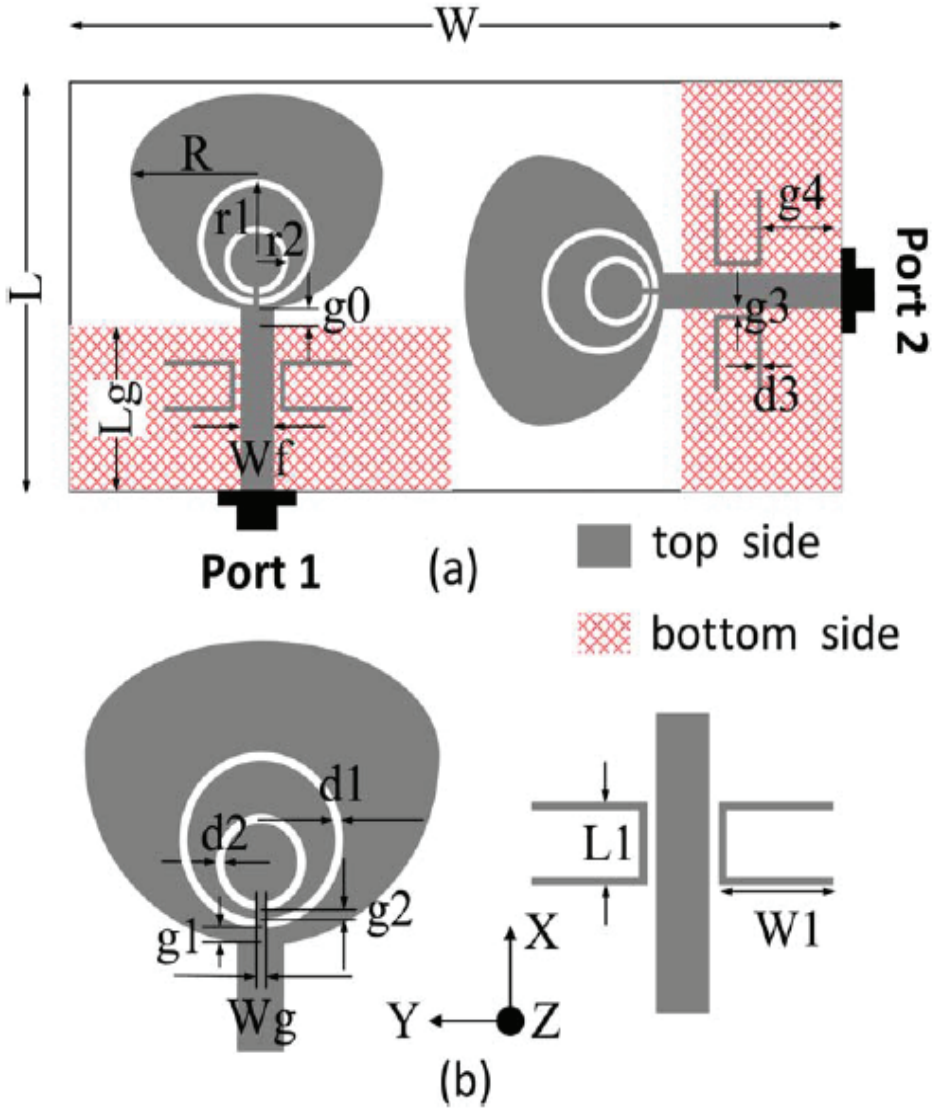

Figure 12: Geometry of the two elements UWB-MIMO antenna presented in [12]. (a) Full view and (b) expanded view.

Due to this placement, orthogonal polarization was achieved which resulted in high isolation. Each element had a main radiator, which consisted of a semicircular and a half ellipse. The ground plane was made rectangle. A small gap was kept

between the edge of the monopole and the rectangular ground plane to achieve the UWB bandwidth. Two CSRR slots were etched on each radiator element. The radius of these slots was fixed at 4.9 mm and 3.2 mm to reject the 3.5 GHz and 5.5 GHz band. To reject the 8 GHz band, two C-shaped stubs were placed on both sides of the microstrip line.

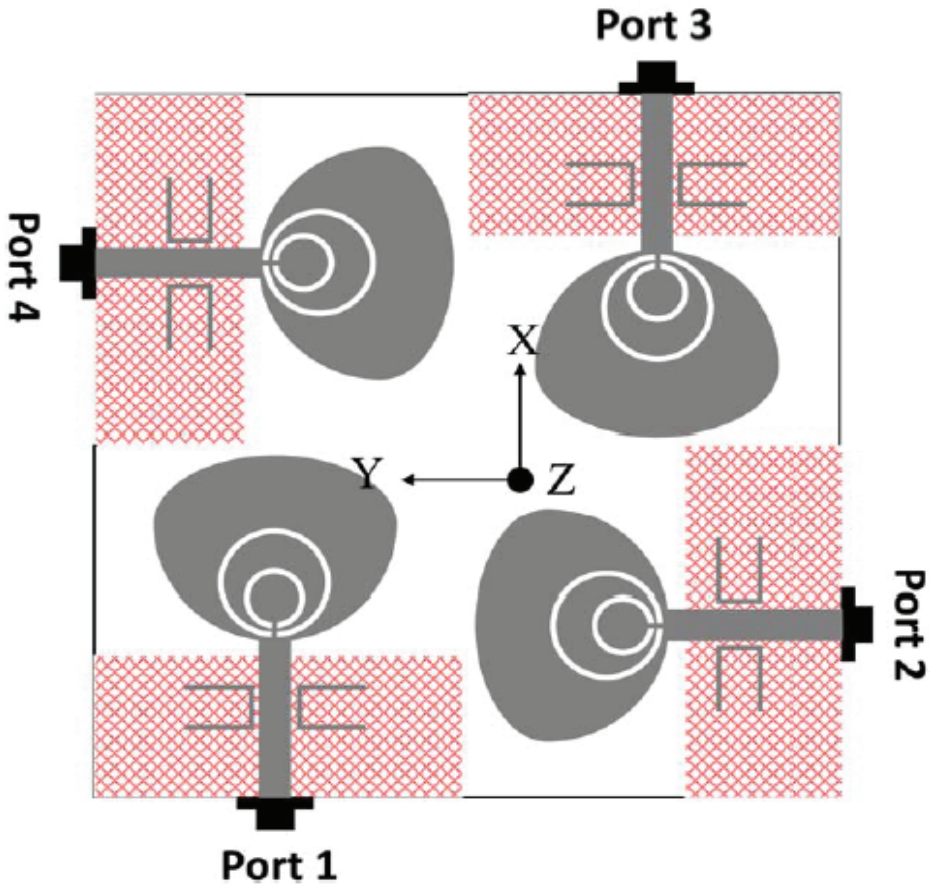

Figure 13: Geometry of the four elements UWB-MIMO antenna presented in [12].

The CSRR slots produced negative effective permittivity to reject the unwanted frequency bands. By changing the radius of CSRR slots and gap between them, the two notches at 3.5 and 5.5 GHZ can be controlled. These slots concentrated the current on their edges at their respective frequencies. Similarly, at 8 GHz, the C-shaped stub absorbed the current. These slots and stub acted as a resonator at their respective frequencies which lead to impedance mismatch and hence notch was

obtained. These elements are placed perpendicularly to each other to convert this two elements UWB-MIMO antenna to four elements as shown in Figure 13. The polarization diversity of nearly placed antenna elements was exploited and CSRR slots and C-shaped stubs were used to reject the three bands. The proposed design is efficient in terms of S-parameters, far-field and band notched characteristics but unavailability of reconfigurability makes it limited to some wireless applications.

2.3. Conformal Antennas

Conformal antennas are being used for the wireless applications that require an antenna to operate on a surface which is not flat (i.e., a singly or doubly curved surface). For most of the previous works, it was assumed that conformal surface was fixed during the operation of antenna. This assumption is useful for some applications, however in modern wireless communication most of the systems require changing conformal surfaces. One of the application of conformal antenna is wearable (textile) antennas. In past, if the antenna is designed for one application than it cannot be applied to different conformal surface without changing the matching and radiation properties. The first attempt to study the affects of conformal antennas on a surface that changes shape was reported in [26]. In recent years many applications are presented which require smaller conformal antennas to change their properties, when the surface is changed.

In [27], a Control Circuit Encoding (CCE) technique was used for calibrating the phased arrays. The calibration system of CCE technique is shown in Figure 14. This method employed orthogonal coding of the digitally controlled attenuators and phase shifters. It measured the relative amplitudes and phases of all the elements within the array. All the elements were calibrated simultaneously, so it required less time from other schemes at that time, where the elements were measured sequentially. This technique was useful for both transmitting and receiving systems. For transmitting

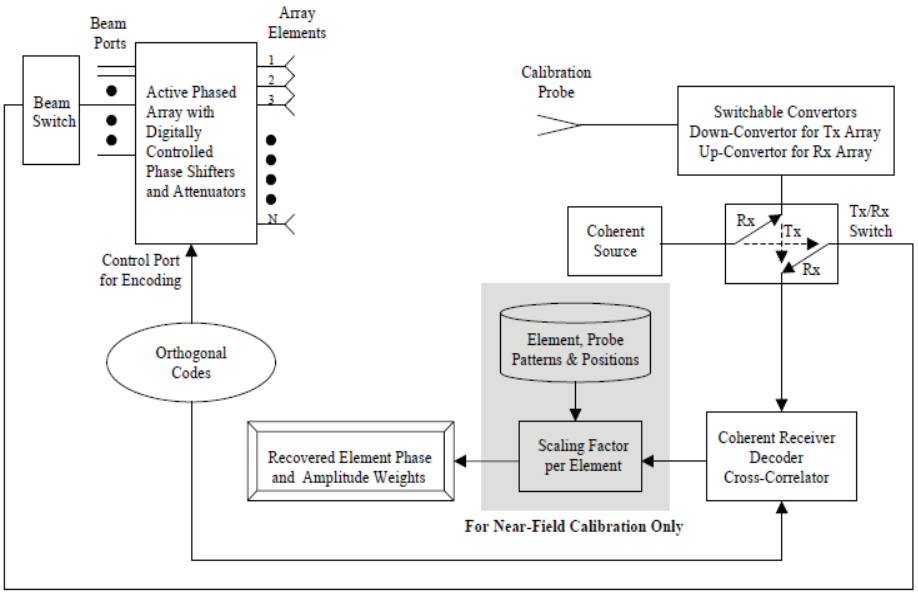

Figure 14: Block diagram of CCE calibration system (transmit/Tx or receive/Rx) for far or near filed presented in [27].

systems, the input beam port of the array was connected with the coherent source, while calibration probe and down-converter received the encoded and radiated signal. This received signal was then sent to the receiver and processor.

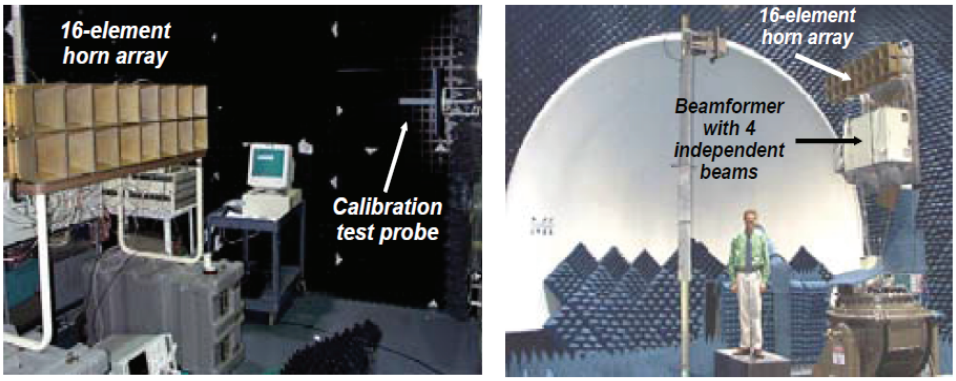

Figure 15: Photo of 16 element horn array during measurement presented in [27]. (a) Near-field range and (b) compact range.

For receiving systems, the signal from the coherent source was forwarded to the up-converter and then it was radiated from the calibration probe. In this process,

the array beam port received the coded signal and forwarded it to the receiver and processor. For both transmitting and receiving systems, the process of coding and decoding was same. To check the performance of the proposed technique, the measurements were taken on different arrays. One setup of measurement is shown in Figure 15. In this measurement, a 16 element horn array was used. In Figure 15(a), the calibration probe was in the near-field of the array, which was moved to the compact range later on as shown in Figure 15(b). The pattern of the array was reconstructed successfully.

In [28], a method was proposed by using the change in the length of the deformation surface to compensate for the induced beam shift. Due to this change in length, the capacitance of the composite right/left-handed transmission was changed, which caused a phase shift in the line. An 18° of beam shift can be corrected by this method. To verify the concept a 10 element linear array resonating at 10 GHz was simulated using CST Microwave Studio. The distance between element was kept at half wavelength. These elements were mounted on a 2 m semi rigid surface with the first element placed at the center of the surface. One end of the surface was fixed as shown in Figure 16.

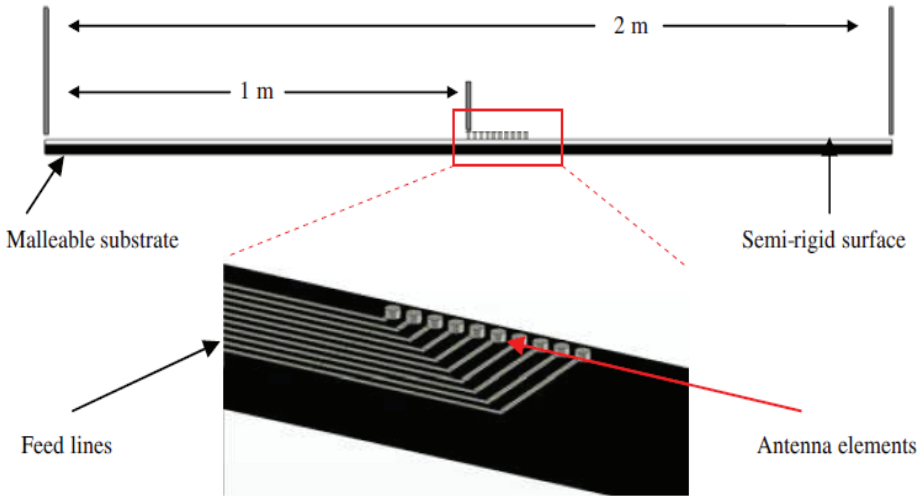

Figure 16: A 10 element array for conformal surface presented in [28].

An individual microstrip was used to fed each element of the array. During simulation, it was assumed that array is flat and the bent with an arc of 30° as shown in Figure 17. The proposed design consisted of shunt inductor and inter-digital capacitors (IDC) as shown in Figure 18.

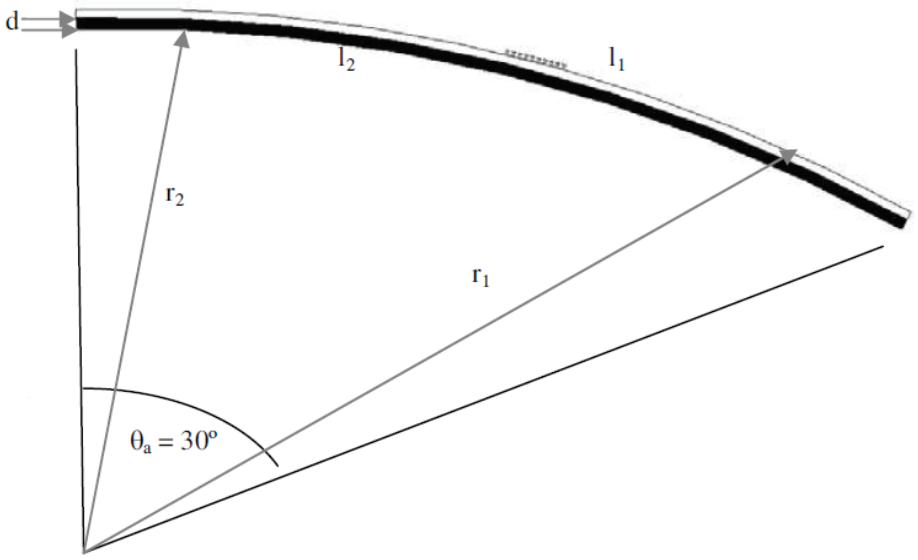

Figure 17: A 10 element array at 30° bend presented in [28].

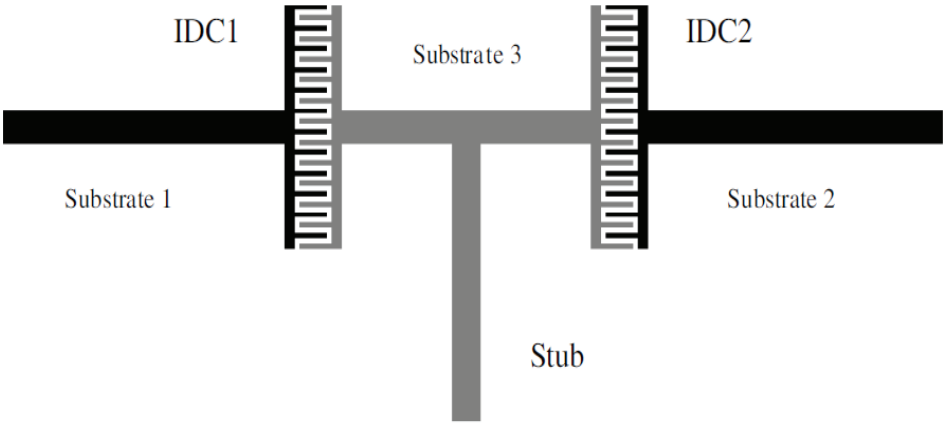

Figure 18: Single CRLH-TL with IDC and a shunt inductor presented in [28].

This structure provided a phase shift, when the length was changed. These IDCs were physically disconnected from each other so that a proper phase could be

achieved at each side. Each IDC created a capacitance related to the gap while each finger of the IDC had a very low inductance as well. The microstrip line produced a separate inductance and its disconnected part produced an inherent capacitance to ground. The transmission line between the IDC and stub was kept half wavelength long. When a bent is applied, than the capacitance produced due to finger was changed. This change in the capacitance was induced on the malleable substrate. This substrate changed its length and a correct phase was induced on the CRLH-TL.

In [29], a four port antenna array operating at 2.45 GHz was developed. Voltage controlled phase shifters and attenuators were used to reconstruct the patterns on the deformed place. The information obtained from this four port array was used to design a 1×4 microstrip array. The schematic of the self adapting 1×4 is shown in Figure 19.

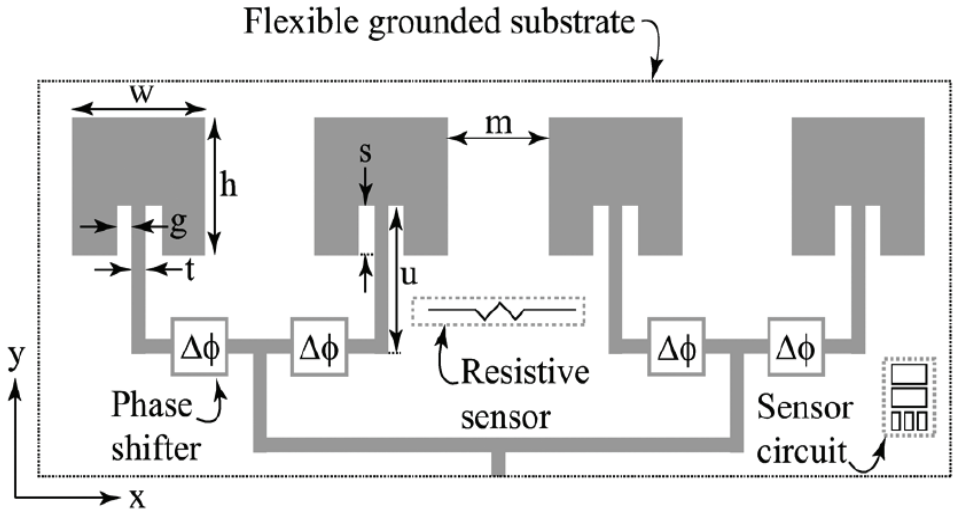

Figure 19: Schematic of 1×4 Selflex array presented in [29].

This array was designed on a flexible ground plane with an embedded sensor. This embedded sensor had the capability of measuring the surface deformation by using flexible resistor and than applying the correct phase voltage at each element by using a sensor circuit. When the array was attached to a wedge or cylindrical

surface, the resistance of the flexible resistor changed. The analog circuit was used to measure this change and then phase shifters were used to apply the correct phase on the array elements. With this technique, by controlling the individual phase shifters in the array, the radiation pattern of the array was recovered. The projection method was used to recover the pattern theoretically. The results were recovered on the 30° wedge, 45° wedge and cylindrical surfaces. The array was designed using HFSS [36]. The spacing between element was kept half wavelength and a flexible 20-mm Rogers RT/duriod 6002 board was used for fabrication of the prototype as shown in Figure 20.

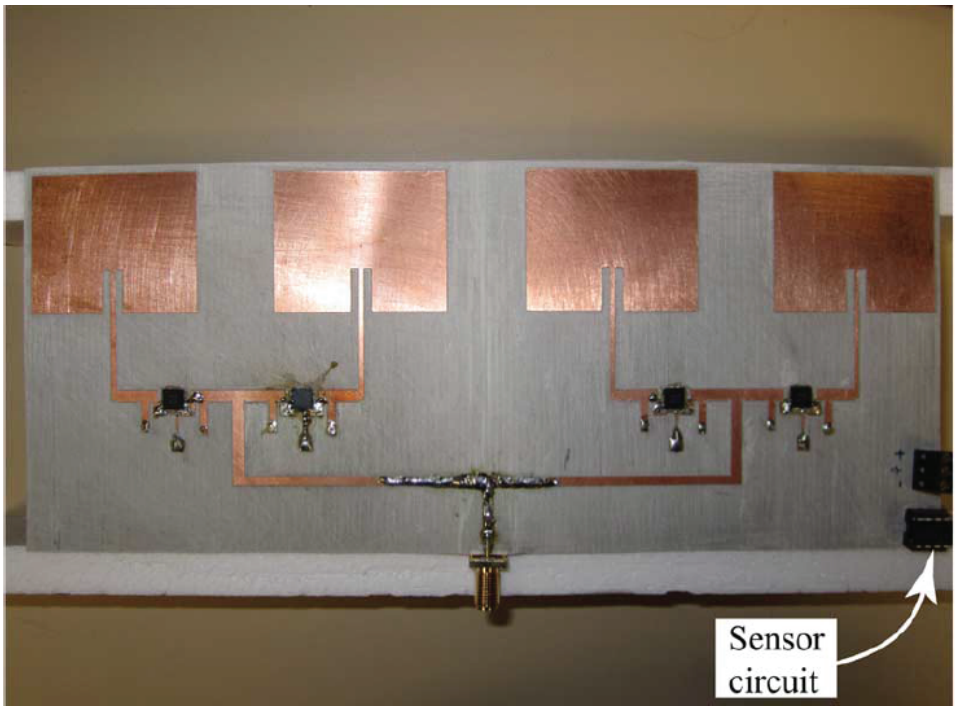

Figure 20: Fabricated prototype of 1 × 4 Selflex array presented in [29].

The sensor circuit which was introducing the correct phase compensation for various values of bending angle was tested separately. For this purpose, a flexible resistor was attached to the wedge shape conformal surface. This resistor was connected with the sensor circuit and the output voltage of the circuit was connected

to the prototype. This experiment was continued and values were taken on different bend angles. When these values were compared with the analytical values, a good comparison was found. When the measurements were taken for different conformal surfaces, the prototype recovered the radiation patterns on those conformal surface.

All the previous techniques focused on single frequency antennas and none of these was applied to the reconfigurable antenna arrays.

2.4. Metamaterial Based Antenna Arrays

Antenna arrays are used to provide high gain and directivity. In the early years linear arrays were formed by cascading the microstirip half wave resonators. The earlier designed arrays have different properties and these arrays provided solid foundation for future work in arrays. The first practical realization of microstrip patch array was series fed array as shown in Figure 21, reported in [30]. In these series fed arrays, the impedance can be altered by changing the length of the microstrip connecting line. Also the phase between array elements can be altered by changing the length of the microstip line. These arrays have very compact feed netwroks and any fabrication tolerance will degrade the performance of overall array.

Figure 21: Microstrip Series-fed array reported in [30].

In antennas, metamaterials are used to exhibit certain electromagnetic properties which are not found in nature. These metamaterials have negative permittivity and permeability and these are referred as left handed materials. The first physicist who realized the concept of left handed material was Veselago in 1967 [31]. During his

investigation, he proved the reversal of snell's law and the Doppler's Effect using left handed metamaterials. Some of the metamaterial based arrays are discussed below.

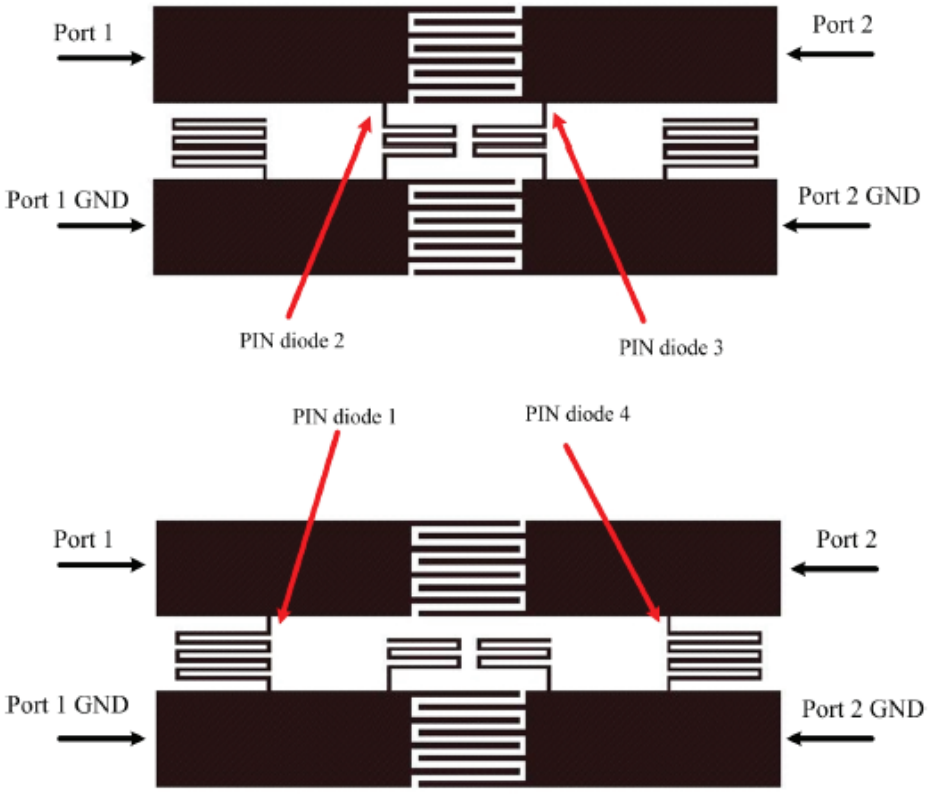

Figure 22: Layout of the interconnect presented in [32].

In [32], a series fed array was designed using non-radiating phase shifting transmission lines. The reconfigurability was attained using RF-PIN diodes. These artificially designed materials exhibited the properties like negative permeability and negative permittivity. These materials also have antiparallel group and phase velocities and they support backward propagation. In this design, dual band CRLH-TLs were adopted instead of meanderline microstrip line. These CRLH-TLs provided the required zero phase at the desired frequency of operation. The layout of the interconnect is shown in Figure 22.

In Figure 22, the interdigitated fingers provided the series capacitance while,

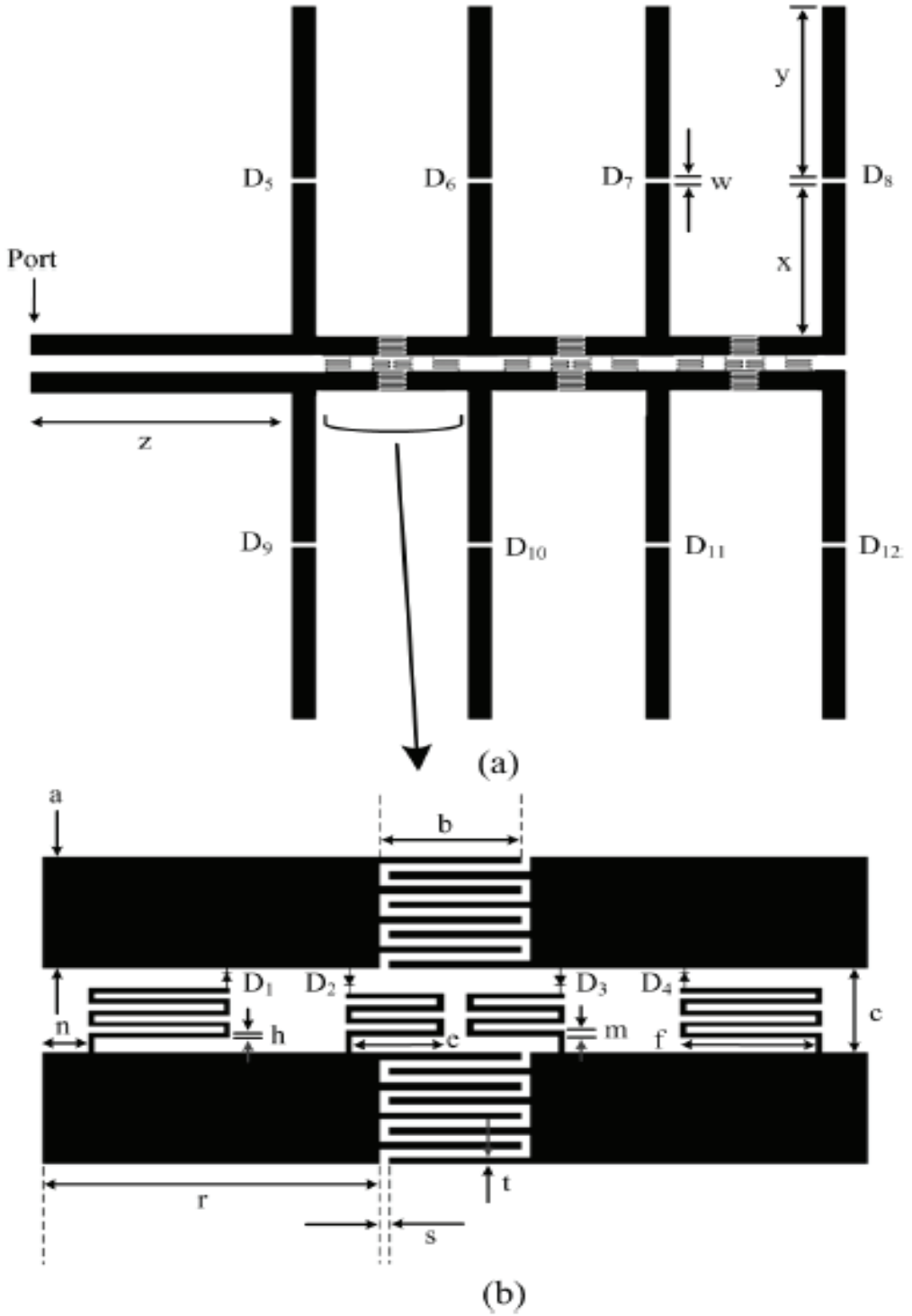

Figure 23: Layout of the reconfigurable series fed array presented in [32]. (a) Full view of array and (b) close view of interconnect.

the meandered line structure provided shunt inductance. The spaces between upper and lower trace provided shunt capacitance while the copper trace provided series inductance. These four parameters exhibited the properties of CRLH. These parameters were adjusted to provide the zero phase at the required frequency. For the first switching frequency, the outer meander inductors were turned on while for second frequency the inner meander conductors were turned on. Final layout of the reconfigurable CRLH-TLs as the interconnections between four reconfigurable dipoles is shown in Figure 23.

According to the layout of the final design, D_2 and D_3 were biased to operate at the higher switching frequency. While D_1 and D_4 were biased along with the other eight diodes at the dipole arms to switch the antenna to the lower frequency. The proposed design was switched efficiently from 2.1 GHz to 2.5 GHz with broad side radiation patterns at both switching frequencies.

Another design of series fed antenna array was proposed in [33]. A dual-band

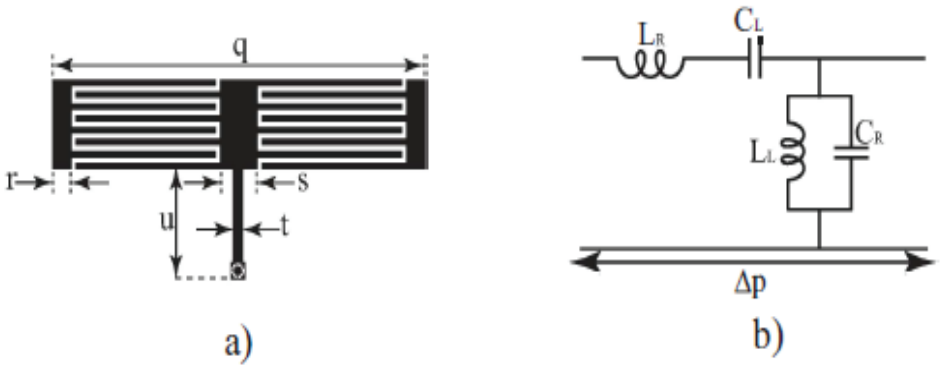

Figure 24: (a)Layout of the CRLH-TL presented in [33] and (b) equivalent circuit of CRLH-TL

CRLH-TLs were used instead of meanderline microstrip lines as shown in Figure 24. These interconnect reduced the overall size of the array. As a first step an interconnect was designed in such a way that it provided S_{21} phase equal to zero at the

desired frequency. Than the phase of the designed interconnect was compared to the traditional transmission line. The comparison showed that the proposed interconnect can achieve the zero phase at the half of the frequency of traditional transmission line. After this a microstrip antenna operating at 2.45 GHz was designed. These interconnects were placed in between the antennas as shown in Figure 25. A small frequency shift was observed but a broad side radiation pattern was obtained at 2.45 GHz.

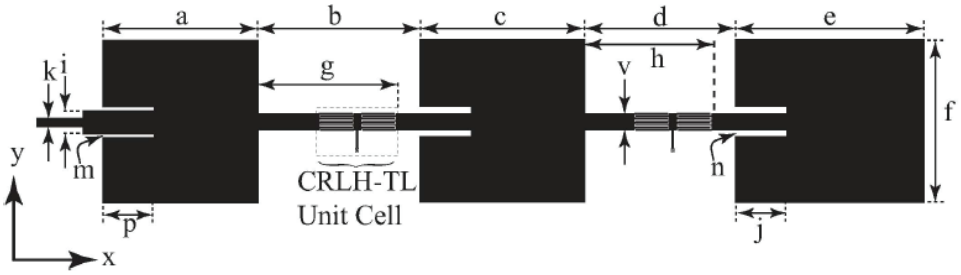

Figure 25: (a)Layout of the series fed-array presented in [33].

CHAPTER 3. DESIGN OF A RECONFIGURABLE SWITCH

Reconfigurable switch is a hardware which is used to alter (reconfigure) the properties of antennas. In reconfigurable antennas these properties are achieved using different techniques. These techniques are summarized below:

1. *Physically Reconfigurable Antennas*

2. *Electrically Reconfigurable Antennas*

   a) By PIN diodes

   b) By Varactors

   c) By RF-MEMS

3. *Optically Reconfigurable Antenna*

   a) By integrated laser diodes

   b) By nonintegrated optical fibers

   c) By integrated optical fibers

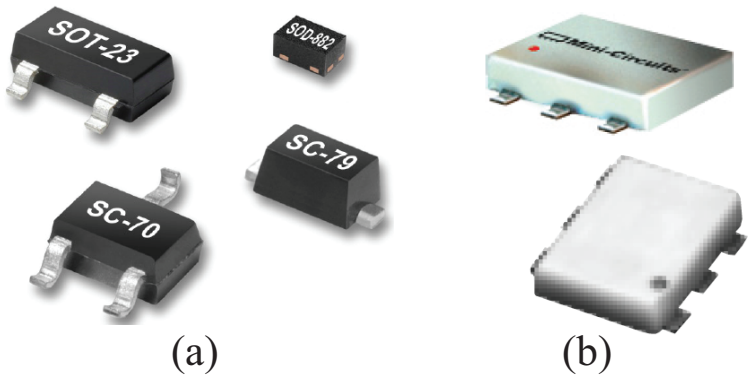

Figure 26: PIN diodes and chokes used for measurements. (a) PIN diodes manufactured by skyworks and (b) chokes manufactured by mini-circuits.

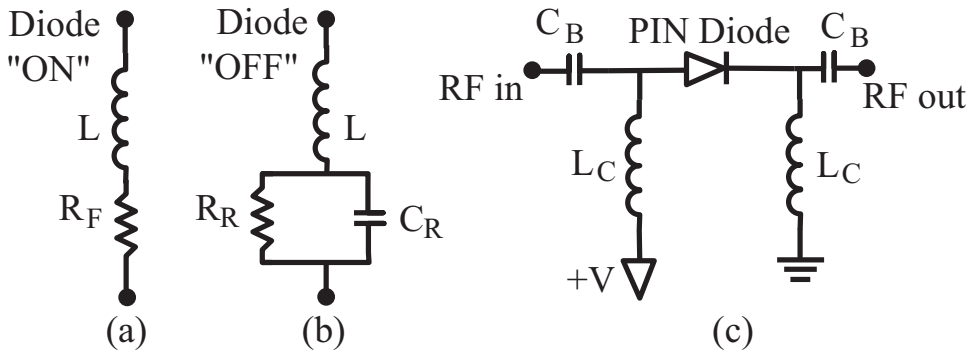

Figure 27: RF PIN diode. (a) Equivalent circuit model for "ON" configuration (b) equivalent circuit model for "OFF" configuration and (c) biasing Network with PIN diode and RF choke model. Parameters are $L = 0.5\ nH,\ R_F = 0.8\ \Omega,\ R_R = 1k\ \Omega,\ C_R = 0.01\ pF,\ C_B = 45\ pF,\ L_C = 200\ nH.$

For all experimental validations, the PIN diodes were used for measurement which were manufactured by Skyworks [34] (part number: SMP 1322) and the RF chokes were manufactured by Mini-circuits (part number: ADCH-80A) [35] as shown in Figure 26. The PIN diodes were modelled in HFSS [36] using the lumped elements shown in Figure 27. In particular, the "ON" and "OFF" state are shown in Figures 27(a) and 27(b), respectively. These diodes are turned "ON/OFF" using a dc bias signal, therefore the DC blocking capacitor $C_B = 45pF$ is used to keep the DC out of the RF portion of the circuit. The biasing network of the PIN diode in Figure 27(c) also shows the RF choke inductance $L_C = 200nH$, which offers high impedance to the RF signals to prevent it from flowing into the DC bias lines.

To design the PIN diode in the HFSS [36], two rectangular or square patches are made between the gap of the copper as shown in Figure 28. These patches are then assigned as lumped RLC elements. For the "ON" (biased) state, the first rectangle is assigned inductor and an arrow is assigned for its boundary excitation 29(a), the second rectangle is assigned as resistor and its value is $R_F = 0.8$ as shown is 29(b). For the "OFF" (unbiased) state, the first rectangular element is not changed but the values of the second lumped elements are changed from R_F to R_R and also a parallel

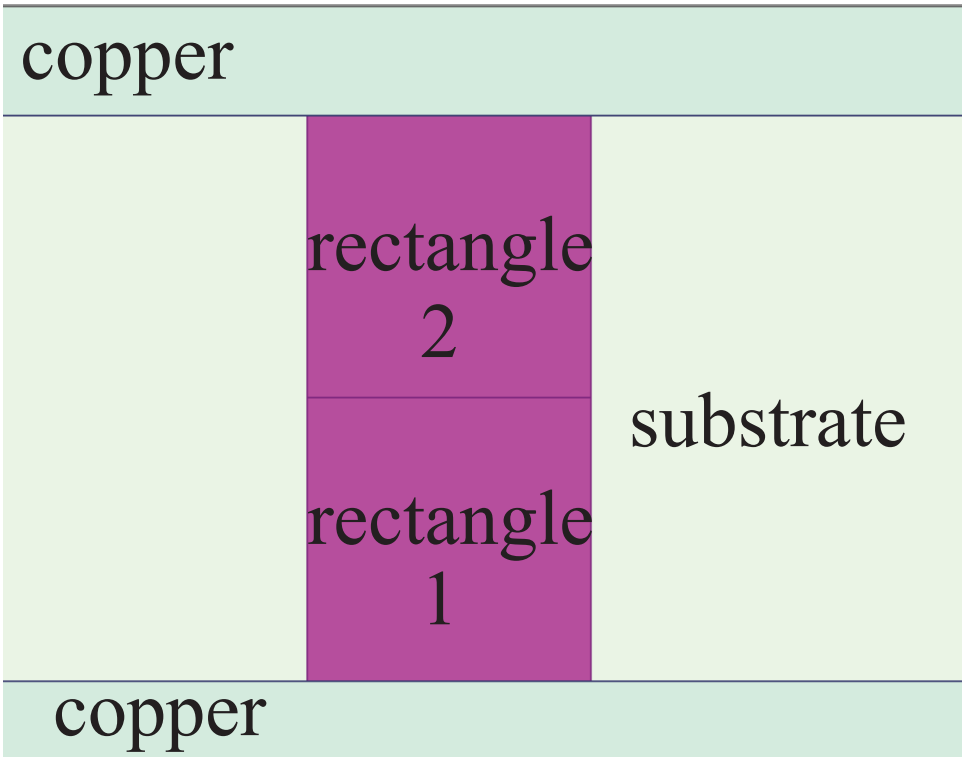

Figure 28: Modelling of PIN diode in HFSS

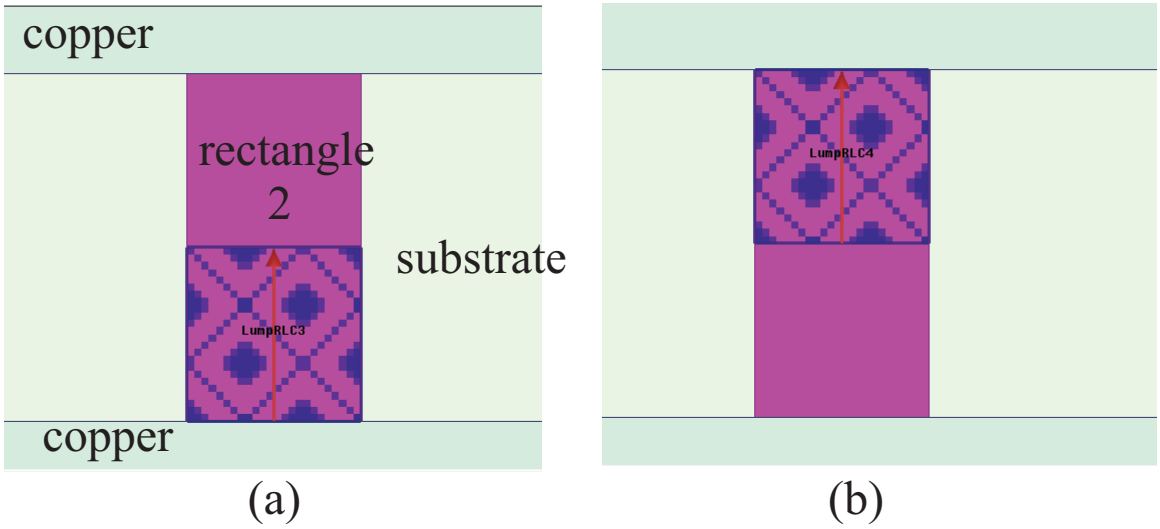

Figure 29: Modelling of PIN diode in HFSS. (a) Assigning first lumped element and (b) assigning second lumped element.

capacitor is added.

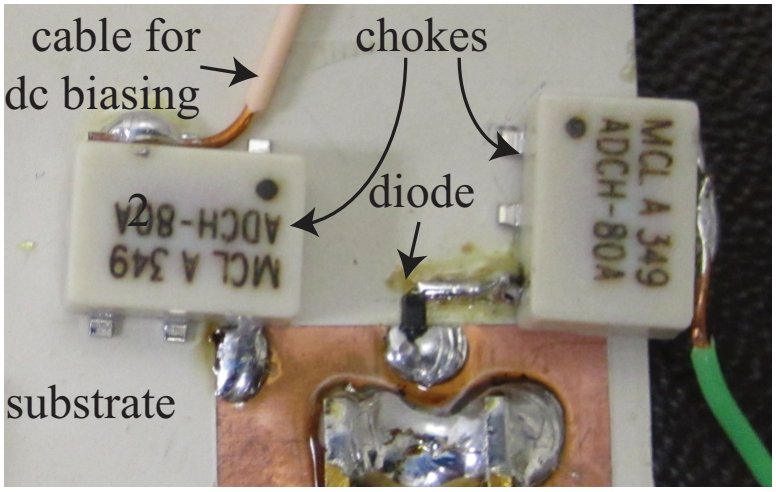

Figure 30: Fabricated prototype with PIN diode and chokes.

During the measurement, PIN diode is soldered between the copper traces. Two chokes are also soldered on both sides of the diodes. The chokes are connected with the cable to provide the dc biasing voltage as shown in Figure 30. A dc biased voltage of 0.7 V is applied for "ON" state and the other part of cable is connected to the ground.

This reconfigurable switch was used for all the prototype measurements.

CHAPTER 4. DIFFERENT RECONFIGURABLE ANTENNAS AND THEIR APPLICATIONS

4.1. An Electrically Small Frequency Reconfigurable Antenna

4.1.1. Introduction

Due to congestion in the electromagnetic frequency spectrum, frequency reconfigurable antennas have received much attention due to their prominent feature of using the spectrum efficiently. Cognitive radio utilizes frequency reconfigurable narrow band antennas to operate at some unoccupied spectrum. Besides, compact size, easy fabrication and low profile structures, other features are also required, such as good frequency selectivity and stable radiation patterns at all frequencies. Antenna reconfigurability can be achieved by employing microelectromechanical systems (MEMS) switches, varactor diodes or PIN diodes as tunable components. Various methods have been introduced to achieve the reconfigurability while maintaining the compactness of the antenna. In [1], a PIN diode is used to reconfigure the dual band patch antenna (2.4 GHz and 3.5 GHz) to a single band (2.4 GHz) but overall dimensions of the antenna are $50 \times 52\ mm^2$. A circular monopolar patch antenna, fed from center and surrounded by four sector-shaped patches, is presented in [2]. Eight varactor diodes are used to bridge the gaps between the circular patch and the sector-shaped patches to operate the antenna between 1.64 GHz to 2.12 GHz. A single (2.4 GHz) or dual band operation (2.4 Ghz and 5.2 GHz) is achieved in [3] by integrating a PIN diode between one of the split-ring radiators and the microstrip feed line. In [4], a printed antenna for WLAN/WiMAX applications is proposed which can be switched to three different frequencies by controlling the states of the switches.

In this work a CPW-fed antenna with switching capabilities is presented and is shown in Figure 31. The resonance at 4.27 GHz is achieved by providing current an extra path to travel on the patch using additional meander lines. Later on PIN

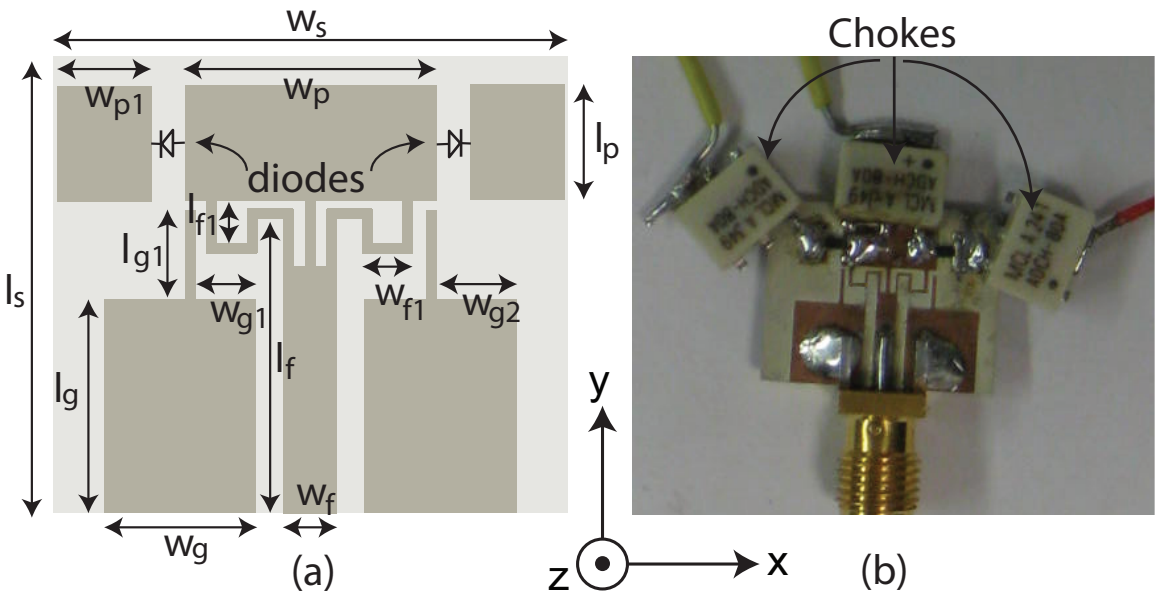

Figure 31: (a) Layout of the proposed antenna with dimensions and (b) fabricated photograph. Optimized dimensions in mm are: $w_s = 14.5$, $l_s = 12.8$, $w_p = 7$, $w_{p1} = 2.25$, $l_p = 3$, $w_g = 4.25$, $w_{g1} = 1.5$, $w_{g2} = 2.25$, $l_g = 7$, $l_{g1} = 1.5$, $w_f = 1.5$, $l_f = 8.3$, $w_{f1} = 1$, $l_{f1} = 1$. Reprinted from [C.1].

diodes are activated to switch the resonance frequency to 3.56 GHz. The proposed antenna is much more compact than the designs presented in [1]-[4].

4.1.2. Antenna Structure and Design Procedure

The layout with the dimensions and the fabricated photograph of the proposed antenna is presented in Figure 31. Initially a CPW-fed antenna with a radiator length l_p and width w_p was designed in HFSS [36] and then additional meander lines with lengths l_{f1} and w_f1 were connected with the radiator to provide an extra path for current from the feedline to the radiator. Due to the extra path, the electrical path of current increases which shifts the resonance frequency to a lower frequency [5]. Good matching was observed at 4.27 GHz. Later on the current path was further increased by connecting the small patches of lengths l_p and width w_{p1} through PIN diodes on both ends of the patch. The PIN diodes are modelled as explained in chapter 3. The lumped elements have negligible effects on the antenna performance because the

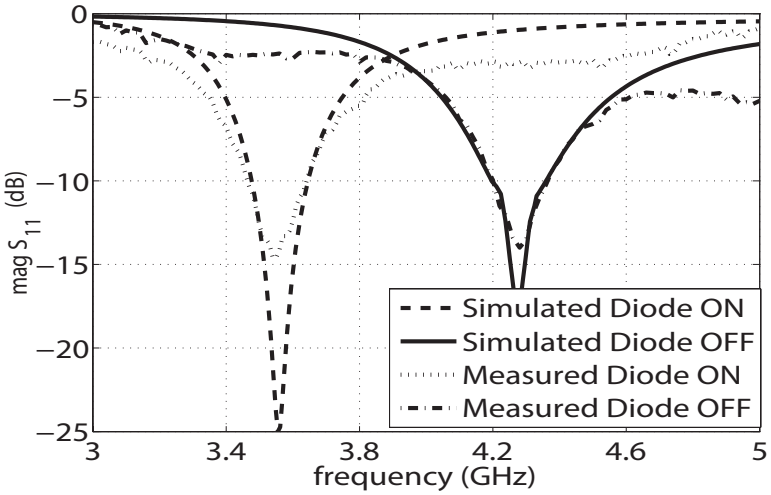

Figure 32: Simulated and measured reflection coefficient. Reprinted from [C.1].

impedance of the antenna is much smaller (lower) than the impedance of the RLC circuit, allowing little currents to flow through.

4.1.3. Experimental Validation

A low loss 1.524 mm thick Rogers TMM4 laminate with a dielectric constant of 4.5 and a loss tangent of 0.002 was used to fabricate the prototype as shown in Figure 31(b). The extra patches were connected via surface-mount voltage controlled PIN diodes and RF chokes were used to place the control voltage (+V = 0.7V) on the conducting surface. The reflection coefficients were measured using the Agilent N5242A PNA-X network analyzer in a full anechoic chamber. It can be seen in Figure 32 that the measured results are in good agreement with the simulated results. The small deviations in the results are due to the non-ideal response of the chokes and diodes. It can be seen in Figure 31(b) that the SMA connector has large dimensions which could affect the properties of the proposed antenna but the simulations were carried out with the SMA connector model to avoid its affects in the measurements.

The radiation patterns of the proposed antenna design were also measured in a fully calibrated anechoic chamber and plotted in Figure 33. The radiation patterns

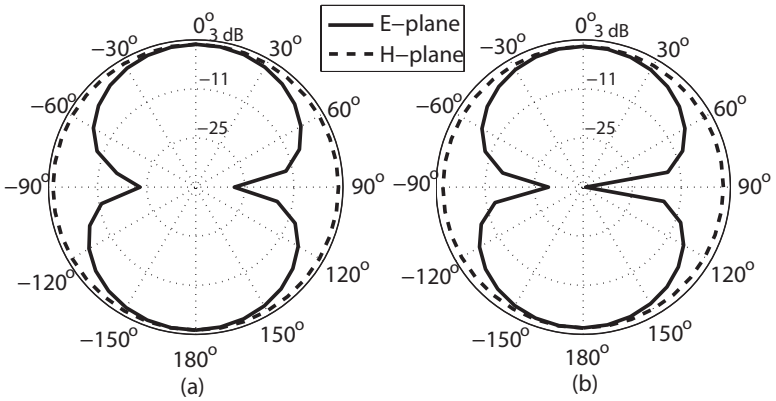

Figure 33: Measured radiation Patterns in E-plane and H-plane (a) 4.27 GHz (b) 3.56 GHz. Reprinted from [C.1].

show a null in the E-plane and are omnidirectional for the H-plane at both switching frequencies. The peak gain was measured in the direction of maximum radiation and found to be 1.3 dBi at 4.27 Ghz but it is reduced to 0.2 dBi at 3.56 GHz due to the losses introduced by the PIN diodes.

4.2. Two Elements Ultra wide-band (UWB) Multiple-Input Multiple-Output (MIMO) Antenna with On-demand WLAN Rejection

4.2.1. Introduction

In high speed wireless personal area networks, UWB MIMO antennas have been considered to be an integral part of the communication system. However, strong WLAN signals may interfere with those of UWB (3.1-10.6 GHz) technology and causing detrimental effects. So, for this reason designers have used different techniques to design band-reject UWB or UWB-MIMO antennas.

The design reported in [24] was an UWB antenna with multiple band notch characteristics using integrated elements in the feed line. Furthermore, a compact dual band notched UWB MIMO antenna using slots in the radiators has also been reported in [7]. In addition to these designs, a pair of slits has been used in the radiators (overall antenna size 36 $\times$ 36 mm^2) to achieve the band-notched functionality in

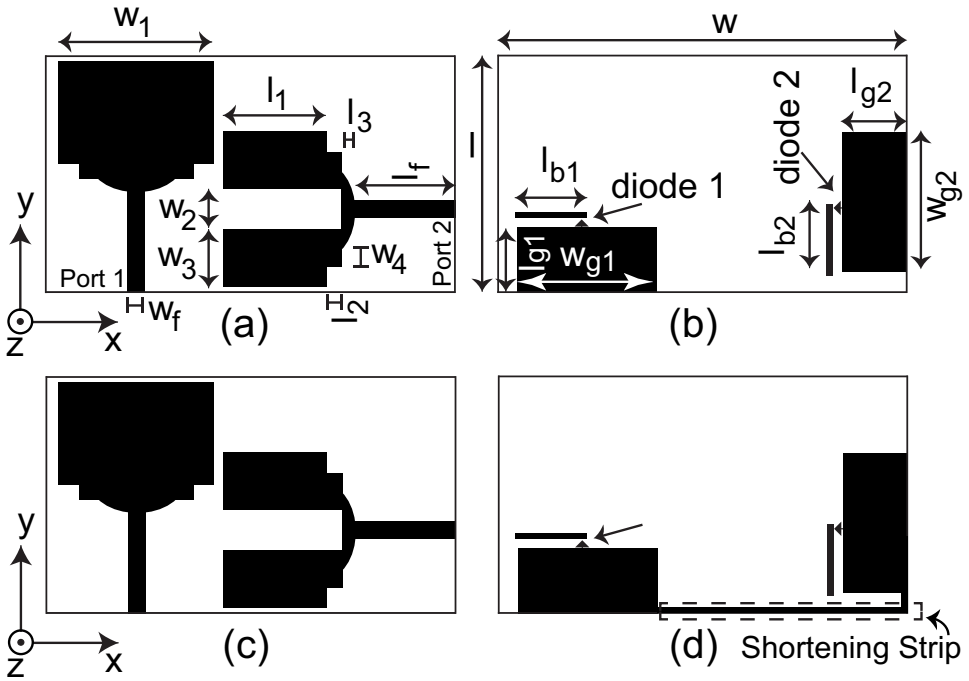

Figure 34: Geometry of proposed UWB-MIMO system. (a) Top view (b) bottom view with separate ground planes (c) top view and (d) bottom view with shared ground plane. Reprinted from [P.9].

[8] and related work in [9] involves the insertion of the stubs in the ground plane (total overall size was 40 $\times$ 68 mm^2). Also, a $\lambda/2$ length open stub on the antenna (with the size of the ground plane being 55 $\times$ 86.5 mm^2) was applied to achieve the band notch operation in [10], but the reflector used in this antenna occupies a large space that limits the overall antennas for further size reduction. Generally, the previous work to reject WLANs either emphasized on rejecting only a portion of the WLAN signals [8] - [10], or multiple bands [24], [7]. However, in all the aforementioned work, the band is permanently rejected. WLAN rejection is not necessary in every case, especially when there are no nearby WLANs. Therefore, the objective of this work is to introduce a more efficient method of using the UWB frequency spectrum by introducing an on-demand rejection mechanism using reconfigurable circuitry with PIN diodes.

In this work, the compact frequency reconfigurable MIMO antenna shown in Figure 34 with on-demand band rejection is proposed. High isolation is achieved by introducing the polarization diversity between the antenna elements. Two PIN diodes connect the ground plane on the bottom side (as shown in Figure 34(b)) with $\lambda/4$ stubs to reject the WLAN band. The proposed technique can be used to reject the other bands (e.g. IEEE 802.11b/g at 2.4 GHz) by changing the length of the stub. The overall size of the proposed antenna is 23×39.8 mm^2, which is smaller as compared to most of the existing designs [8] - [10]. Furthermore, the proposed antenna design can be used as a stand-alone antenna system similar to wireless body area networks [37] and good isolation can be achieved by separating the ground plane [38] - [39], and again, in this design the antennas are placed perpendicularly to exploit the polarization diversity and to obtain high isolation. The compactness of the proposed antenna makes it suitable for small portable devices.

4.2.2. Antenna Structure Configuration

The two radiators in Figure 34, including the tapered section connected to microstrip feeding lines, are placed orthogonal to each other with only 1 mm spacing between them. A U-shaped slot is inserted in radiator 2 to improve the broadband matching characteristics [40] as well as the isolation [41]. Two stubs are placed on the bottom side near each ground plane and the length of the stubs are determined using eqn. (4.1):

$$L_{b1} = L_{b2} = \frac{\lambda}{4} = \frac{c}{4f_o.\sqrt{\epsilon_r}} \tag{4.1}$$

where $f_o = 5.5$ GHz is central frequency of the rejected band and ϵ_r is the relative permittivity of the substrate. When the diodes are ON, the stubs act as a stop band resonator since the gap between the stubs and ground planes acts as a capacitor and the stubs themselves act as an inductor [9]; resulting in a structure that can be

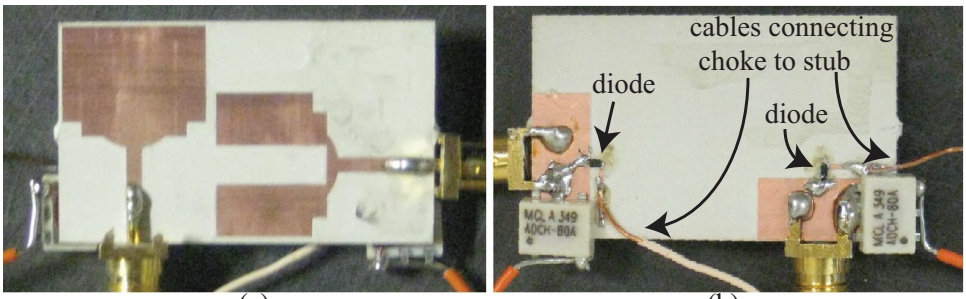

Figure 35: Prototype of proposed antenna. (a) Top view and (b) bottom view without common ground. Optimized dimensions are $w = 39.8\ mm$, $l = 23\ mm$, $w_1 = 15\ mm$, $w_2 = 4\ mm$, $w_3 = 5.5\ mm$, $w_4 = 2.26\ mm$, $l_1 = 10\ mm$, $l_2 = 1.5\ mm$, $l_3 = 1.1\ mm$, $w_f = 1.6\ mm$, $l_f = 9.85\ mm$, $w_{g1} = w_{g2} = 13.5\ mm$, $l_{g1} = l_{g2} = 6.25\ mm$, $l_{b1} = l_{b2} = 6.25\ mm$. Reprinted from [P.9].

thought of an equivalent band-stop filter.

4.2.3. Prototype Testing

To demonstrate the functionality of the proposed antenna, a prototype was fabricated on a 23 mm × 39.8 mm × 1.524 mm Rogers TMM4 substrate with a relative permittivity of 4.5 and a loss tangent 0.002, as shown in Figure 35. The stub was connected to the ground plane via surface-mount voltage controlled PIN diodes and the control voltage (+V = 0.7V) was placed on the conducting surface with RF chokes. The reflection coefficient and isolation for "ON-ON" (i.e., both diodes are biased, the stubs are physically connected with ground) and "OFF-OFF" (i.e., both diodes are un-biased, the stubs are physically disconnected from ground) states were measured using the Agilent N5242A PNA-X network analyzer and the prototype was fed with a semi-rigid cable surrounded by ferrite-beads.

This minimized the current traveling on the outer conductor and the associated parasitic radiation. These results are shown in Figures 36 - 38 and are denoted as "Measured (diodes)". Next, to determine the effects that the diodes and associated RF biasing circuitry may have on the S-parameters, two separate prototypes without the components were manufactured. Except in these prototypes, a printed copper

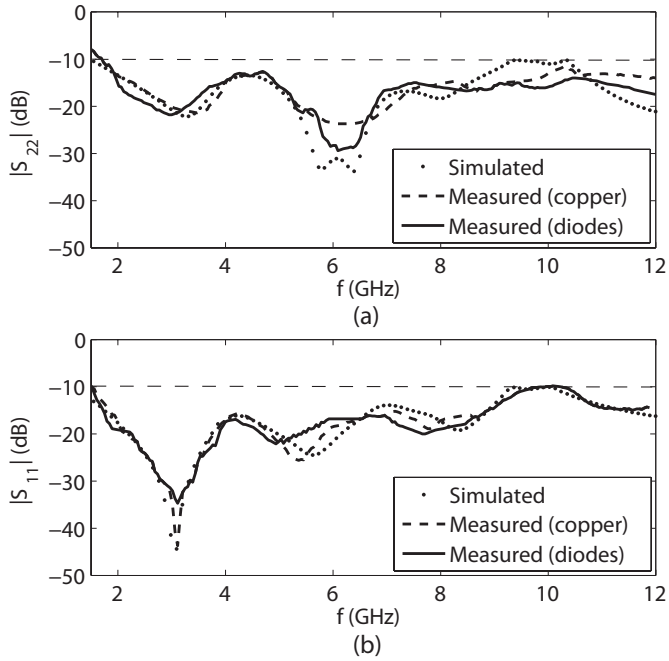

Figure 36: (a) $|S_{22}|$ and (b) $|S_{11}|$ of the prototype when both diodes are "OFF". Reprinted from [P.9].

conductor was used to represent a biased diode in one design and the copper was then removed to represent an un-biased diode in the other design. This then allowed the study of the proposed antenna without the effects of the diode and biasing circuitry. The S-parameters were then measured and the results are shown in Figures 36-38 and are denoted as "Measured (copper)". Overall, good agreement can be seen between the simulated, copper and diodes results; indicating that the lumped components have a small effect on the S-parameters up to 12 GHz. Finally, the isolation is more than 20 dB in all cases, as shown in Figure 38.

The two PIN diodes have 4 possible switching states, namely ON-OFF, OFF-ON, OFF-OFF and ON-ON states. For the sake of brevity only the results of these last two states are plotted in Figures 36-38. In the "ON-OFF" state, antenna 1 rejects the band from 4.8 to 6.4 GHz while in the "OFF-ON" state antenna 2 rejects the band from 4.8 to 6.2 GHz. (It should be noted that some of the applications require the

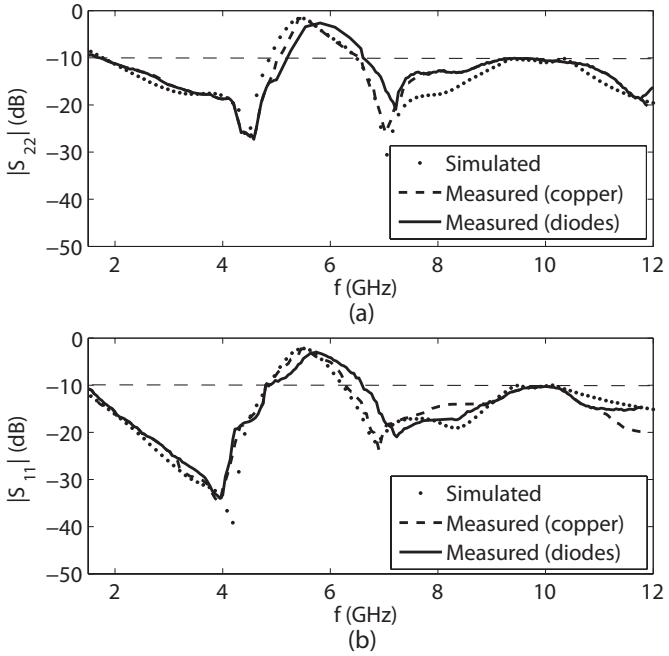

Figure 37: (a) $|S_{22}|$ and (b) $|S_{11}|$ of the prototype when both diodes are "ON". Reprinted from [P.9].

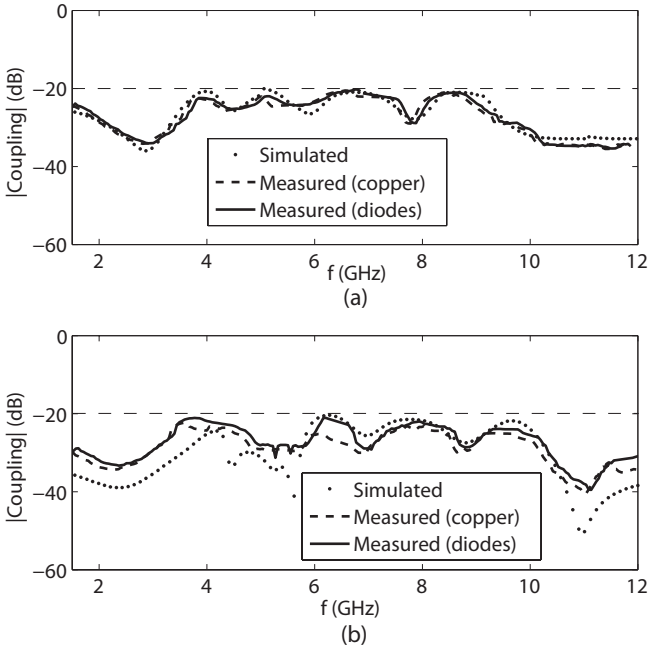

Figure 38: Coupling between the ports for the diodes (a) "OFF" and (b) "ON". Reprinted from [P.9].

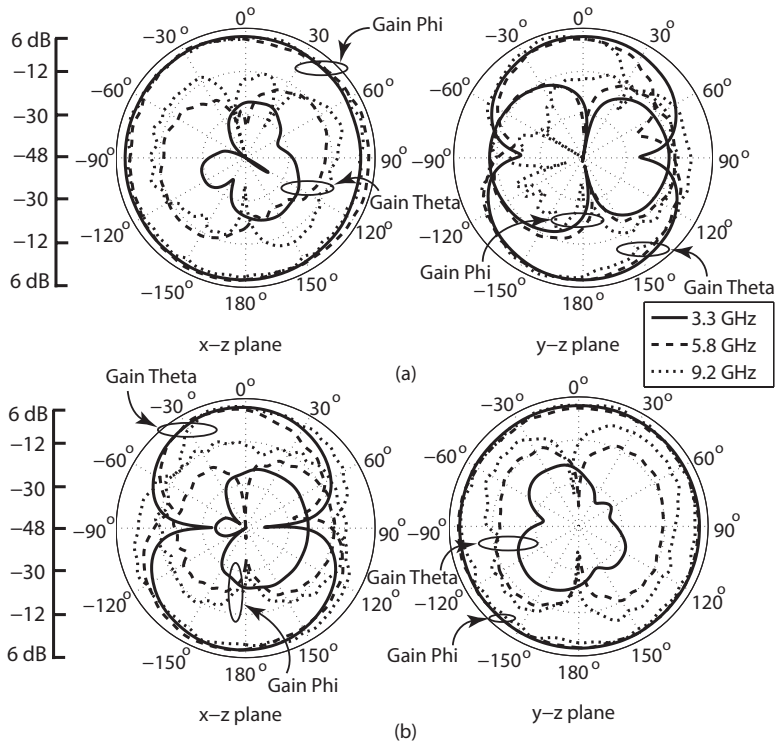

Figure 39: Measured radiation patterns at 3 GHz, 5.8 GHz and 9.2 GHz, when both diodes are "OFF" for (a) port 1 being driven and (b) port 2 being driven.

common ground plane. So a shortening strip as shown in Figure 34 was used to see the affect of common ground plane on the antenna elements. When ground was made common, only slight variations were observed. The bandwidth was reduced from 2.7 to 12 GHz but band rejection characteristics were not changed in the scattering parameters.)

4.2.4. Radiation Patterns, Gain and Efficiency

For further validation, the radiation patterns of the proposed antenna were measured in an anechoic chamber for the "OFF-OFF" and "ON-ON" states. During the pattern measurements, a cable with ferrite bead rings was used to block the return current. Figure 39 shows the patterns of the "OFF-OFF" state at 3, 5.8 and 9.2 GHz in $x-z$ and $y-z$ planes, while Figure 40 shows the patterns of the "ON-ON" state. Notice, the antenna radiation intensity in the rejected band is smaller in all directions

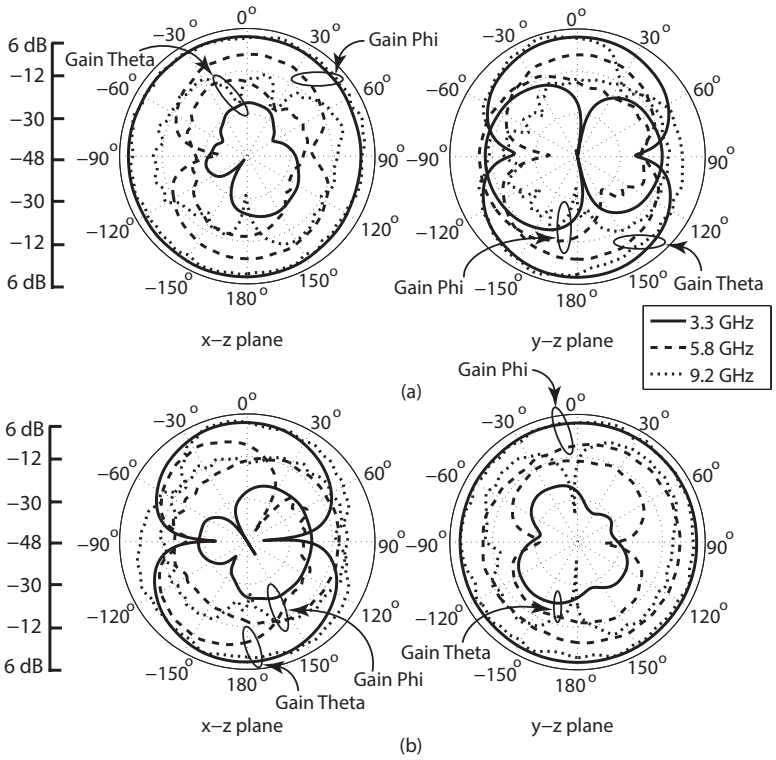

Figure 40: Measured radiation patterns at 3 GHz, 5.8 GHz and 9.2 GHz, when both diodes are "ON" for (a) port 1 being driven and (b) port 2 being driven.

when both diodes are "ON" and its gain is dropped by more than 6 dB.

Next, the peak gain measurements are reported in Figure 41 with respect to frequency for the "OFF-OFF" and "ON-ON" states. When both diodes are "ON", the peak gain reduces by 6.4 dB for antenna element 1 and 6.3 dB for antenna element 2 at 5.8 GHz, where G_{off1} = 3 dBi while G_{on1} = -3.4 dBi and G_{off2} = 2.8 dBi while G_{on2} = -3.5 dBi. The peak gain has low variation in the complete band and it lies in the range of 1.89 dBi to 4.4 dBi. The total efficiency of the proposed antenna array has also been calculated for the "OFF-OFF" and "ON-ON" states. In particular, the total efficiency was numerically calculated using HFSS [36] by functionality taking into account losses in metals and dielectrics, and the efficiency remains above 85% and reduces to 15% in the rejected band when both diodes are "ON".

Finally, to verify, the polarization diversity, the difference between the two

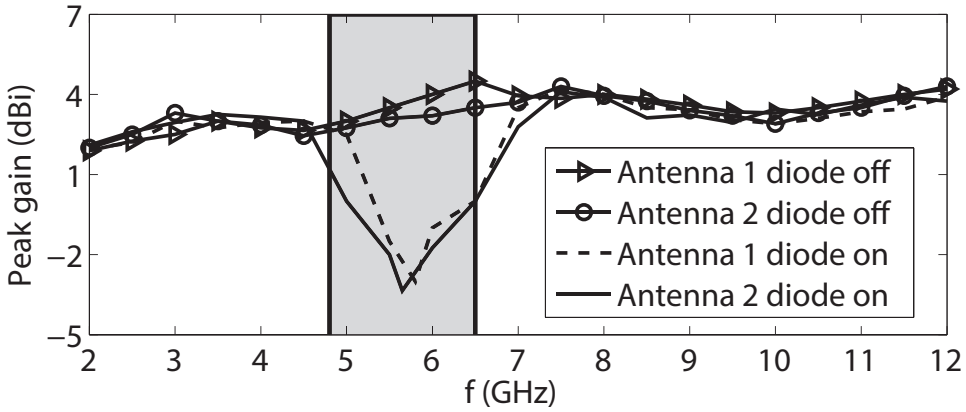

Figure 41: Measured Peak gain over the complete spectrum for the "OFF-OFF" and "ON-ON" states. Reprinted from [P.9].

Table 1: Power Level Difference in the Selected Planes (θ Component Peak Value Minus ϕ Component Peak Value)

Freq	y-z plane		x-z plane	
(GHz)	Radiator 1	Radiator 2	Radiator 1	Radiator 2
2.0	18.1 dB	-10.3 dB	-18.5 dB	10.7 dB
4.0	19.0 dB	-10.4 dB	-15.8 dB	13.0 dB
6.0	19.2 dB	-13.9 dB	-16.8 dB	14.0 dB
8.0	17.2 dB	-09.4 dB	-13.8 dB	14.8 dB
10.0	16.1 dB	-10.8 dB	-13.9 dB	14.1 dB
12.0	17.3 dB	-12.5 dB	-14.9 dB	15.7 dB

polarization components (θ component minus ϕ component) in the $x-z$ and $y-z$ planes as calculated in [41], was calculated. The results from these computations are shown in Table 1 and it is shown that radiator 1 is polarized in the $y-z$ plane and radiator 2 is polarized in the $x-z$ plane.

4.2.5. Diversity Analysis

The correlation coefficient and diversity gain are closely related. The lower correlation coefficient represents a higher antenna diversity as well as better diversity gain. The relationship between ECC (ρ_e) and diversity gain (G_d) can be expressed mathematically [42] as: $G_d = 10\sqrt{1-|\rho_e|}$ and the correlation coefficient can be

numerically calculated from the scattering parameters as [43]:

$$\rho_e = \frac{|S_{11}^* S_{12} + S_{21}^* S_{22}|^2}{(1 - |S_{11}|^2 - |S_{21}|^2)(1 - |S_{22}|^2 - |S_{12}|^2)} \tag{4.2}$$

When the diodes are "ON" or "OFF", the numerically calculated value of the ECC for our proposed UWB diversity antenna from the measured S-parameters is below -20 dB across the entire bandwidth except the band which is rejected, as shown in Figure 42. Since the correlation value of our proposed antenna system is very low, it guarantees good diversity performance over the entire bandwidth. The ECC has also been calculated using the far-field radiation patterns as explained in [43], for isotropic, indoor and outdoor environments and its value was found to be less than 0.5, except for the rejected band when the diodes are "ON".

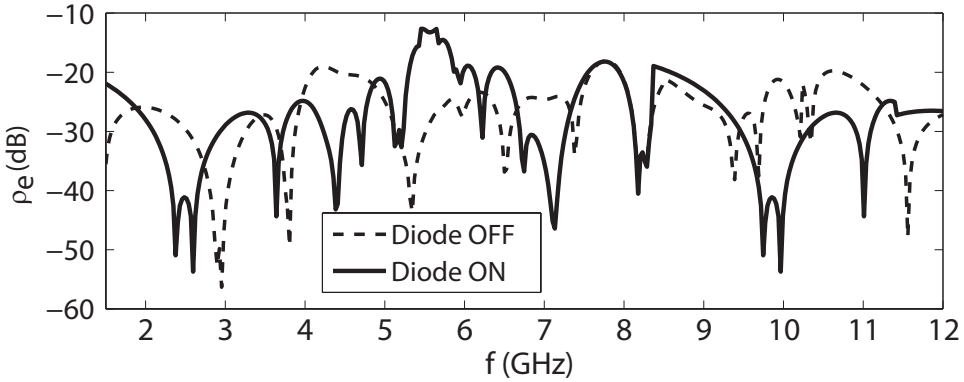

Figure 42: Numerically calculated envelop correlation coefficient from measured S-parameters. Reprinted from [P.9].

4.3. Four Elements Ultra wide-band (UWB) Multiple-Input Multiple-Output (MIMO) Antenna with On-demand WLAN Rejection

4.3.1. Introduction

In high speed wireless communication technologies such as, wireless personal area networks, UWB MIMO antennas have been considered to be an integral part of the communication system. However, WLAN signals (in the 5.15-5.35 and 5.75-5.8225

GHz bands) may interfere with those of UWB (3.1-10.6 GHz) technology and causing detrimental effects. So, for this reason designers have used different techniques in band-reject UWB or UWB-MIMO antennas [7]-[15]. In [7], slots have been used in the radiator to get the dual band notched characteristics, while in [8] a pair of slits has been inserted in the radiators to achieve the band-notch functionality. Moreover related works in [13]-[15] involve insertion of stubs to reject the WLAN bands and introduction of the polarization diversity to improve the isolation amongst the elements. An electromagnetic bandgap (EBG) structure has also been implemented to reject the WLAN band along with the band-stop filter for coupling suppression in [11]. Rejection of WLAN band has been implemented using a short stub and parasitic meander lines were inserted to reduce the mutual coupling in [10]. In [12], different types of resonators were used to attain the band notch functionality and also polarization diversity between nearly placed elements was exploited to attain high isolation. Another technique in [9], involves the insertion of stubs in the ground plane to mitigate the interference between the UWB and WLAN bands. Moreover, a $\lambda/2$ length of open stub has also been used on the ground plane ($55 \times 86.5\ mm^2$) of the antenna having a large reflector size [10]. Generally, previous works dealing with the band rejection either emphasized on rejecting the multiple bands or a portion of the band only permanently. Also, most of the designs in the literature focus on the band rejection feature of two elements UWB MIMO antennas.

In this work, a four elements frequency reconfigurable UWB MIMO antenna shown in Figure 43 is proposed for the on-demand band rejection. Two UWB monopole radiators in the proposed structure have rectangular slot whereas the others have circular slots. The ground plane of all the four radiators is shared using a rectangular shortening strip, as shown in Figure 43(b). In the proposed design, high isolation between the elements was achieved by exploiting the polarization diversity

between nearly placed elements. The on-demand band rejection is achieved by using the PIN diodes which connect the shared ground plane with the band-stop design. The detailed description of the design, and simulated and measured results will be discussed in the following sections.

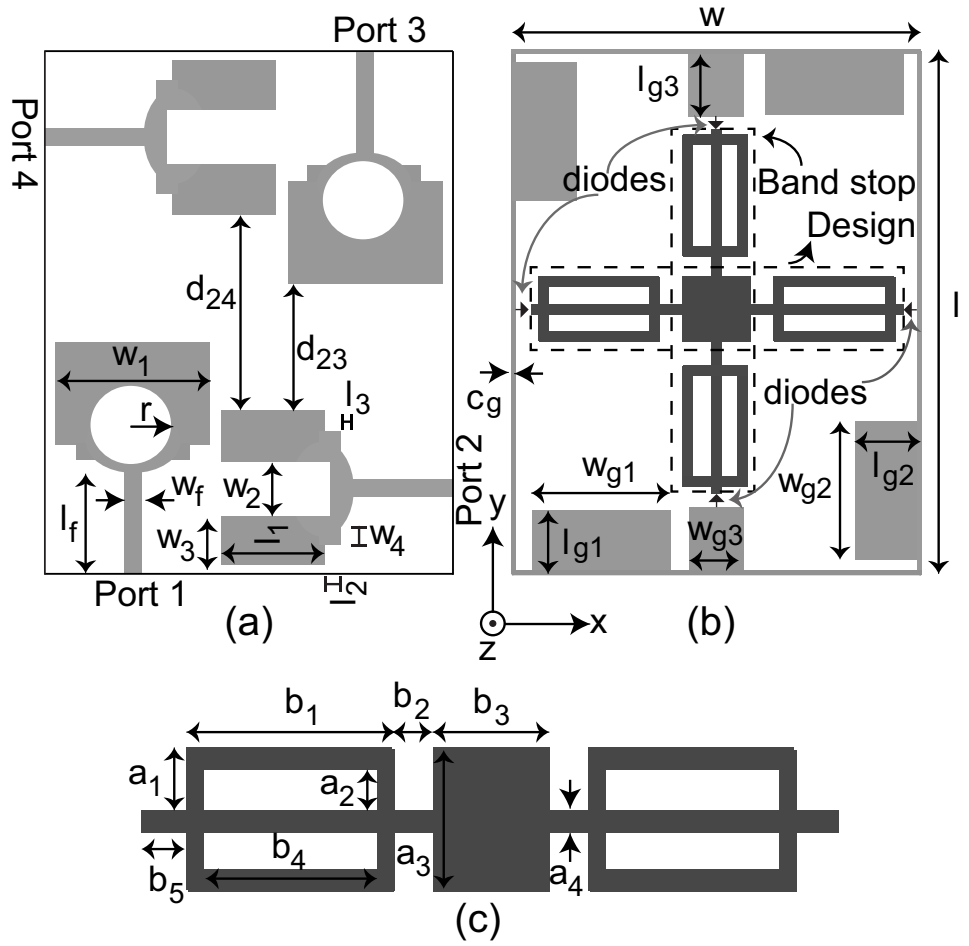

Figure 43: Geometry of the proposed UWB-MIMO antenna. (a) Top view (b) bottom view and (c) band-stop design. Optimised dimensions in millimetres are: $w = 39.8,\ l = 50,\ w_1 = 15,\ w_2 = 5,\ w_3 = 5,\ w_4 = 2.26,\ l_1 = 10,\ l_2 = 15,\ l_3 = 1.1,\ w_f = 1.5,\ l_f = 9.85,\ d_{23} = 12,\ d_{24} = 18.95,\ w_{g1} = w_{g2} = 13.5,\ w_{g3} = 5,\ l_{g1} = l_{g2} = 6.25,\ l_{g3} = 5.1,\ c_g = 0.5,\ a_1 = 2,\ a_2 = 1,\ a_3 = 5,\ a_4 = 1,\ b_1 = 13.7,\ b_2 = 1.7,\ b_3 = 5,\ b_4 = 11.7$ *and* $b_5 = 0.5$. Reprinted from [P.1].

4.3.2. Antenna Geometry

The detailed geometry of the proposed design is shown in Figure 43. Two U-shaped slot monopole radiators and two circular slot monopole radiators with tapered

section feeding are shown in Figure 43. One U-shaped slot radiator was placed orthogonally to the circular slot radiator at a distance of 1 mm. Similarly, the second U-shaped slot radiator was placed perpendicular to the other circular slot radiator at a same distance. These slots had been used to improve the broadband matching. The placement is chosen in such a way that there exists broadband matching characteristic, polarization diversity, and high isolation. Later on, the ground planes of all these radiators were connected through a shortening strip of $c_g = 0.5$ mm width. A small change in the return loss and isolation was observed. But the impedance matching in the 2.7 to 12 GHz frequency range was achieved. A small patch of size $l_{g3} \times w_{g3}$ was also connected with the ground plane so that a symmetrical design of band-stop design could be attached to the ground plane to reject the WLAN band. Next, on the bottom side of the proposed structure a band stop design is inserted and the length of the band stop design is determined using the formula:

$$L_{b1} = \frac{\lambda}{2} = \frac{c}{2f_o \cdot \sqrt{\epsilon_r}} \tag{4.3}$$

where $f_o = 5.5$ GHz is the central frequency of the rejected band and ϵ_r is the relative permittivity of the substrate. The stubs in the band stop design act as an inductor whereas, gaps between the stubs act as a capacitor. When diodes are biased, the band-stop design act as a LC band-stop resonator having an additional inductance of the PIN diode whereas, in the diodes unbiased states additional capacitance stemming from the diodes prevents the on-demand WLAN rejection. Thus, the overall structure can be thought as an equivalent band stop filter. The surface current distribution of the band-stop design with the four PIN diodes in the biased and unbiased states is shown in Figure 44, when port 1 was excited at 5.5 GHz. It can be seen from the Figure 44(b) that a very little current is induced on the stop-band design through coupling when all four diodes are unbiased,

while a strong flow of the current can be seen from the stop-band design when all diodes are biased as shown in Figure 44(d), providing the on-demand rejection in the WLAN band. It can also be seen in Figure 44(d) that the most of the current is passed through the band-stop design which is closer and along the direction of the element 1. Similarly when other port is excited, the current passes through the section of band-stop design which is near to that port and rejects the WLAN band.

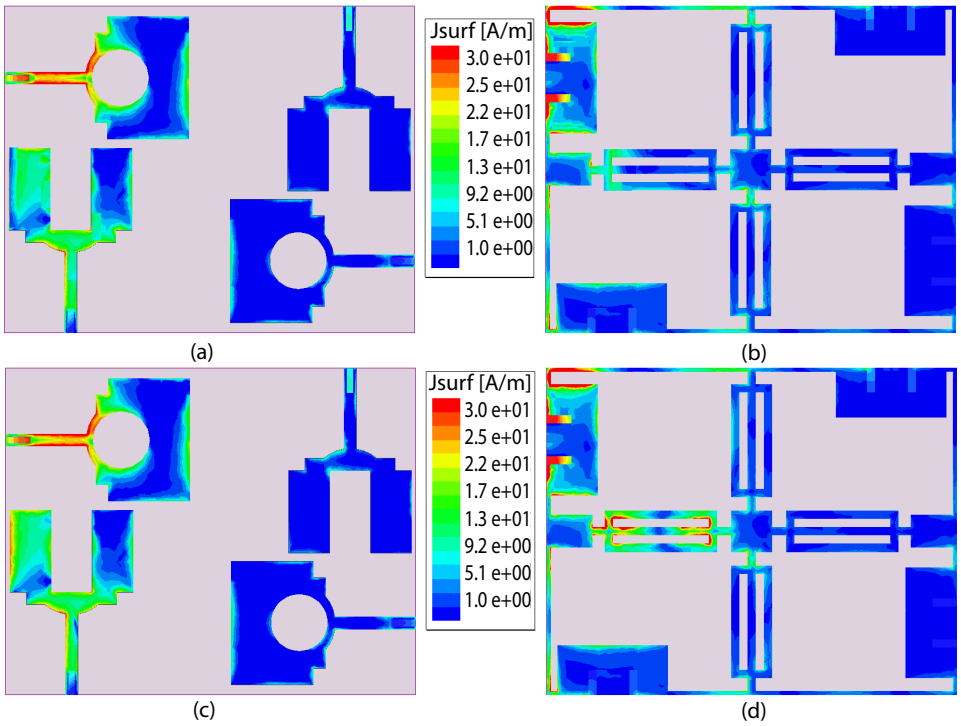

Figure 44: Simulated surface current distribution at 5.5 GHz, when port 1 is excited for the unbiased state. (a) Top view (b) bottom view, for the biased state (c) top view and (d) bottom view. Reprinted from [P.1].

4.3.3. Fabrication of the Prototype

A prototype of the layout in Figure 43 was fabricated on a 1.524 mm thick Rogers TMM4 substrate ($\epsilon_r = 4.5$, $tan\delta = 0.002$) to demonstrate the functionality of the proposed structure. The fabricated prototype is shown in Figure 45.

The band stop design having stubs is connected to the shared ground plane

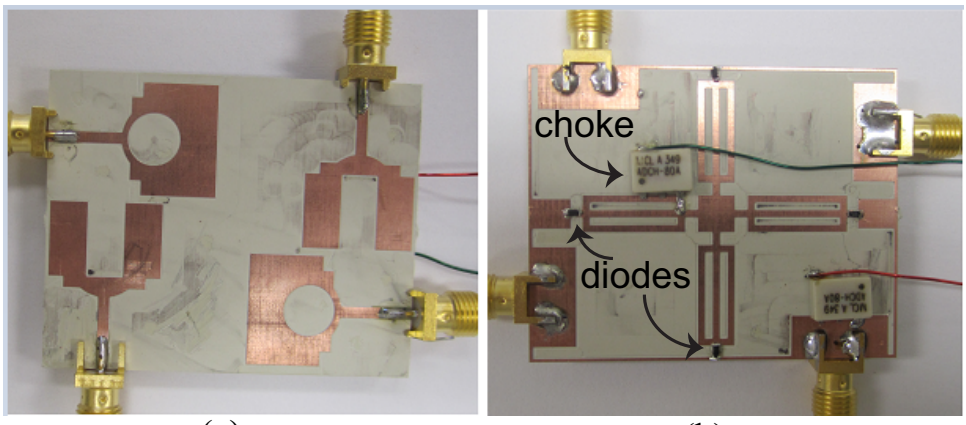

Figure 45: (a) Top view of the fabricated prototype and (b) bottom view of the fabricated prototype. Reprinted from [P.1].

via surface mount voltage controlled PIN diodes and RF chokes are used for biasing the RF current and DC current. These diodes are designed in HFSS [36] using the guidelines explained in chapter 3. Furthermore, effects of the diodes and biasing circuitry on the S-parameters and performance of the proposed structure were studied by fabricating the prototype and discussed in the following section.

4.3.4. S-parameters

The reflection coefficient and isolation for the four diodes in biased state (i.e. band stop design physically connected to the ground) and unbiased states (i.e. the band stop design disconnected from the shared ground plane) were measured using a calibrated Agilent N5242A PNX-A network analyzer. To minimize the current travelling on the outer conductor and the associated parasitic radiations, the prototype was fed with a semi-rigid cable surrounded by ferrite-beads. Figure 46(a) shows the comparison between simulated and measured reflection coefficients while Figure 46(b) shows the measured isolation; the results were obtained when the PIN diodes were in unbiased states. The comparison of simulated reflection coefficients with the measured is shown in Figure 47(a) while measured isolation is shown in Figure 47(b) for the PIN diodes biased states. Overall good agreement between the simulated

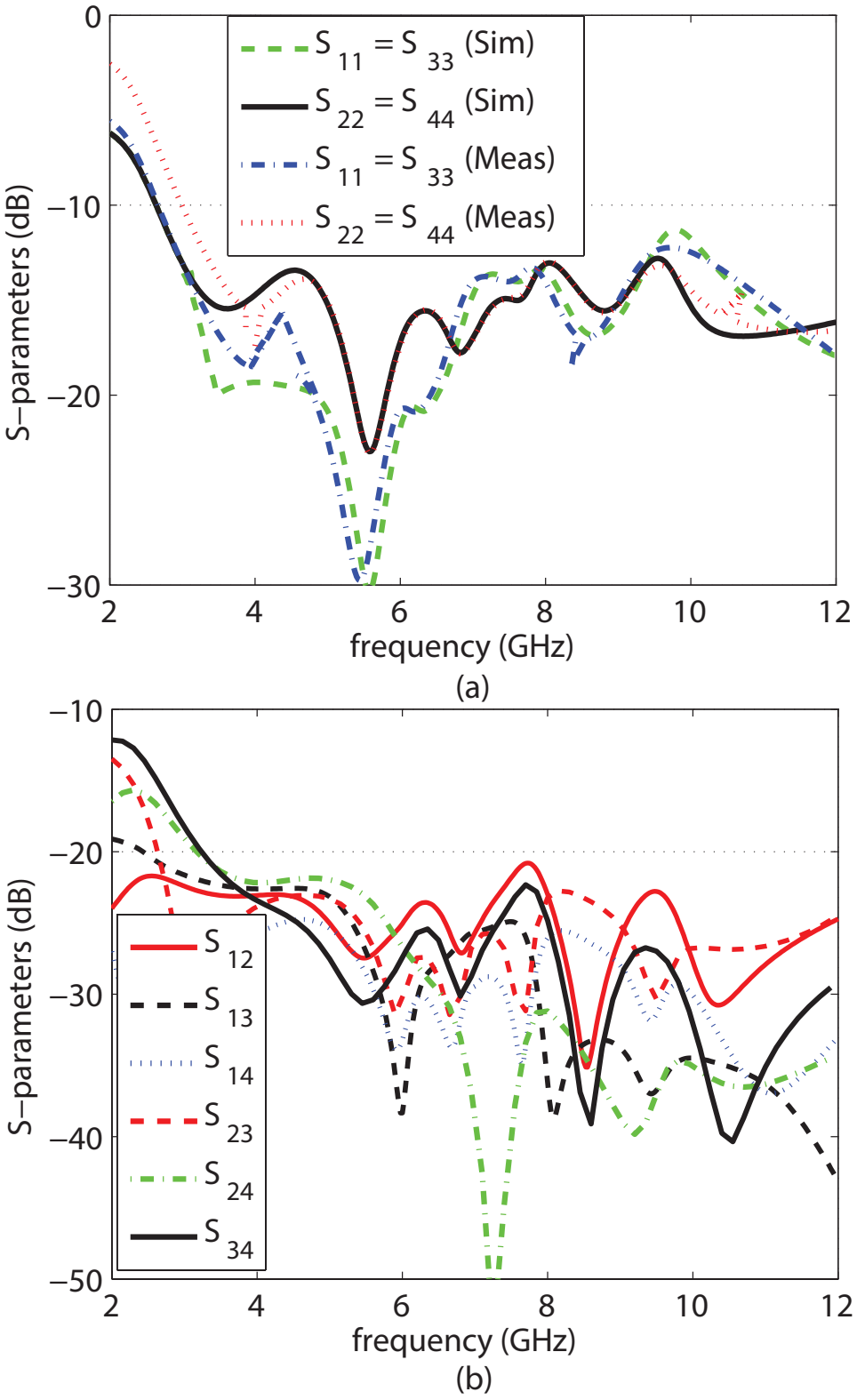

Figure 46: Simulated and measured S-parameters of antenna for the PIN diodes unbiased states. (a) Simulated and measured S_{11} and S_{22} and (b) measured mutual coupling. Reprinted from [P.1].

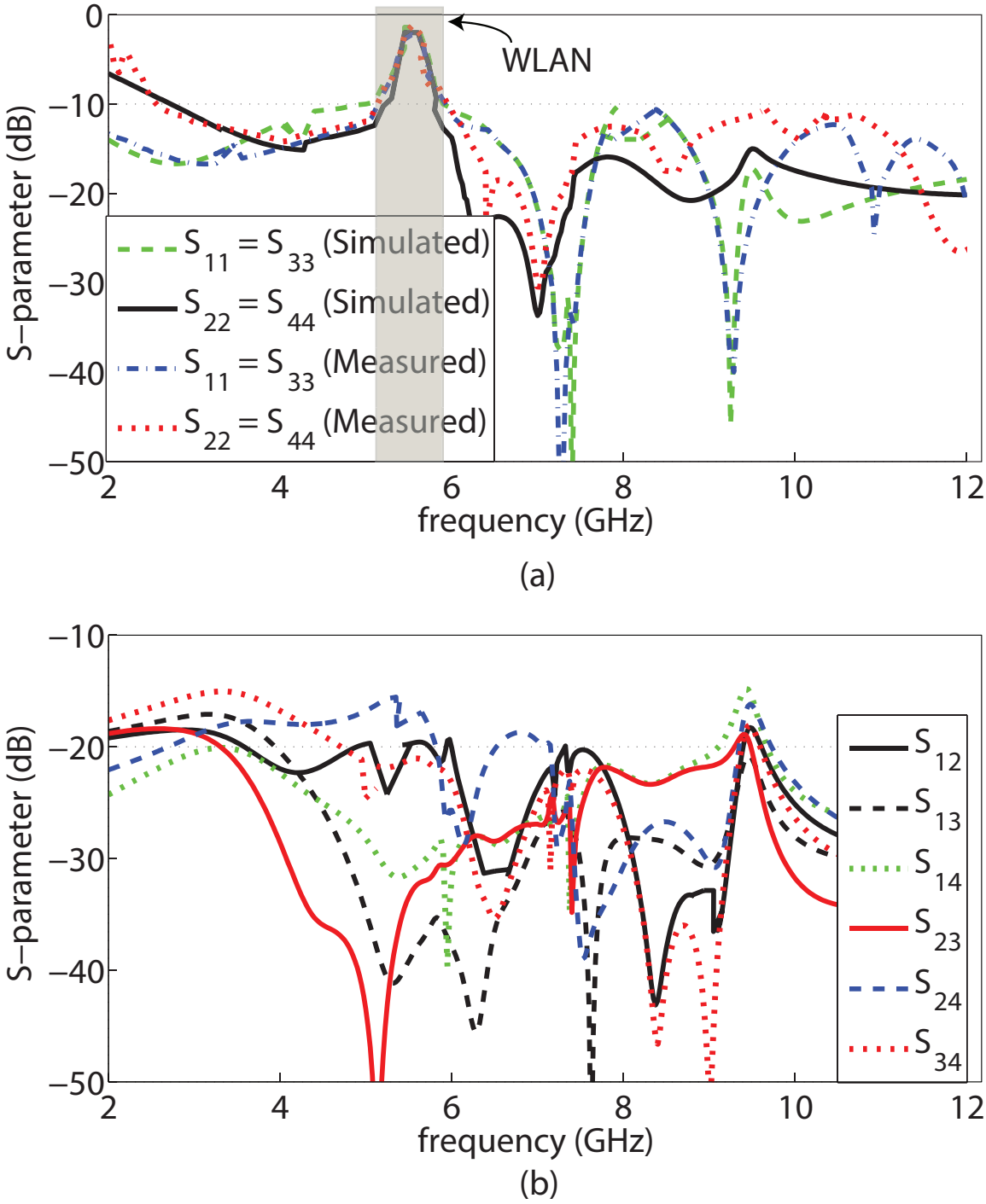

Figure 47: Simulated and measured S-parameters of antenna for the PIN diodes biased states. (a) Simulated and measured S_{11} and S_{22} and (b) measured mutual coupling. Reprinted from [P.1].

and measured results was observed, indicating that the lumped components have not any significant effects on the S-parameters up to 12 GHz. For sake of clarity only measured isolation results are plotted in Figure 46(b) and Figure 47(b). Moreover, the isolation between the radiators is found higher than 17 dB in all cases. The four PIN diodes have sixteen possible states but for sake of brevity only the results of ON-ON and OFF-OFF states are plotted in Figures 46-47.

4.3.5. Radiation Patterns and Gain

Next, the radiation patterns of the proposed four elements UWB MIMO antenna were measured in an anechoic chamber for both the unbiased and biased states. Figure 48 shows the patterns in the x-z and y-z planes at 3, 5.8, and 9.2 GHz when the diodes are in unbiased states whereas, Figure 49 shows the patterns in the diodes biased states. The port 1 was excited during the measurements while port 2, 3 and 4 were terminated using 50 Ω loads. In Figure 49 the intensity of the patterns at 5.5 GHz is lower than in the Figure 48 because of the rejected band. Since polarization diversity is employed in the proposed structure, the patterns of element 1 and element 3 in the x-z and y-z are observed almost identical to the element 2 and element 4 in the y-z and x-z planes, respectively. Figures 50 and 51 show the peak gain of the proposed UWB diversity antenna in the unbiased and biased states, respectively. Note that the antenna radiation intensity in the rejected WLAN band is smaller in all directions in the diodes biased states and its gain is less than 6 dBi as shown in Figure 51.

Since the proposed antenna is for MIMO applications, it must be characterized for the diversity performance. Diversity performance of an antenna system can be evaluated by using the envelope correlation coefficient (e), according to [44]: Using eqn. (5) of [44], the envelope correlation between the antenna elements i and j in the (N, N) MIMO system can be calculated. In the case of i = 1, j = 2, and N =

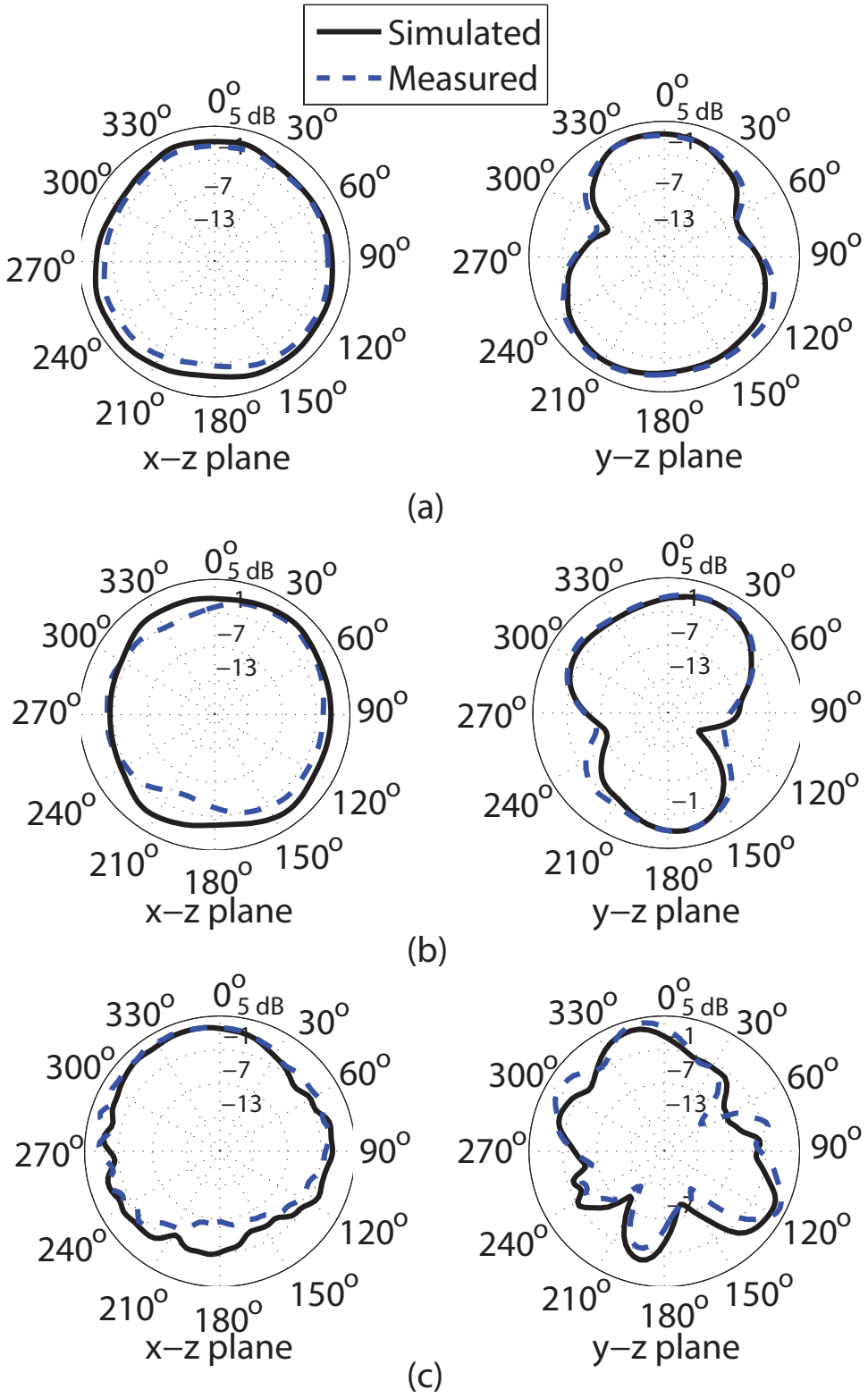

Figure 48: Simulated and measured radiation patterns of the proposed antenna for the PIN diodes unbiased states, only port 1 was excited (a) 3 GHz, (b) 5.5 GHz, and (c) 9 GHz. Reprinted from [P.1].

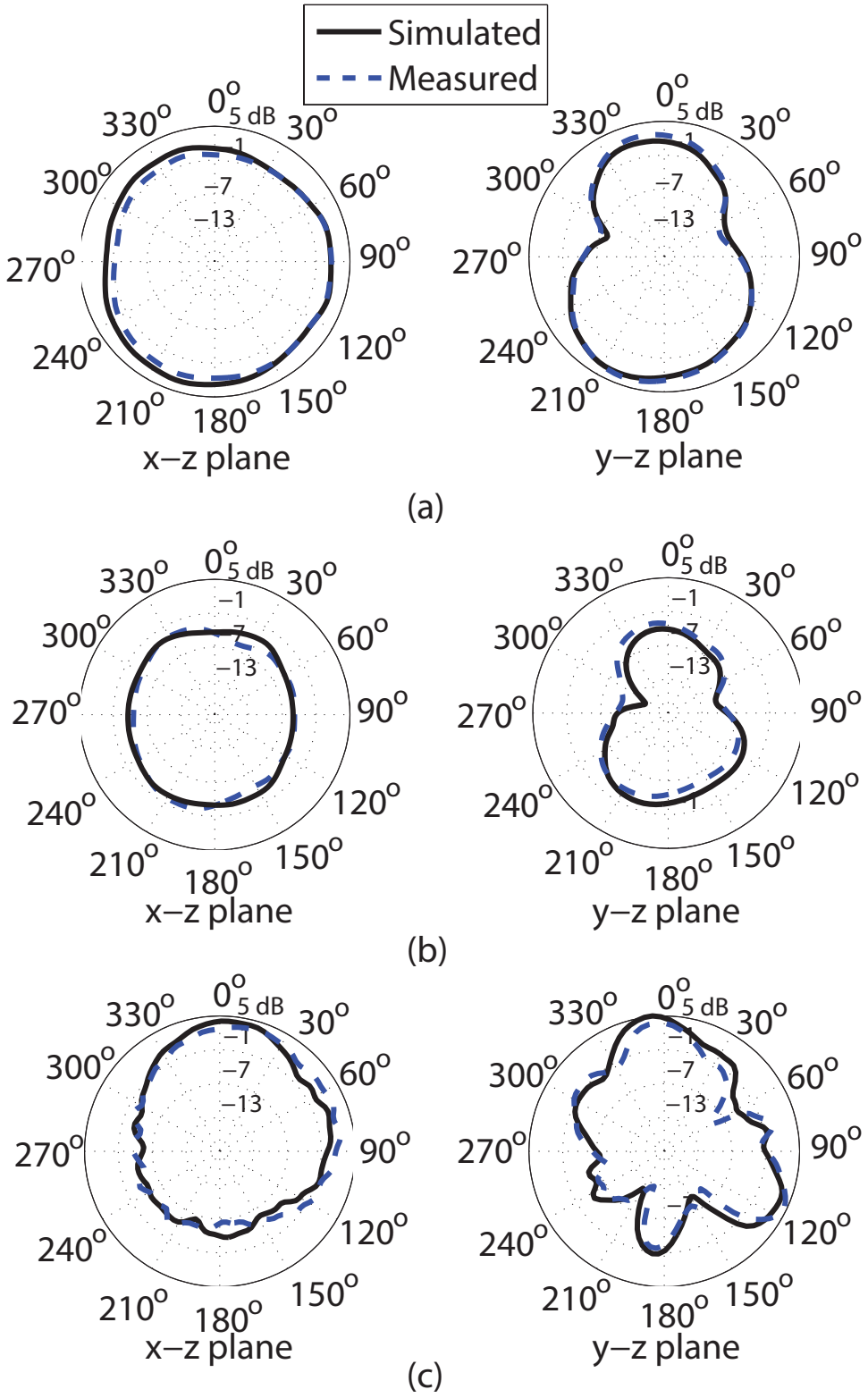

Figure 49: Simulated and measured radiation patterns of the proposed antenna for the PIN diodes biased states, only port 1 was excited (a) 3 GHz, (b) 5.5 GHz, and (c) 9 GHz. Reprinted from [P.1].

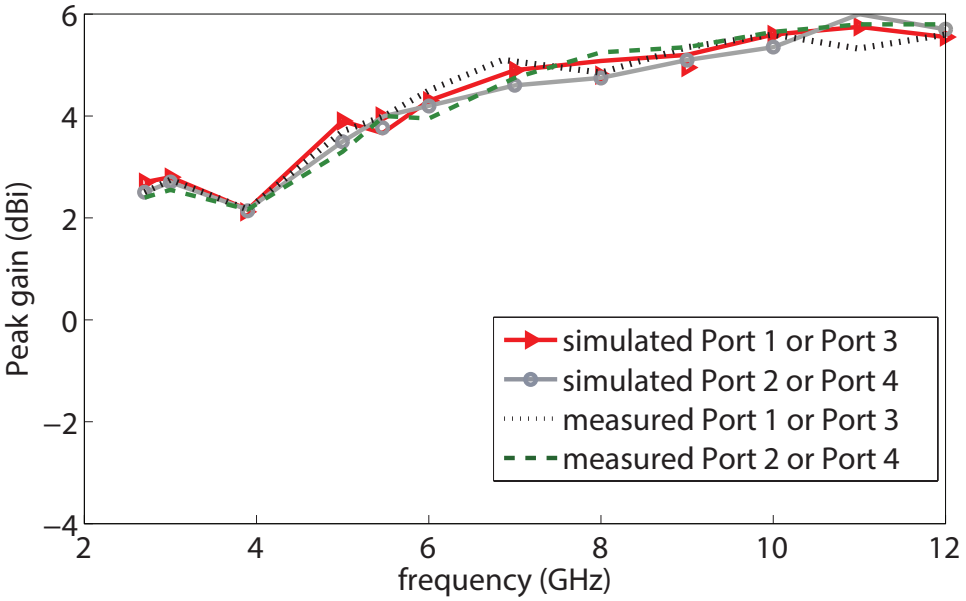

Figure 50: Simulated and measured peak gain of the proposed antenna for the PIN diodes unbiased states over complete radiating band. Reprinted from [P.1].

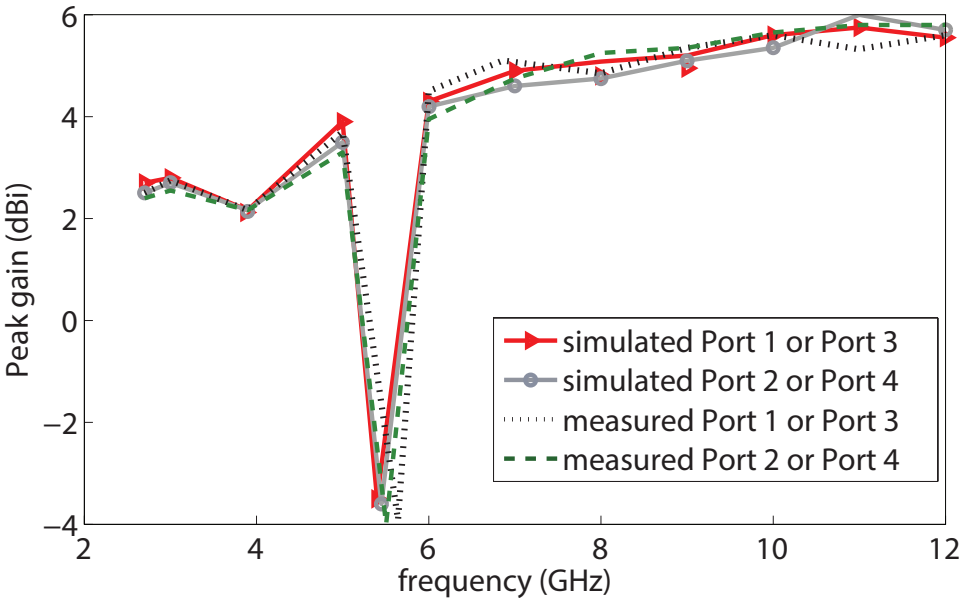

Figure 51: Simulated and measured peak gain of the proposed antenna for the PIN diodes biased states over complete radiating band. Reprinted from [P.1].

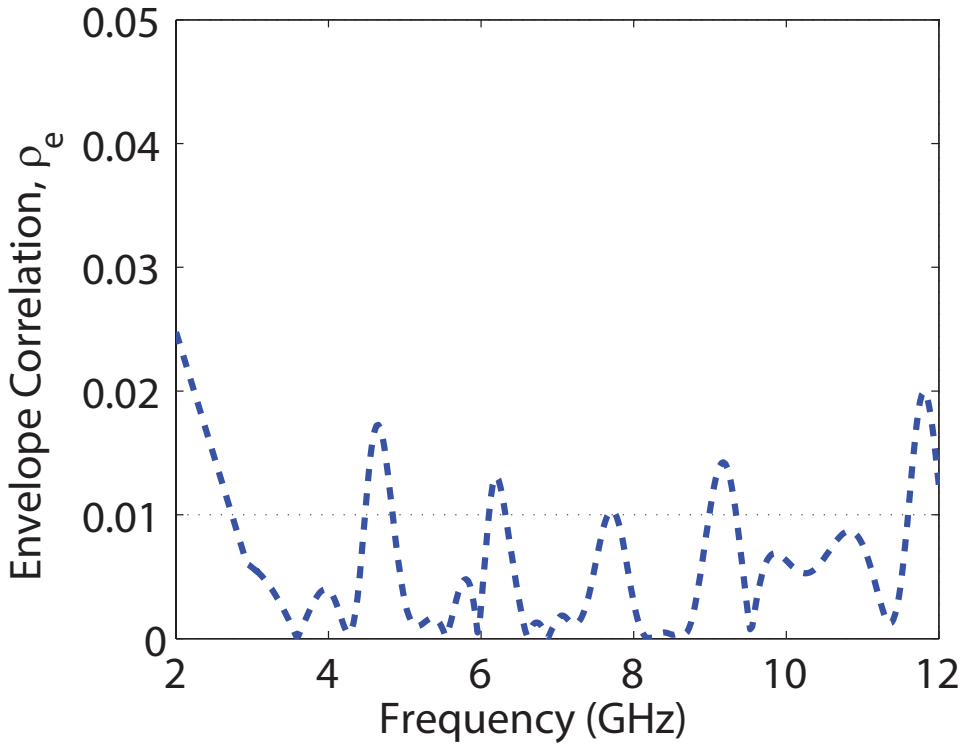

Figure 52: Numerically calculated ECC from the measured S-parameters. Reprinted from [P.1].

4, the envelope correlation of the proposed MIMO antenna is computed and shown in Figure 52. The computed value of ECC for the proposed MIMO antenna from measured S-parameters is below 0.025 across the entire bandwidth. The correlation value of the proposed antenna system is very low, which guarantees good diversity performance over the entire bandwidth.

4.4. Frequency Reconfigurable Self-Adapting Conformal Array

4.4.1. Introduction

As the applications of modern wireless communication systems grow, the antenna requirements become evermore complex. Some of these requirements include load-bearing capabilities [45]-[46], wearable functionality [47]-[52], vibration tolerances [53]-[54] and extreme environmental immunity [55]. To meet some of these challenges, designers have turned to the development of conformal antennas [29],[56]-

[61]. However, one of the drawbacks of using conformal antennas to meet some of the aforementioned requirements is the unwanted radiation pattern distortion caused by the deformation of the surface on which the antenna is attached upon [61]-[62]. Fortunately, some preservation of the radiation pattern of a changing conformal antenna can be achieved by implementing mechanical [63]- [64] and electrical [26]-[29], [65]-[68], [69]-[70] compensation at a single frequency band into the design.

In addition to conformal antennas, frequency reconfigurable antennas are being used by wireless platforms to increase coverage and access multi-band provider services such as GPS, Bluetooth, 3G, WiMax, WiFi and UWB services [71]-[75]. By using a reconfigurable antenna, a designer can avoid the implementation of multiple antennas in a device and use the additional benefit of the resonant frequency of the antenna to avoid complicated and expensive multi-band filtering [71]. However, much of the development of reconfigurable antennas, with the exception of the work in [76], has been limited to single element antennas on planar and conformal surfaces.

In this work, the benefits of self-adapting conformal antennas and reconfigurable antennas are combined into one design. In particular, the objective of this communication is to present the autonomous self-adapting capabilities of the frequency reconfigurable conformal array shown in Figure 53(a) on a changing wedge- and cylindrical-shaped conformal surface. The antenna array consists of reconfigurable microstrip patch antennas each individually connected to voltage controlled phase shifters with identical SMA cables. SMA cables were chosen to allow for the antenna elements to be placed on various conformal surfaces. The phase shifters are then connected to the ports of a 4-way power combiner. The wedge- and cylindrical-shaped surface deformation is then measured by the reconfigurable sensing circuit shown in Figure 53(b). The circuit then in turn provides an output voltage that drives the voltage controlled phase shifters to implement phase compensation. By

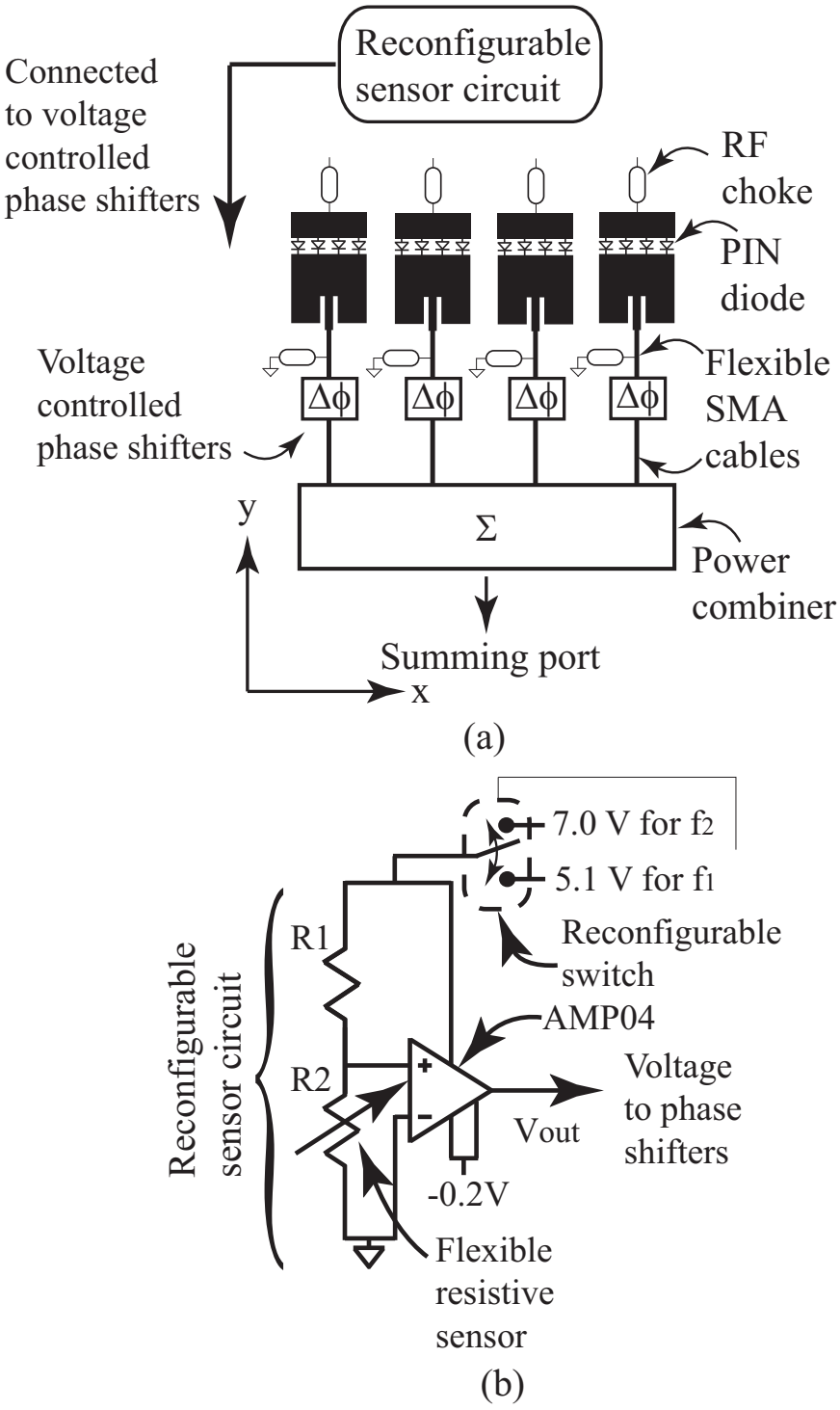

Figure 53: (a) Topology of the frequency reconfigurable self-adapting conformal antenna and (b) schematic of the reconfigurable sensing circuit used to control the voltage controlled phase shifters ($R_1 = 1.0\ M\Omega$, $R_{gain} = 4.0\ K\Omega$ - connected between pins 1 and 8).

choosing the appropriate circuit design, the array in Figure 53(a) can autonomously preserve the radiation pattern in both frequency reconfigurable bands using phase compensation (i.e., electrical compensation).

With the development of this new antenna, designers will be able to develop wireless communication systems for much more complicated and compact structures. For example, the antenna could be directly integrated into the enclosure of a multi-band multi-radio device and the requirement of having multiple antennas on flat surfaces could be removed.

Finally, for this work, it was assumed that the direction of maximum radiation was fixed in both frequency reconfigurable operating bands. This then requires the phase-compensation circuitry to operate correctly in both bands.

4.4.2. Theoretical Background on Wedge-shaped Surfaces

To determine the amount of phase-compensation required, the problem in Figure 54 is considered. The problem consists of four antenna elements, denoted as $A_{\pm n}$ where $n = \pm 1, \pm 2$, on a wedge-shaped conformal surface with a bend angle θ_b. For this work, it is assumed that the direction of maximum radiation is along the z-axis (or $\phi_s = \pi/2$) and the inter-element spacing along the surface of the wedge is fixed at L. One method to ensure that radiation is along the z-axis in Figure 54 is to add a phase shift to elements $A_{\pm 2}$ such that the fields from these elements arrive at the reference plane with the same phase as the fields radiated from elements $A_{\pm 1}$. This then results in a broadside radiation to the reference plane. To determine the amount of phase required on elements $A_{\pm 2}$, the distance Δz_w in Figure 54 from the elements to the reference plane must be computed [29]. Then, Δz_w can be used in the following equation to compute the amount of phase required to cancel the phase introduced by the free-space propagation from the elements $A_{\pm 2}$ to the reference plane [29]:

$$\Delta\phi_{\pm 2} = k\Delta z_w \tag{4.4}$$

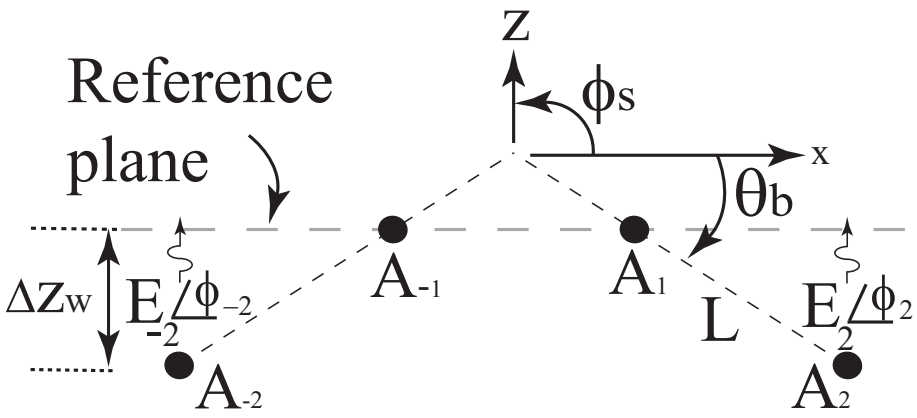

Figure 54: An illustration of a 1×4 array on a wedge-shaped conformal surface with a bend angle θ_b.

where $\Delta z_w = L|n|sin\theta_b$, $0 \leq \theta_b \leq \pi/2$, $(x_{\pm 2},\ z_{\pm 2})$ is the location of the $A_{\pm 2}$ element, respectively, and k is the free space wave number. Notice that the value of eqn. (4.4) is positive to cancel the negative phase introduced by the free-space wave propagation. Next, since the values of eqn. (4.4) depend on frequency, two expression will be defined (one for each operating band). If the lower operating band is f_1 and the upper operating band is f_2, then the associated wavelengths at these frequencies are denoted as λ_1 and λ_2, respectively. This then gives $k_1 = 2\pi/\lambda_1$ and $k_2 = 2\pi/\lambda_2$. Using this notation in eqn. (4.4) gives the following equations:

$$\Delta\phi_{\pm 2}^{w1} = k_1 \Delta z_w \tag{4.5}$$

and

$$\Delta\phi_{\pm 2}^{w2} = k_2 \Delta z_w \tag{4.6}$$

where the superscript is used to denote the phase compensation required in operating bands f_1 and f_2, respectively, on the wedge-shaped surface.

4.4.3. Theoretical Background on Cylindrical-shaped Surfaces

In a manner similar to the wedge-shaped surface, expressions for the phase-

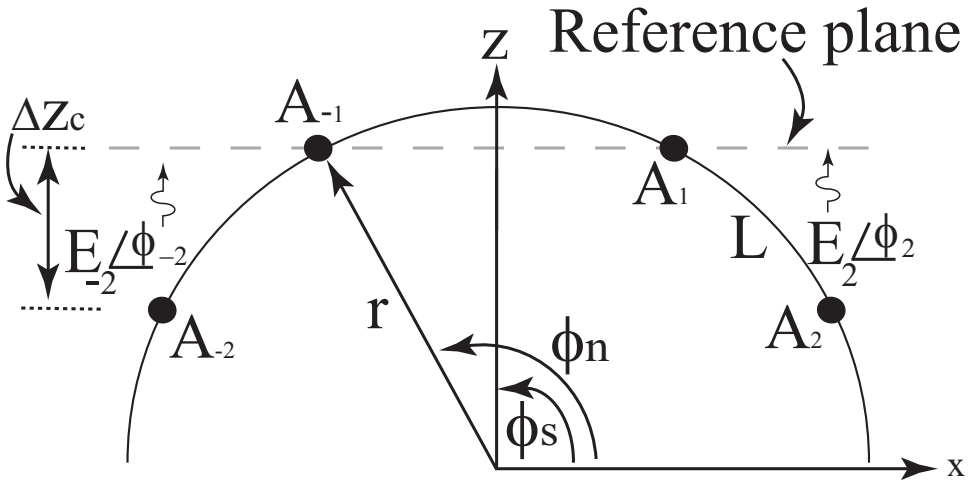

Figure 55: An illustration of a 1×4 array on a cylindrical-shaped conformal surface with a radius r.

compensation will be presented for the four-element array on a cylindrical surface with radius r. The problem being considered is shown in Figure 55 and again the inter-element spacing along the cylindrical surface is fixed at L, and the elements that require the phase-compensation are denoted as $A_{\pm 2}$. Next, it can be shown that Δz_c can be computed as [29]:

$$\Delta z_c = r|sin(\phi_n) - sin(\phi_{n-1})| \tag{4.7}$$

where ϕ_n is defined in Figure 55. This then gives:

$$\Delta\phi_{\pm 2}^{c1} = k_1 \Delta z_c \tag{4.8}$$

and

$$\Delta\phi_{\pm 2}^{c2} = k_2 \Delta z_c \tag{4.9}$$

Again, the superscript is used to denote the phase compensation required in operating bands f_1 and f_2, respectively, on the cylindrically-shaped surface.

In summary equations (4.5)-(4.6) and (4.8)-(4.9) are the required phase-compensation values in both of the operating bands f_1 and f_2 for the wedge- and cylindrical-shaped surfaces, respectively. This now allows the theoretical computations required to develop a frequency reconfigurable self-adapting conformal antenna. Next, a prototype sensing circuit that is frequency reconfigurable and used to implement the self-adapting conformal array is presented.

4.4.4. Development of Frequency Reconfigurable Sensing Circuit

The overall role of the sensing circuitry is to measure the deformation of the wedge- and cylindrical-shaped surface on which the conformal antenna is attached upon and use this information to introduce the appropriate phase-compensation (in both bands) to elements $A_{\pm 2}$ to radiate along the z-axis as the surface changes shape. Thus, this part of the antenna design is key to enabling the development of a self-adapting reconfigurable conformal array. Another way to think about the sensing circuity is as a mapping between the shape (i.e., values of θ_b and r) of the wedge- and cylindrical-shaped conformal surfaces and $\Delta\phi_{\pm 2}$. To create this mapping an appropriate phase-shifter must be chosen. For this work, connectorized phase-shifters (part number: HMC928LP5E) manufactured by Hittite Microwave Corporation [77] were chosen, and the upper and lower operating frequencies were defined to be $f_1 = 2.43$ GHz and $f_2 = 3.15$ GHz, respectively. Next, a prototype circuit was manufactured and a picture of the reconfigurable sensing circuit is shown in Figure 56(a) and the measured output for various values of θ_b are shown in Figure 56(b). The resistive sensor used to measure the surface was manufactured by Spectra Symbol [78] and an AMPO4 instrumentation amplifier was used for the OpAmp. The results show that the sensing circuit can be reconfigured to measure the surface deformation

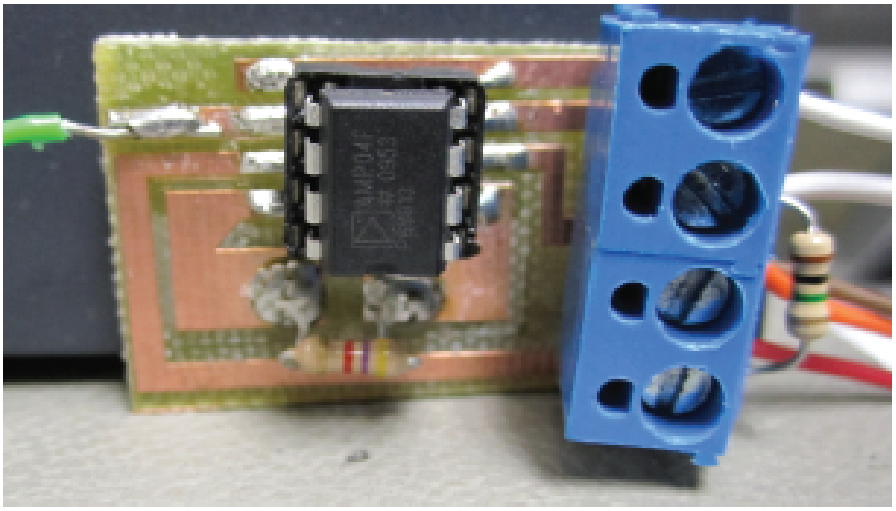

(a)

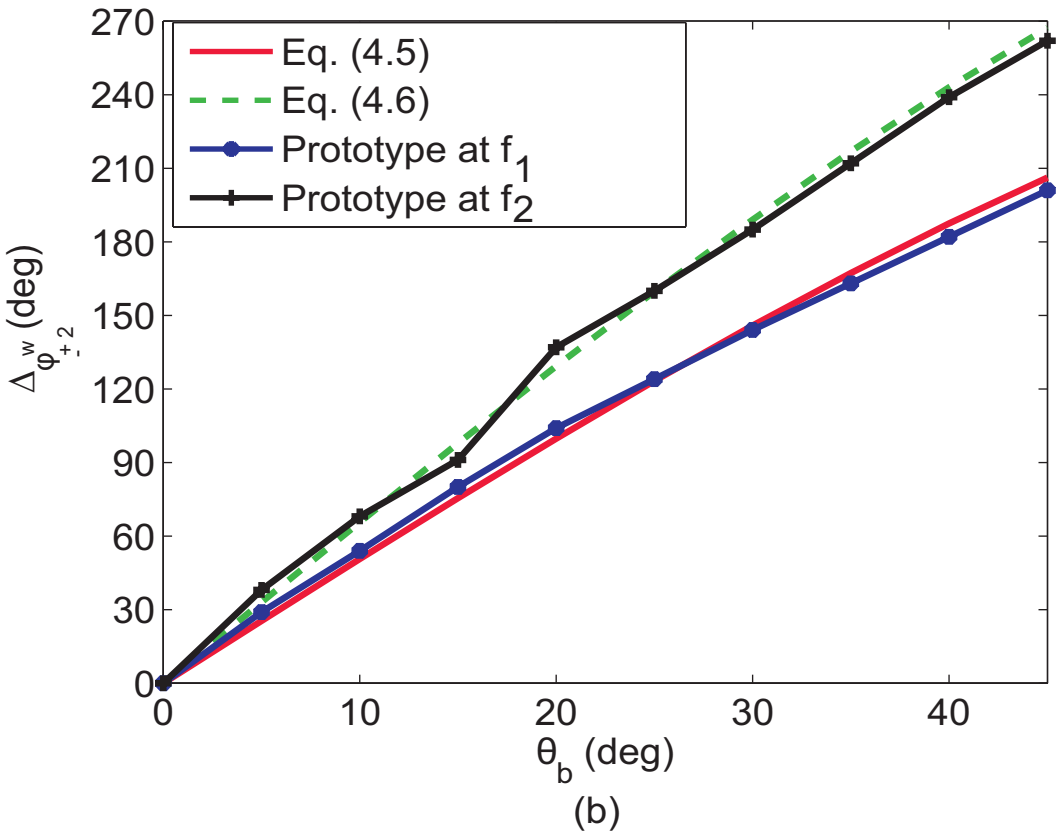

(b)

Figure 56: (a) A photograph of the prototype sensor circuit and (b) normalized phase shift values measured from the Hittite phase shifters and compared to the values determined by eqns. (4.5) and (4.6) for accuracy.

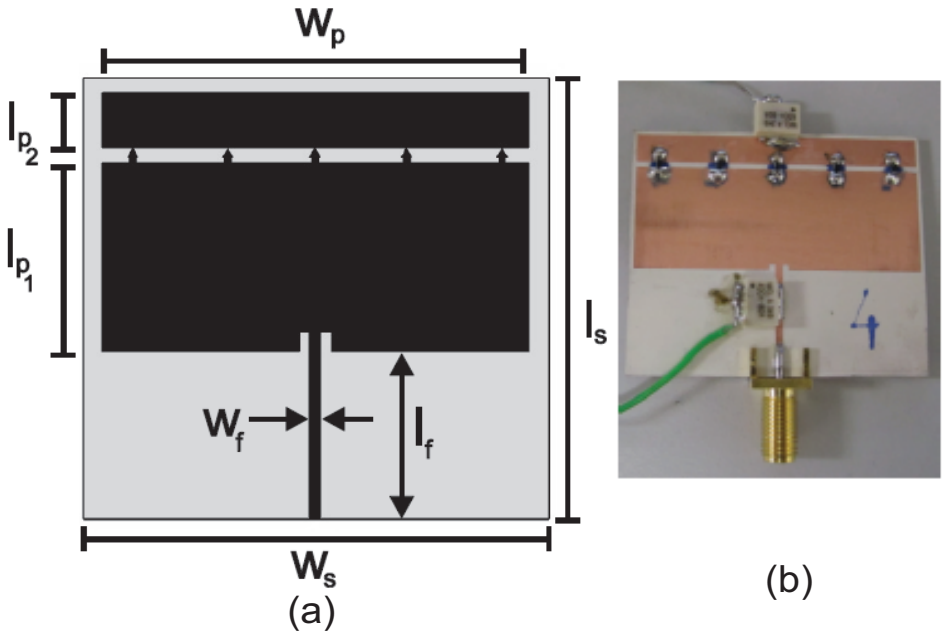

Figure 57: (a) Drawing of the frequency reconfigurable microstrip patch element in the 1×4 array and (b) photograph of the prototype element ($l_s = 42$ mm, $w_s = 50.5$ mm, $l_{p1} = 17.7$ mm, $l_{p2} = 4.8$ mm, $w_p = 49$ mm, $l_f = 17.6$ mm, $w_f = 1.3$ mm.

of a wedge at both frequencies. Similar agreement was also observed between the circuit and equations (4.8) and (4.9). In brief, the results in Figure 56(b) show that the prototype sensor circuit is operating correctly and can now be used in the development of a frequency reconfigurable self-adapting conformal antenna array, which is shown next.

4.4.5. Development of Antenna for Conformal Surfaces

To have the convenience of attaching the prototype array to various conformal surfaces, a topology that consists of four individual frequency reconfigurable microstrip patches was chosen. This avoided the need of finding a much larger flexible substrate to print the antennas on. A drawing with the dimensions of the reconfigurable patch is shown in Figure 57(a). The reconfigurable antenna switches between f_1 and f_2 by connecting the parasitic element to the top of the microstrip patch using PIN diodes. This connection makes the patch electrically larger and

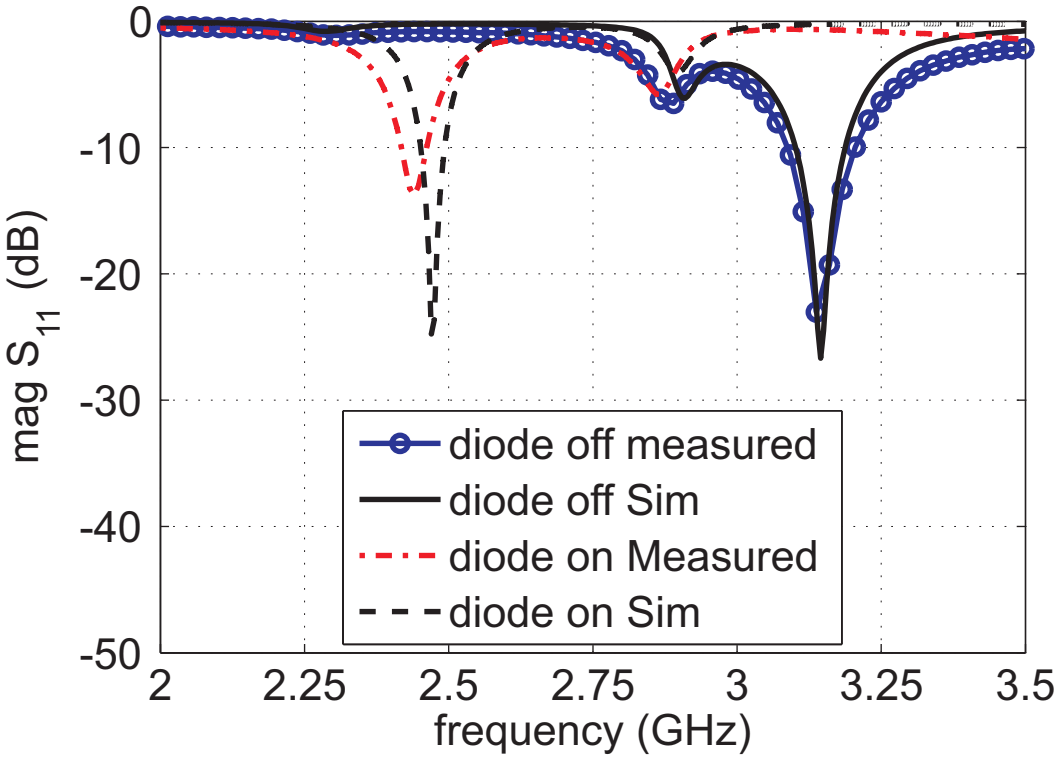

Figure 58: Measured and simulated S-parameter values for the single frequency reconfigurable patch in a full anechoic chamber.

reduces the operating frequency to f_1. The PIN diodes are biased through the RF chokes. Then, when the bias voltage is removed, the patch is electrically smaller and operates at f_2. To evaluate the performance of the individual patch design, the prototype in Figure 57(b) was designed, manufactured and tested in a full anechoic chamber. The antenna was simulated in HFSS [36] on a 1.524mm thick TMM4 Rogers Substrate [79]. The PIN diodes were purchased from Skyworks [34] (part number: SMP1322). The S-parameter results are shown in Figure 58 and it is shown that the patch is switching between f_1 and f_2. Next, the prototype array shown in Figure 59 (shown attached to the wedge-shaped conformal surface) was manufactured. This array consisted of four of the single frequency reconfigurable microstrip patches connected to four Hittite phase shifters through four identical SMA cables. The phase shifters were then connected to the port of a four-way power combiner (manufactured

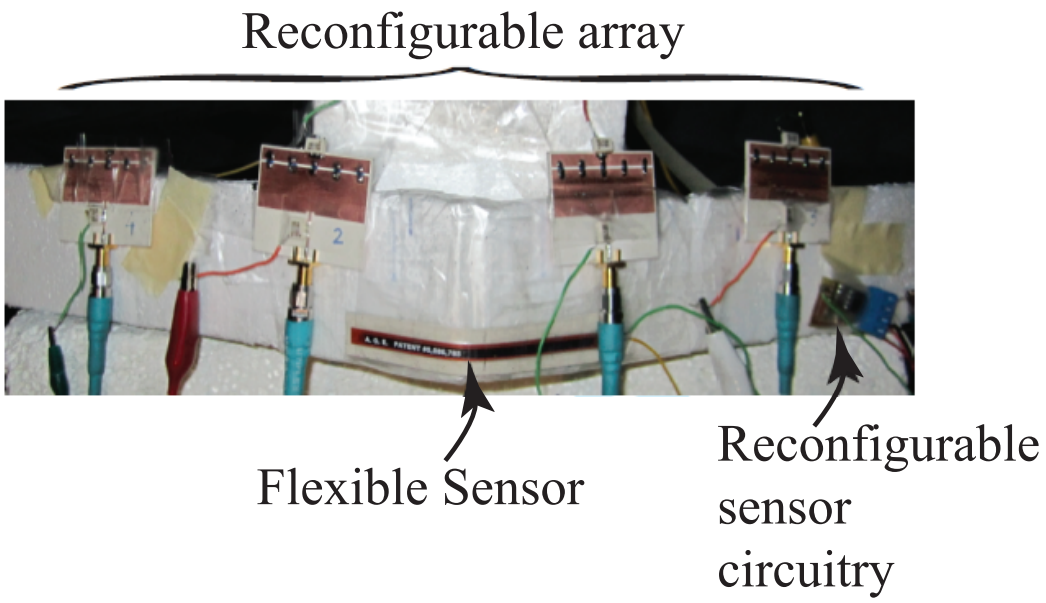

Figure 59: Photograph of the prototype array on the wedge-shaped conformal surface.

by Mini-circuits [35] with part number: WP4R+). Then, the reconfigurable sensor circuitry was connected to the voltage controlled Hittite phase shifters to create the frequency reconfigurable self-adapting conformal array.

4.4.6. Simulated and Measured Results

To validate the performance of the proposed reconfigurable self-adapting array, the wedge-shaped surface with the array attached was placed in a full anechoic chamber. The interelement spacing was $L_1 = 0.83\lambda_1$ and $L_2 = 1.0\lambda_2$. The pattern of the array was then measured at both f_1 and f_2 for $\theta_b = 30°$ and $45°$. The results from these measurements are shown in Figures 60-63. For validation, these measurements were compared to the analytical computations using the Array Factor expressions presented in [57]. Good agreement can be observed and self-adapting characteristics at both reconfigurable frequencies f_1 and f_2 are demonstrated. Next, the array was attached to a cylindrical-shaped surface with r = 16 cm and an inter-element spacing of $L_1 = 0.83\lambda_1$ and $L_2 = 1.0\lambda_2$. The results from these measurements are shown in Figures 64 and 65. Again, for comparison, these measurements were

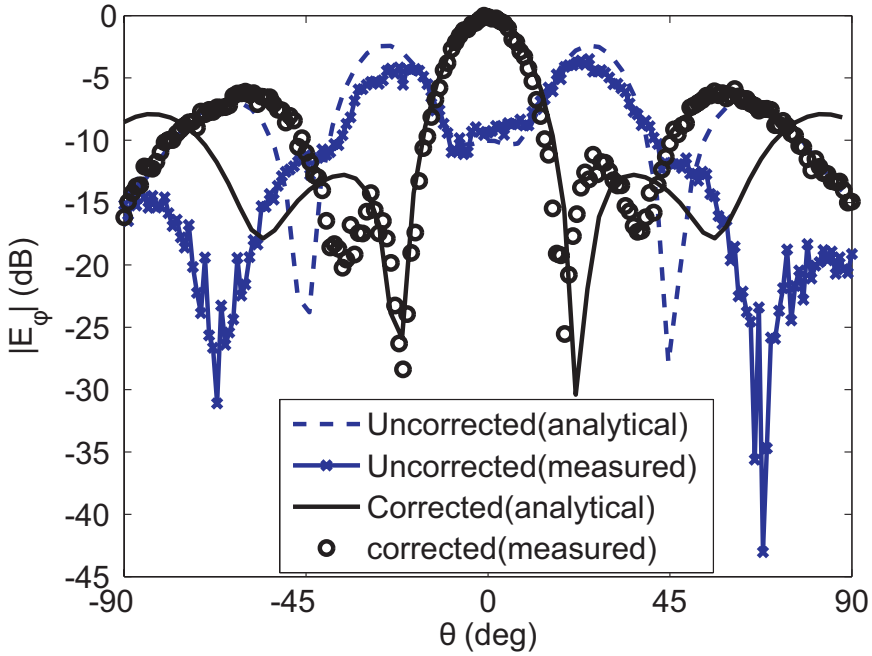

Figure 60: Analytical and Measured patterns of antenna array at 2.43 GHz (f_1) in the x-z plane for the wedge-shaped conformal surface with $\theta_b = 30°$.

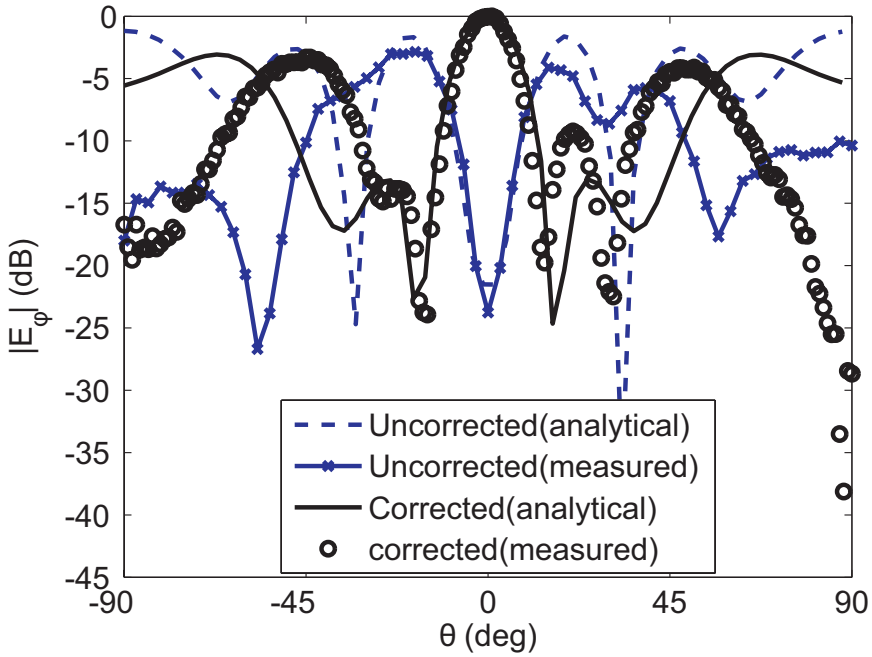

Figure 61: Analytical and Measured patterns of antenna array at 3.15 GHz (f_2) in the x-z plane for the wedge-shaped conformal surface with $\theta_b = 30°$.

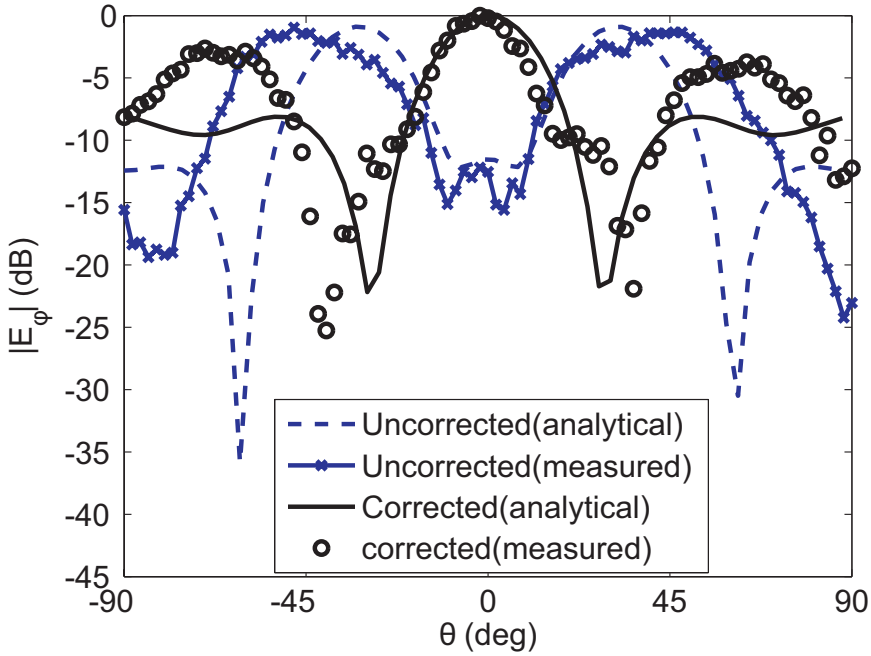

Figure 62: Analytical and Measured patterns of antenna array at 2.43 GHz (f_1) in the x-z plane for the wedge-shaped conformal surface with $\theta_b = 45°$.

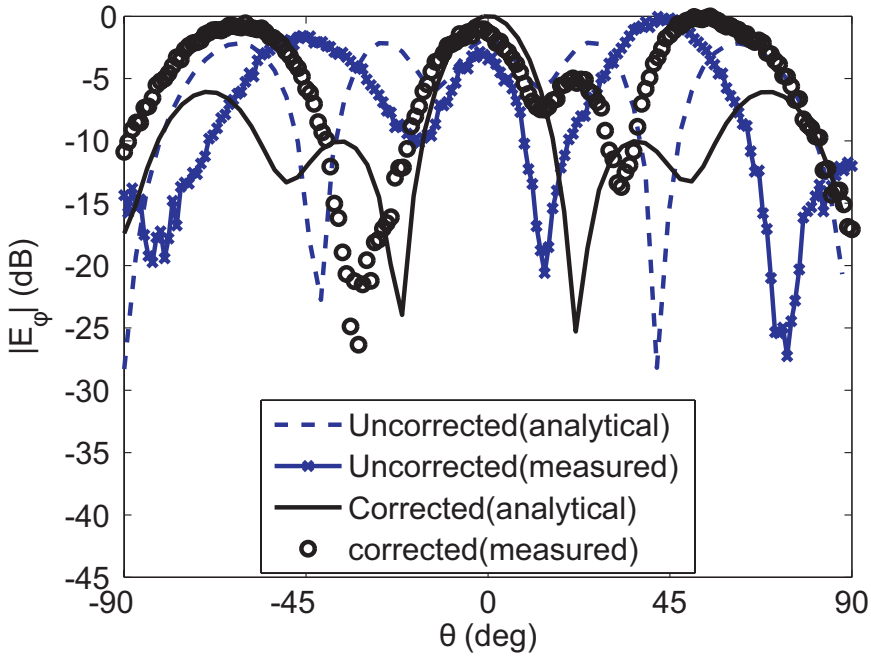

Figure 63: Analytical and Measured patterns of antenna array at 3.15 GHz (f_2) in the x-z plane for the wedge-shaped conformal surface with $\theta_b = 45°$.

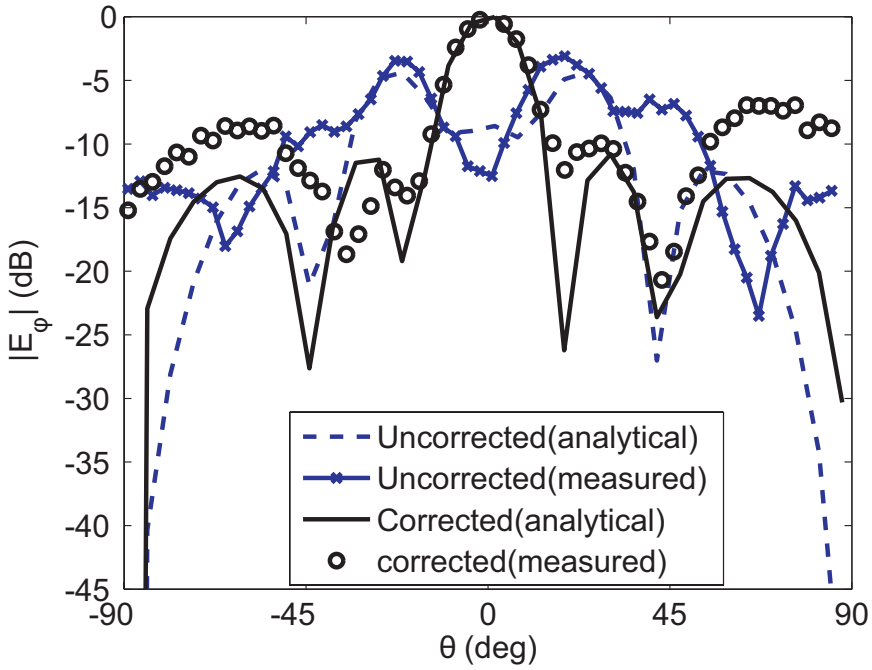

Figure 64: Analytical and Measured patterns of antenna array at 2.43 GHz (f_1) in the x-z plane for the cylindrical-shaped conformal surface.

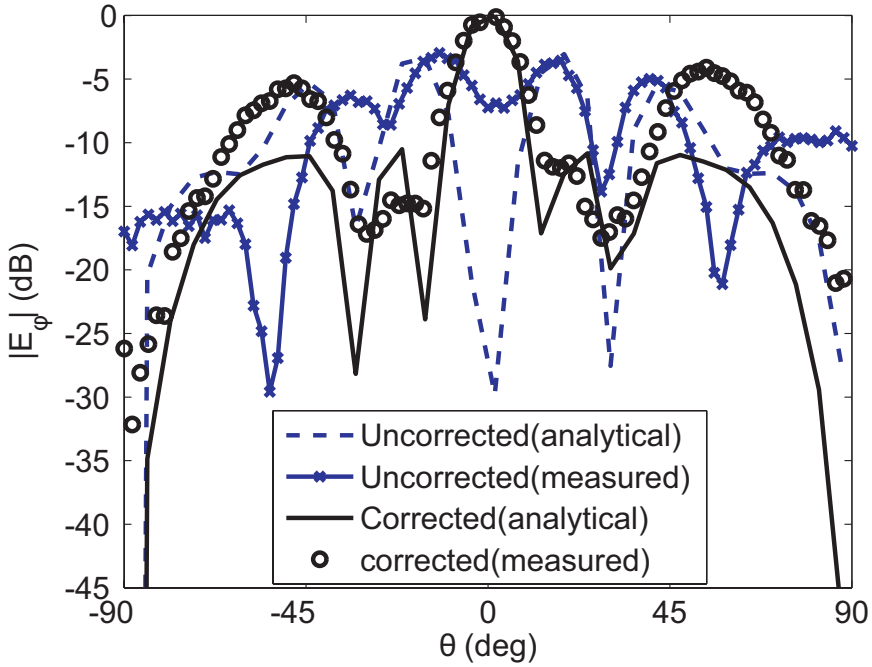

Figure 65: Analytical and Measured patterns of antenna array at 3.15 GHz (f_2) in the x-z plane for the cylindrical-shaped conformal surface.

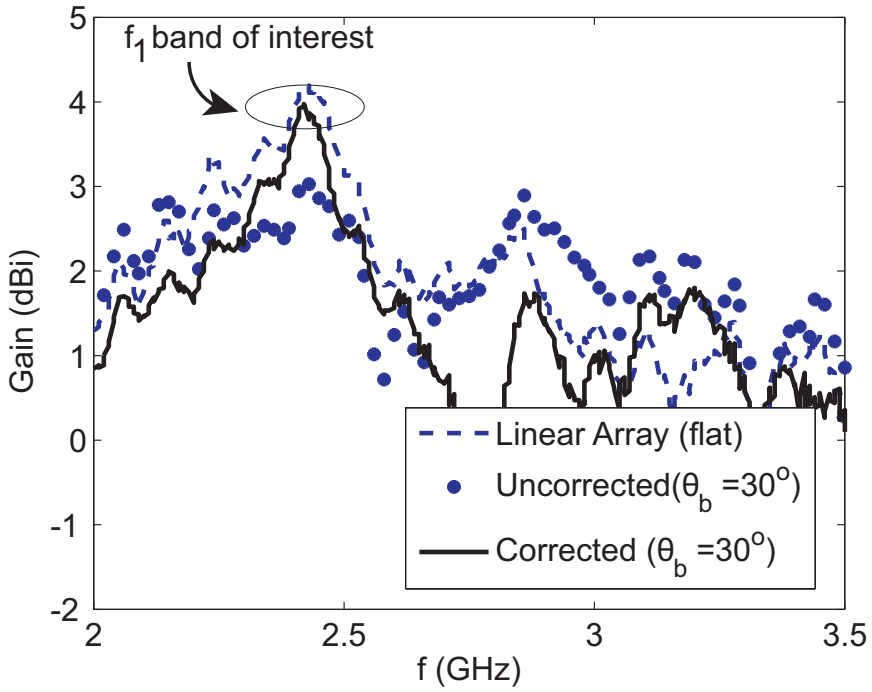

Figure 66: Measured gain of the self-adapting antenna prototypes at f_1 for $\theta_b = 30°$.

compared to the analytical computations using the Array Factor expressions presented in [57]. Good agreement is also observed; indicating that the antenna is autonomously correcting the radiation pattern in both operating bands on three difference conformal surfaces.

Finally, to illustrate that the antenna was operating in the bands of interest, the gain of the antenna was measured on the wedge- and cylindrical-shaped surfaces in the calibrated anechoic chamber. The results for the wedge-shaped surface with $\theta_b = 30°$ are shown in Figures 66 and 67. The results show that the array is reconfiguring between the f_1 and $_2$ operating bands, and since the gain is the maximum in these bands, it shows that the antennas are also self-adapting autonomously. Finally, it should be mentioned that a similar gain improvement was observed for the wedge angle $\theta_b = 45°$ and the cylindrical surface, and these results are presented in Figures 68-71.

The following comments can be made about the antenna presented in this work:

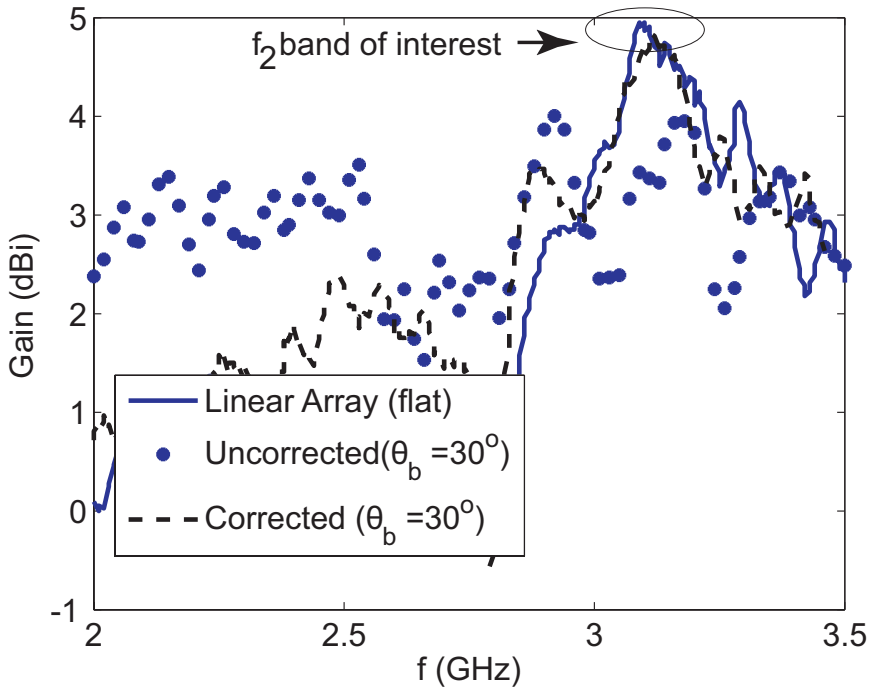

Figure 67: Measured gain of the self-adapting antenna prototypes at f_2 for $\theta_b = 30°$.

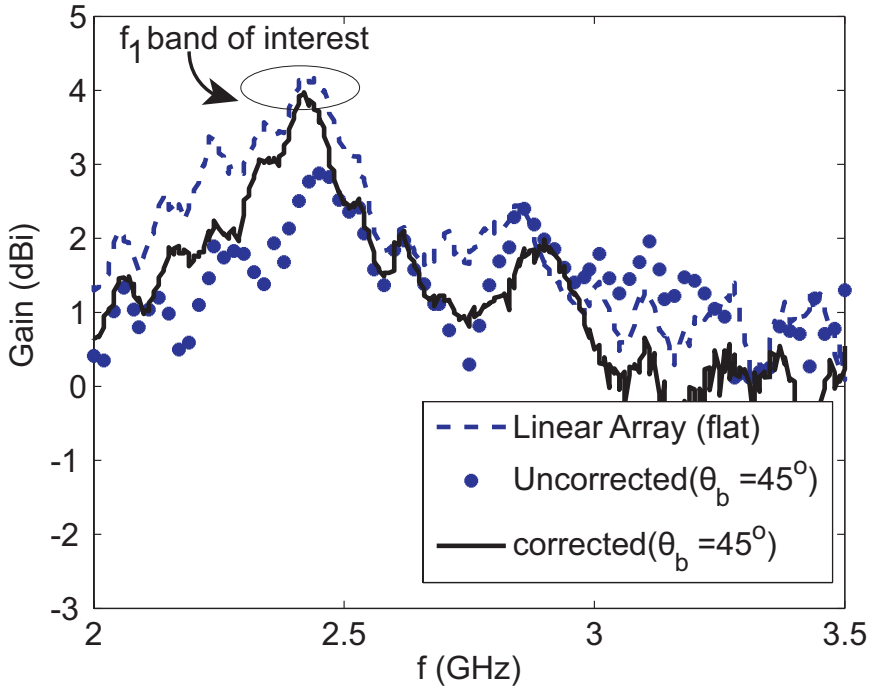

Figure 68: Measured gain of the self-adapting antenna prototypes at f_1 for $\theta_b = 45°$.

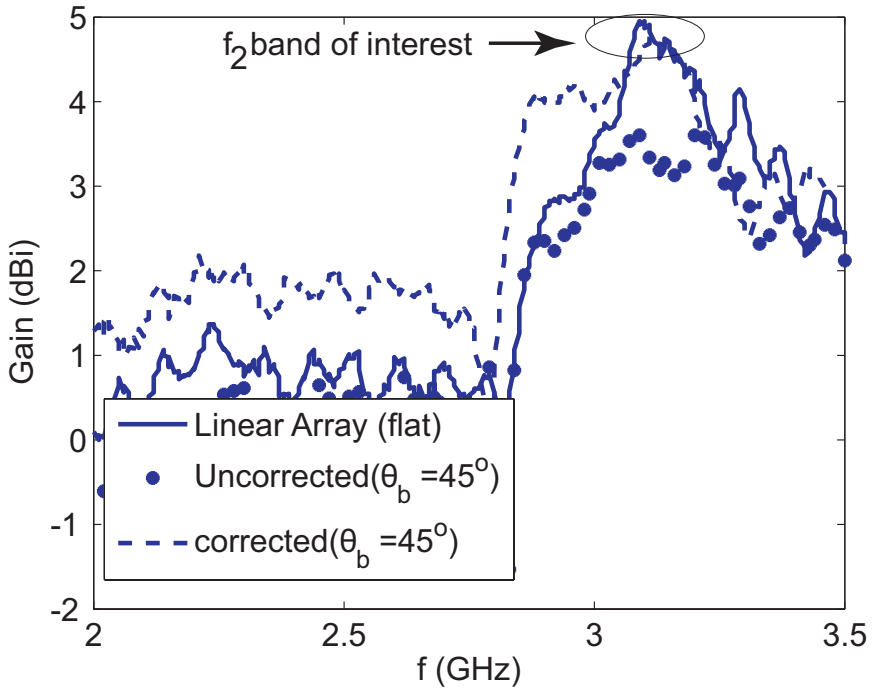

Figure 69: Measured gain of the self-adapting antenna prototypes at f_2 for $\theta_b = 45°$.

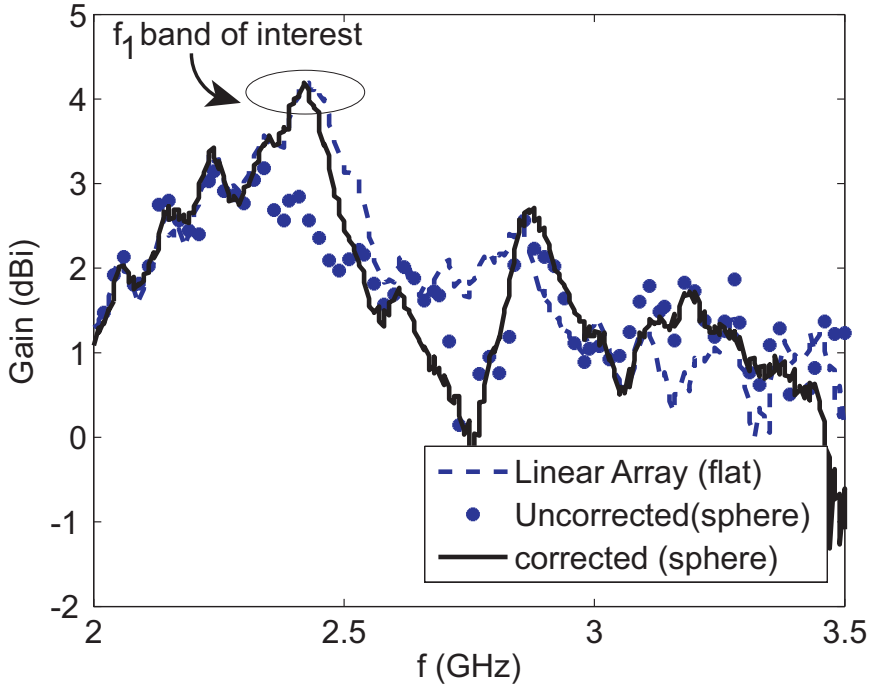

Figure 70: Measured gain of the self-adapting antenna prototypes at f_1 for the cylindrical surface.

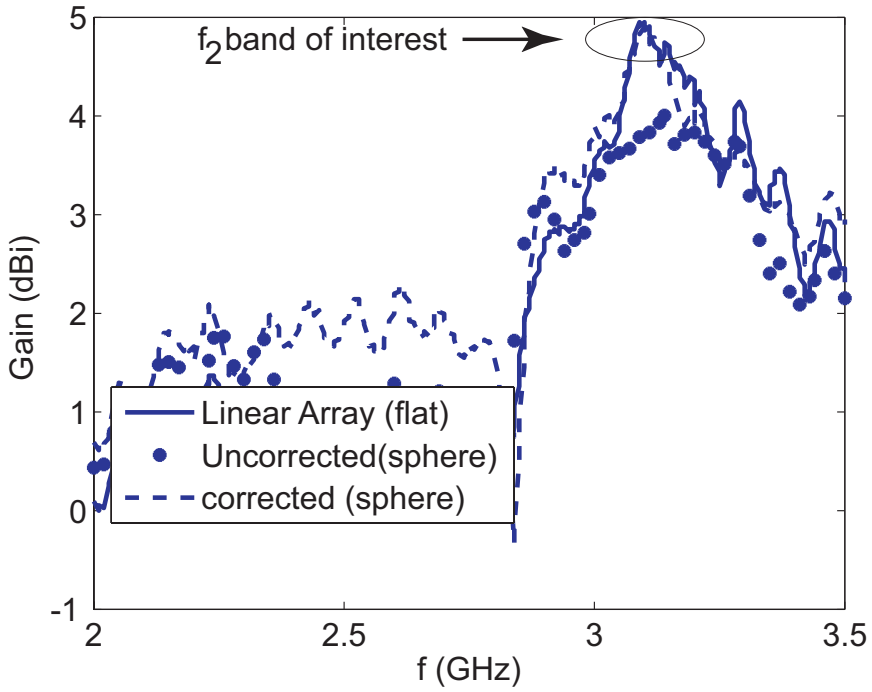

Figure 71: Measured gain of the self-adapting antenna prototypes at f_2 for the cylindrical surface.

1. The results in Figure 56 show that a frequency reconfigurable sensor circuit was successfully developed and implemented the theoretical expressions shown in equations (4.5)-(4.6) and (4.8)-(4.9).

2. The results in Figures 60-65 show that the radiation pattern of the prototype array can be autonomously recovered for various wedge- and cylindrical-shaped surfaces.

3. The gain results in Figures 66-71 show that the antenna pattern recovery is occurring in both frequency reconfigurable bands.

4.5. Frequency Reconfigurable Series-Fed Microstrip Patch Array with Interconnecting CRLH Transmission Lines

4.5.1. Introduction

Rapid growth in the areas of WiMax, WiFi, GPS, Bluetooth and UWB [80] has

led to the development of multi-band platforms capable of accessing these wireless services. A major benefit of a reconfigurable antenna is the capability to access multiple services in a device without the need of multiple antennas, thus potentially saving space. In many of the reconfigurable antenna designs in published literature, PIN diodes, RF MEMS switches and optical switches have been used to reconfigure the antennas [81] - [84]. Furthermore, microstrip patch antenna arrays are of great interest because of their small size, low cost, light weight, ease of manufacturing and useful radiation patterns [85]. Typically, series-fed antenna arrays are driven from a single point and the radiating elements are connected in series by using conventional transmission lines of suitable length for the operating frequency. These transmission lines can be replaced by meandered-lines and drive the elements of the array with the same voltage phase in order to achieve a broadside radiation pattern. However, at low microwave frequencies meander-lines can be very large. A possible way to overcome this size problem is to incorporate composite right/left-handed transmission lines (CRLH-TLs) into the feed network of a series-fed antenna array [86]-[90]. Efforts have been made previously to minimize the overall size of an array using CRLH-TLs [33], [91]-[92]; however, these designs were limited to a single band of operation.

In this work, the benefits of metamaterial-based transmission lines are combined with frequency reconfigurability to develop a compact series fed microstrip patch array. The layout of the proposed array is shown in Figure 72. It consists of three radiating patches and two non-radiating CRLH-TL interconnections between the radiating elements. The PIN diodes activate one of the CRLH-TLs at a time along with the particular sections of the main microstrip patch. These electrical switches re-route the current in a specific direction and alter the electrical lengths in the overall array, hence controlling the operating frequency of the array. Furthermore, this work is related to the single frequency design reported in [33].

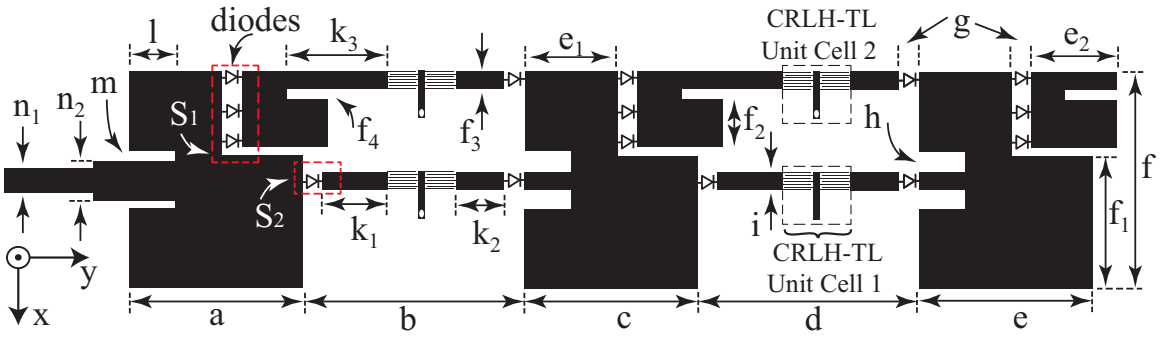

Figure 72: Layout of the reconfigurable series fed array with CRLH-TL interconnects. (a) Top view and (b) bottom view. Dimensions are: $a = 43.2$ mm, $b = 39$ mm, $c = 43.7$ mm, $d = 39$ mm, $e = 44.4$ mm, $f = 49.5$ mm, $f_1 = 26.5$ mm, $f_2 = 15.3$ mm, $f_3 = 2.7$ mm, $f_4 = 2.5$ mm, $e_1 = 24.7$ mm, $e_2 = 24.5$ mm, $g = 1$ mm, $h = 2.65$ mm, $i = 2.7$ mm, $k_1 = 16.9$ mm, $k_2 = 8.2$ mm, $k_3 = 23.8$ mm, $l = 12.4$ mm, $m = 2$ mm, $n_1 = 3.65$ mm and $n_2 = 4.86$ mm. Reprinted from [P.8].

4.5.2. Design of the Array

The equivalent impedance model of a series-fed antenna array is shown in Figure 73(a), which is classified as a standing wave array [93]. In these particular arrays, the feed is a single point and Z_1, Z_2 and Z_3 represent the input impedance of each radiating element. The impedance of each antenna element and interconnecting transmission line has an important role in matching [94]. Furthermore, for a broadside radiation pattern, each element must be fed with the same voltage phase. This can be done by either designing the length of each interconnection to be a multiple of the TL wavelength or to introduce the CRLH-TLs that can be tuned to have a zero phase constant near the operating frequency [90] (i.e., a zero-phase frequency). To make the antenna array compact and reconfigurable, the switching mechanism shown in Figure 73(b) was used. When the arm of the switch was connected to S_1, the CRLH-TL2 interconnects were activated. Then, when switch S_2 was connected to the arm, the CRLH-TL1 interconnects provided the path for current to travel along the array.

The layout and equivalent circuit of the CRLH-TL interconnects is shown in Figure 74. It consists of series impedances (series-connected C_L and L_R) as well

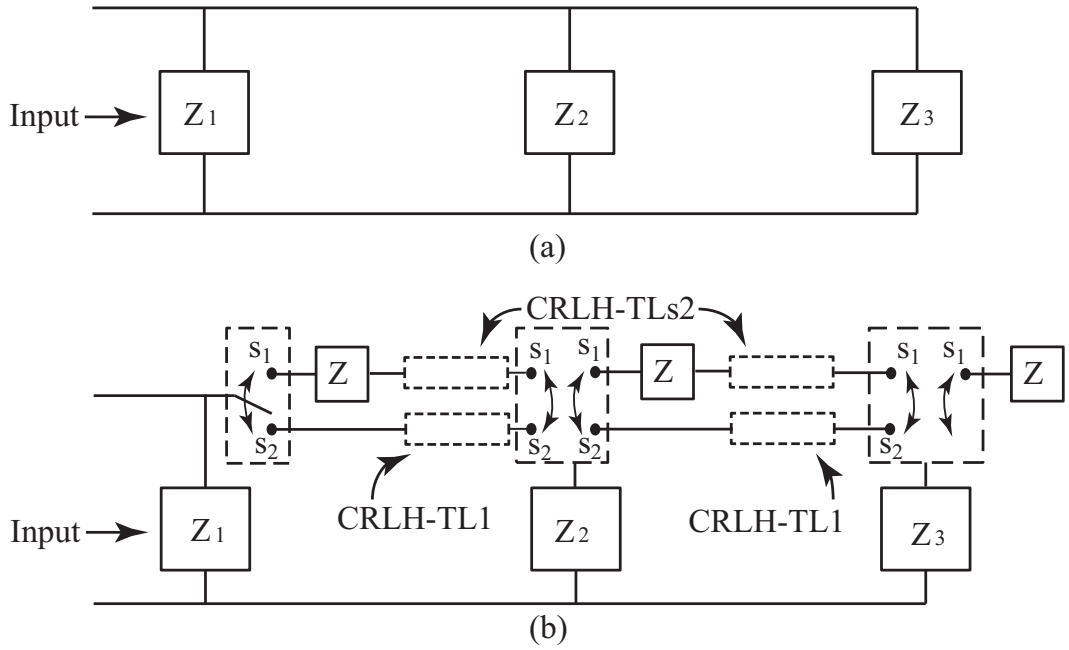

Figure 73: (a) Circuit representation of a 3-element series-fed array with conventional microstrip interconnects and (b) circuit representation of a 3-element series-fed array with CRLH-TL interconnections showing the switching mechanism. Reprinted from [P.8].

as shunt impedances (parallel connected L_L and C_R). L_R represents the parasitic inductance of the TL supporting wave propagation and C_R represents the parasitic capacitance between the ground and the printed conductors on the top of the substrate. C_L represents the interdigitated capacitance between the fingers of the unit cell and L_L is introduced due to the shunt stubs. When L_L and C_L are dominant for the frequencies of interest, a positive phase shift will be introduced by the CRLH-TL unit cell of length k. This phase shift can be changed to a particular frequency by adding a shunt per-unit-length capacitor, C_m, followed by a series per-unit-length inductor L_m on both sides on the CRLH-TL unit cell. With this configuration, the multi-band CRLH-TL characteristics can be achieved.

The CRLH-TL unit cells shown in Figure 74(a) and (b) were simulated in HFSS with the dimensions mentioned in the caption of Figure 74. A Rogers RT/Duriod 5880 substrate with a thickness of 1.57 mm, $\epsilon_r = 2.2$ and the loss tangent of 0.0009 was

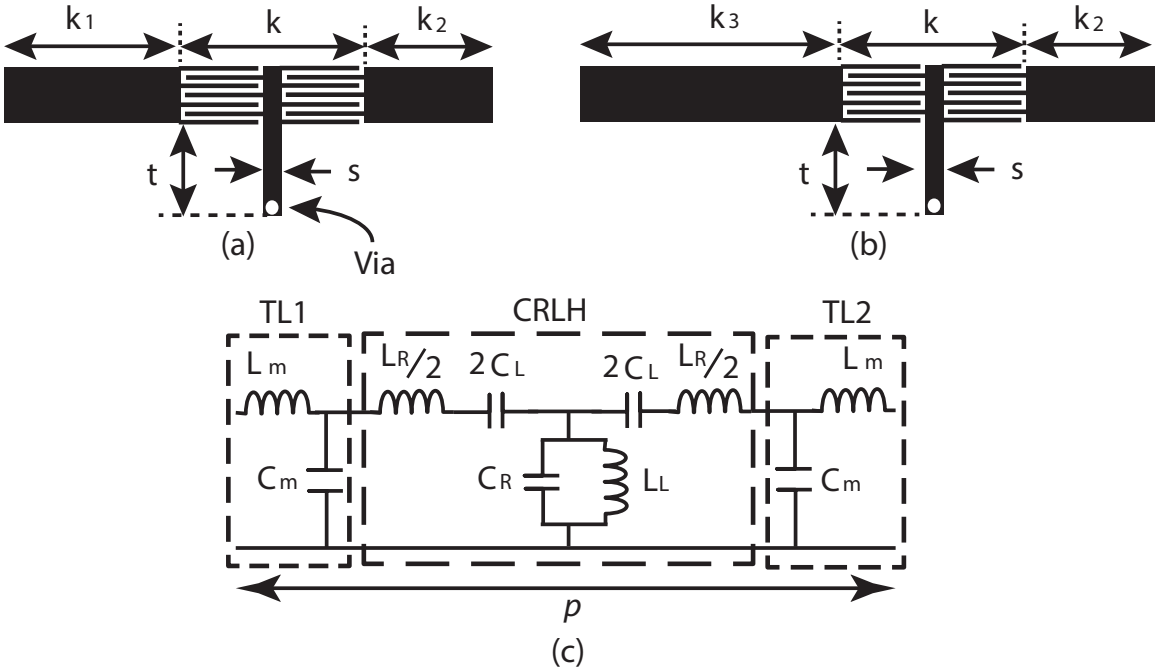

Figure 74: (a) Layout of CRLH-TL unit cell 1 (b) layout of CRLH-TL unit cell 2 and (c) circuit representation of CRLH-TL Unit Cells. Dimensions are: $k = 11.9$ mm, $k_1 = 16.9$ mm, $k_2 = 8.2$ mm, $k_3 = 23.8$ mm, $S = 1.3$ mm, $t = 7.26$ mm. Reprinted from [P.8].

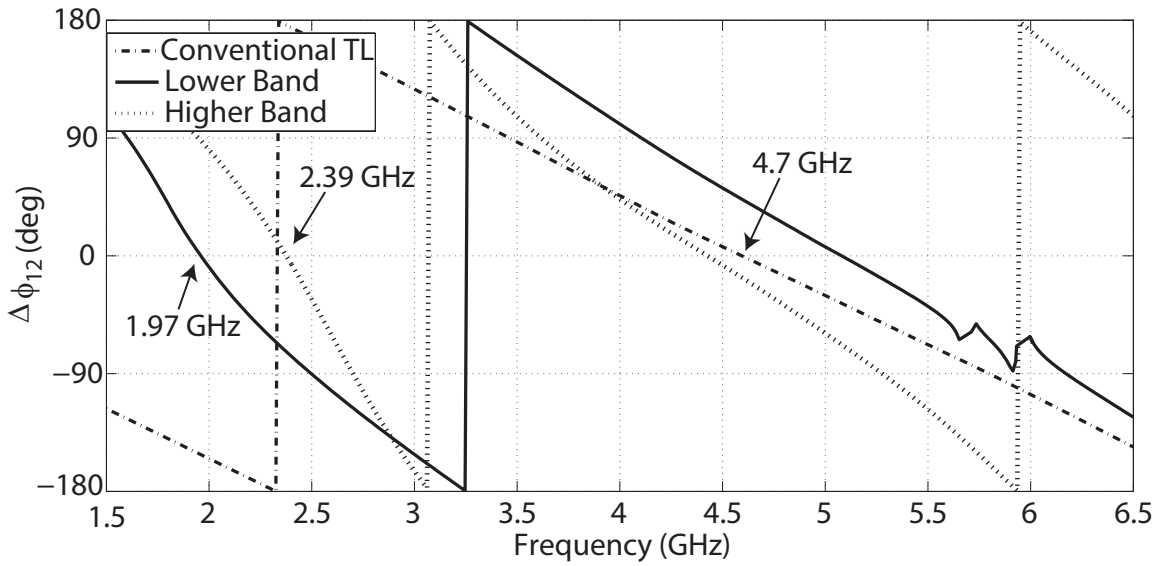

Figure 75: Simulated S_{12} phase for the conventional transmission line with a total length of k_1+k+k_2, higher band (unit cell 1) and lower band (unit cell 2). Reprinted from [P.8].

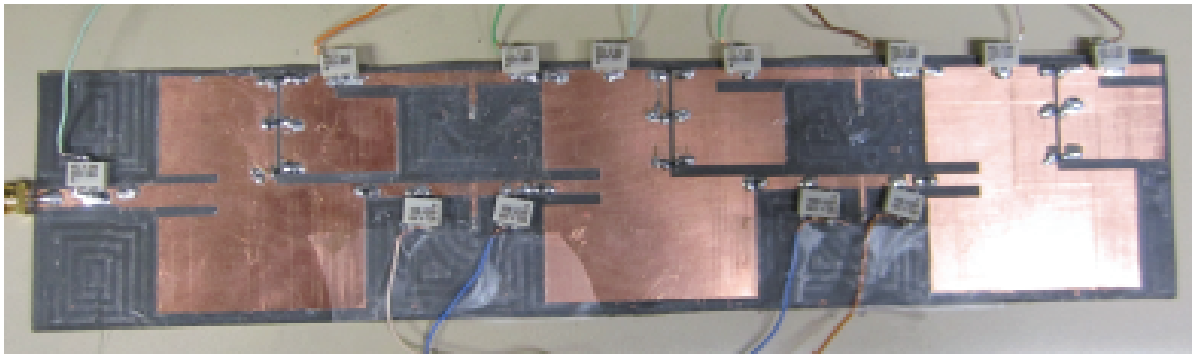

Figure 76: Picture of the manufactured prototype. Reprinted from [P.8].

used in the simulation environment. The S_{12} phase of the unit cells at both operating frequencies is shown in Figure 75. It can be seen that the zero-phase occurs at 2.39 GHz when unit cell 1 (in Figure 74(a)) was simulated. Then, when the length of the TL was increased the zero-phase frequency was shifted to the lower band, as shown in Figure 75. For comparison, the phase introduced by a conventional 50 Ω microstrip interconnect is also plotted in Figure 75. The length of this interconnect was chosen equal to the length of the CRLH-TL unit cell 1 in Figure 74(a). It can be seen that the zero-phase frequency occurs at 4.7 GHz, which is almost double the zero-phase frequency of the CRLH-TL unit cell 1. Once the zero-phase configurations were determined, the CRLH interconnects were added to the array as shown in Figure 72. Finally, it should be mentioned that the zero-phase can be moved to other frequencies by changing the series inductance L_m of the CRLH-TL. In fact, to shift the zero-phase to a lower frequency the length of the TL connecting with CRLH-TL is changed from k_1 to k_3 changing the series inductance L_m.

4.5.3. Prototype Testing

To demonstrate the functionality of the proposed frequency reconfigurable series-fed array, a prototype was fabricated on the same Rogers RT/Duroid 5880 substrate as the simulations and is shown in Figure 76. The CRLH-TL unit cells were connected

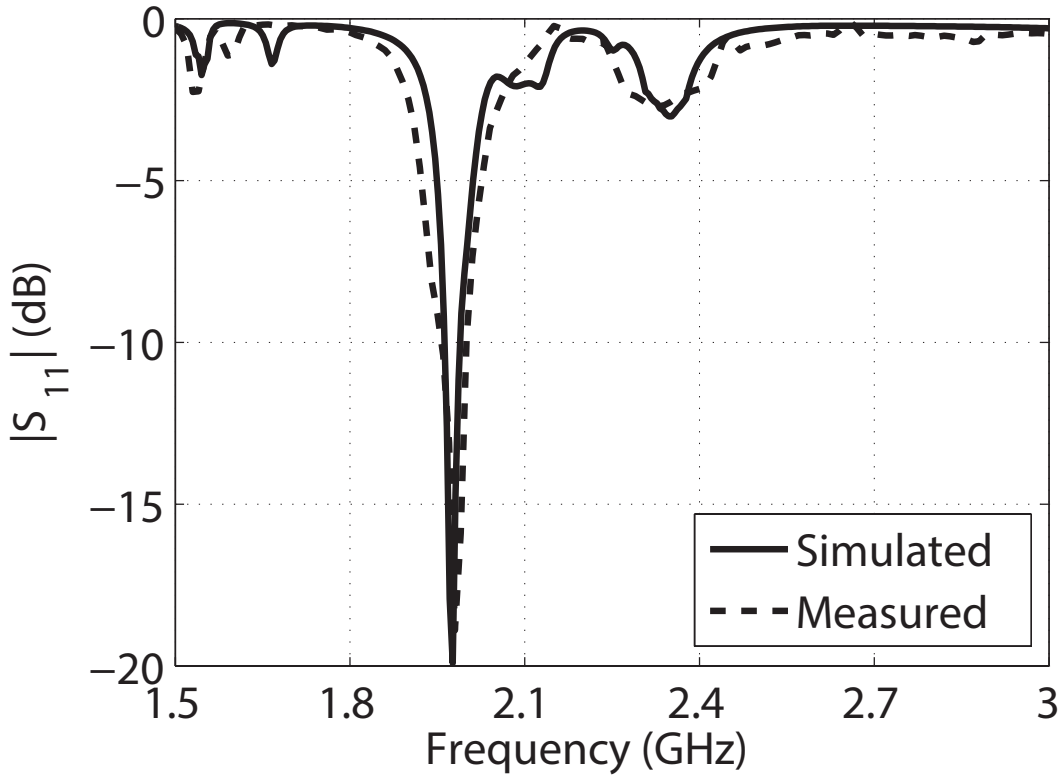

Figure 77: Simulated and measured $|S_{11}|$ for the lower band with S_1 activated. Reprinted from [P.8].

to the array elements with switches consisting of surface-mount voltage controlled PIN diodes. The control voltage (+V = 0.7V) was applied to the conducting surface with RF chokes.

The PIN diodes were modelled using the equivalent circuit defined in chapter 3. Figures 77 and 78 show the comparison of the S-parameters of the array. When switch S_2 was activated, the antenna had a smaller electrical length and the current was passing through the CRLH-TL unit cell 1, hence resonating at the higher resonant frequency of 2.37 GHz (as shown in Figure 78). When S_2 was turned "OFF" and S_1 was turned "ON", then a longer current path through the CRLH-TL unit cell 2 was introduced. This then resulted in the lower reconfigurable frequency of 1.97 GHz (as shown in Figure 77). A good comparison between simulated and measured results

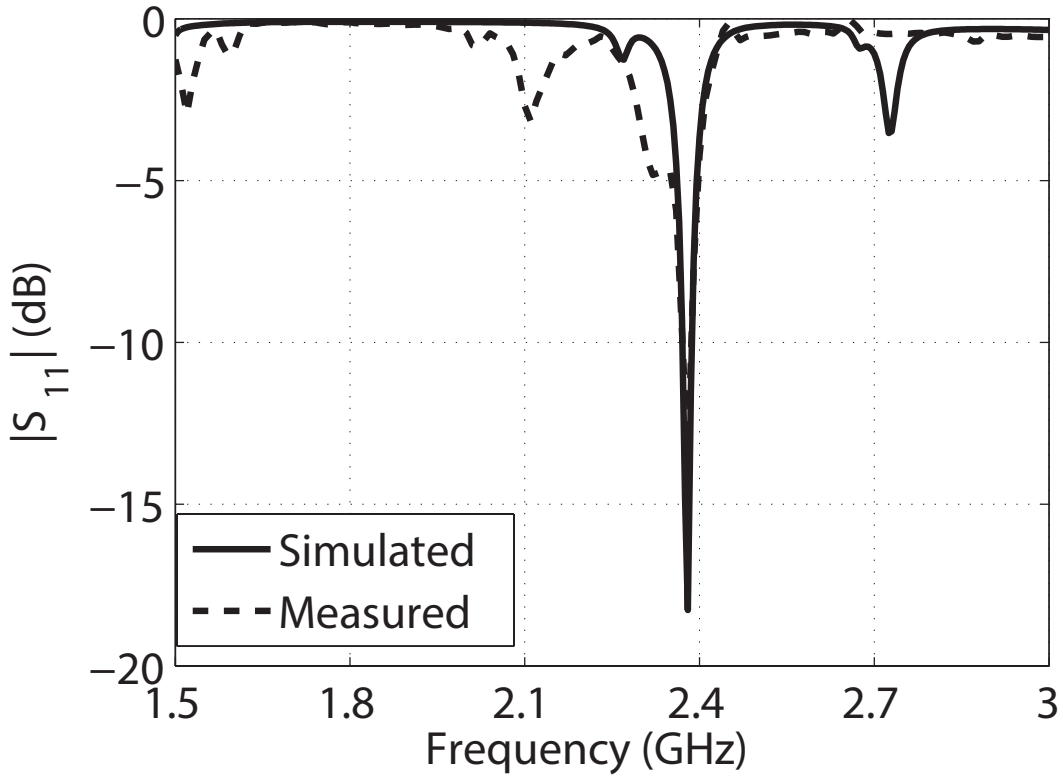

Figure 78: Simulated and measured $|S_{11}|$ for the upper band with S_2 activated. Reprinted from [P.8].

can be seen.

4.5.4. Surface Current

The surface current distribution at both operating frequencies is shown in Figure 79. When the array is operating at the lower band, the current finds a path through the small patches to the CRLH-TL unit cell 2. There is a small induced current on CRLH-TL unit cell 1 as well, but it does not contribute to the lower resonant band due to its weak intensity. Similarly, when the array is operating at the upper band, the current finds a path through CRLH-TL unit cell 1 and there is a little current induced on the small patches and CRLH-TL unit cell 2.

4.5.5. Radiation Pattern

Next, the normalized radiation pattern of the array was measured in both the

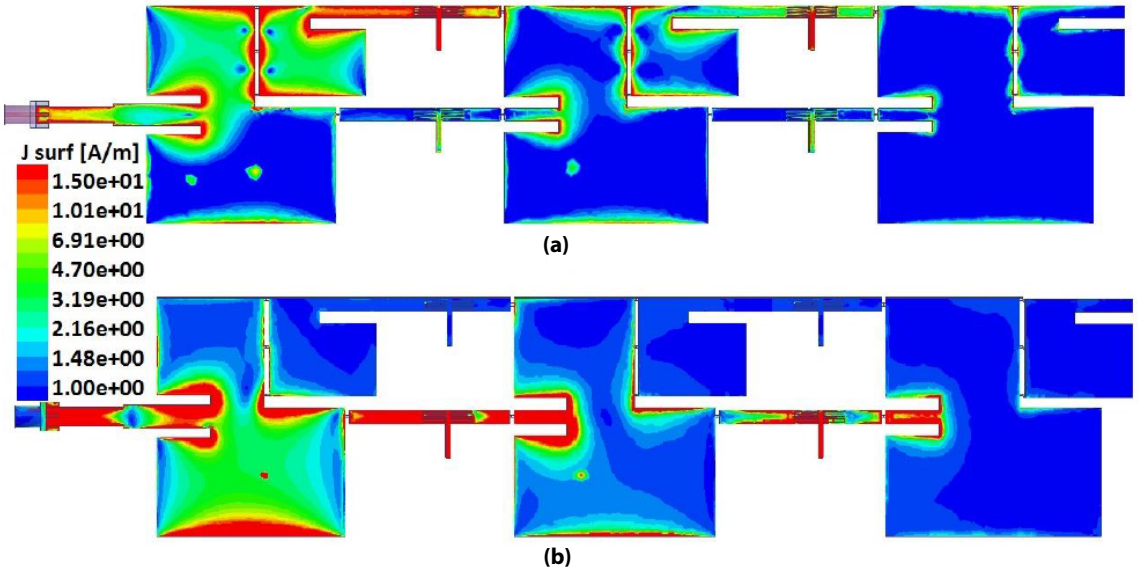

Figure 79: Surface current distribution for (a) 1.97 GHz and (b) 2.37 GHz. Reprinted from [P.8].

lower and upper reconfigurable bands. In particular, the E_θ component in the y-z plane was measured at 1.97 GHz and 2.37 GHz. The results from the measurements are shown in the Figure 80. Both switching frequencies have a broadside radiation pattern. Small variations in the measured results are due to the loading parasitics introduced by the PIN diodes and fabrication tolerances.

4.5.6. Gain and Efficiency

Next, the gain of the proposed reconfigurable antenna array was measured in a fully calibrated anechoic chamber and compared with the simulated gain values from HFSS. When the array was configured for the lower band, the measured gain at the 1.97 GHz (resonant frequency) was 1.9 dBi while the simulated gain was 2.45 dBi. Also, while still configured for 1.97GHz, the gain at 2.37 GHz (non-resonant frequency) was measured to be -6.0 dBi and simulated to be -5.2 dBi. This illustrated that the radiation from the antenna is in the desired lower reconfigurable band. Similarly, when the array was reconfigured for the upper operating band, the

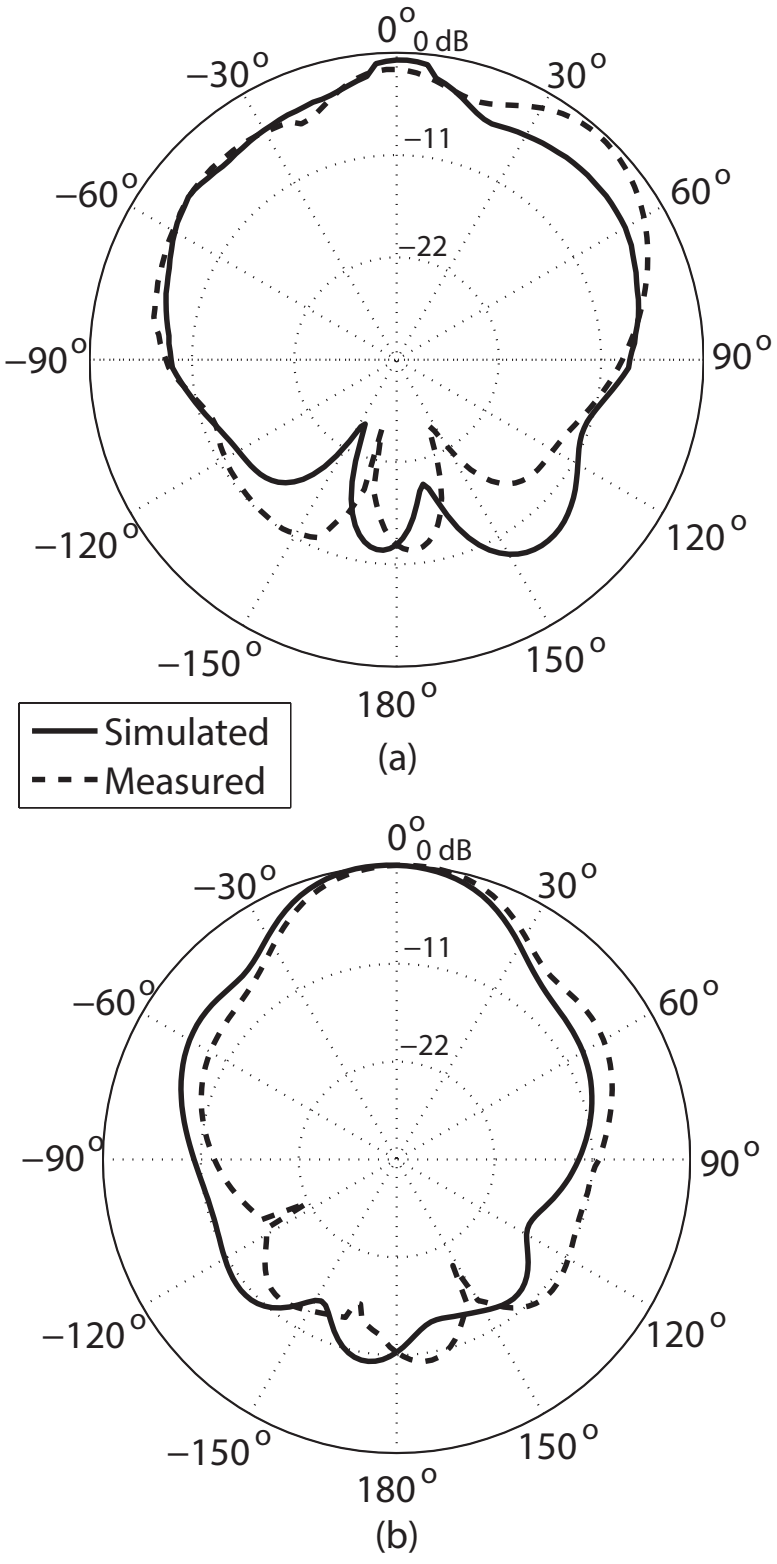

Figure 80: Simulated and measured radiation pattern in the y-z plane for (a) 1.97 GHz and (b) 2.37 GHz. Reprinted from [P.8].

measured gain at 1.97 GHz (non-resonant frequency) was -5.5 dBi and the simulated gain was -4.75 dBi. Then, the measured gain at 2.37 GHz (resonant frequency) was 3.5 dBi and the simulated gain was 3.95 dBi. Finally, the efficiencies of the proposed series-fed array were simulated in HFSS. The efficiency at 2.37 GHz was determined to be 0.785 and at 1.97 GHz it was reduced to 0.47. This was due to the diodes used in switching at the lower band. Thus, one draw back of using RF PIN diodes on an antenna array is a reduction in efficiency; however, the array shows reasonable gain at both operating frequencies and efficiency can be improved using MEMs switches or better diodes.

CHAPTER 5. CONCLUSION AND FUTURE DIRECTION

In this work, five different printed reconfigurable antennas having different properties were designed. Chapter 1 discussed the problem statement along with the motivation for future research in this area. The background of some different types of antenna was presented in Chapter 2. In Chapter 3, the steps involved for designing the reconfigurable switch were discussed.

Chapter 5 discussed the design of these five reconfigurable antennas with simulation and measured results. The first design was a compact frequency reconfigurable CPW-Fed antenna. The electrical length of the conductor was modified using PIN diodes and antenna was efficiently switched from 4.27 GHz to 3.56 GHz. The prototype was fabricated on Rogers TMM4 and comparison of S-parameters and radiation pattern was shown. A good agreement between simulated and measured results was observed. Another design involved a UWB-MIMO antenna with two radiating elements. The antenna was made compact by placing two radiators perpendicularly and very close to each other. The WLAN band was rejected by using the stubs on the ground plane. These stubs were connected to the ground plane by using PIN diodes. Good comparison between simulated and measured S-paramters and Far-field characteristics was observed. The antenna efficiently rejected the bandwidth of 1.4 GHz around 5.5 GHz center frequency. The second UWB-MIMO design was made with four antenna elements. The ground was made common using shortening strips. A band stop design was placed between the ground planes and it was connected with a rectangular patch which was placed exactly at the center of the ground plane. The band stop design was connected to ground plane by using PIN diodes. The current travelled through the ground plane and the notch was obtained around 5.5 GHz. The surface current illustrated that each band-stop design only affects the antenna which is placed nearly and along the direction of band stop design. Again good

comparison between simulated and measured results was observed. The low envelope correlation co-efficient and low gain variation makes this antenna suitable for portable devices. A reconfigurable antenna array was designed for conformal surfaces. The array was made with four individual microstrip patch elements and PIN didoes were used to reconfigure each patch. These patches were reconfigured from 3.15 GHz to 2.43 GHz. A sensing circuit was designed which provided the correct phase to each element attached to the conformal surface. The input voltage to the sensing circuit was changed to configure it for other switching frequency. The patterns were successfully recovered at both switching frequencies. A good comparison between analytical and measured results was observed. In the final design a series-fed array with three microstrip patches was designed. These patches were connected by using CRLH-TLs. CRLH-TLs were designed in such a way that these provided a zero phase at the connecting element. The array was switched to the other frequency by using small patches which were connected to the patch by using PIN diodes. Also the second CRLH-TL was activated to provide the correct phase at the connecting element. The broadside radiation pattern was obtained at both switching frequencies. Also simulated results showed good agreement with measured results.

5.1. Future Research

During the study of this thesis, only active elements were used to reconfigure the antennas. One of the draw back of these elements is that they insert losses due to which the efficiency and gain of antenna reduces. So the other elements should be explored like magnetic switches which could be very useful to reconfigure the antenna whit out decreasing its efficiency. Magnetic switches use the external magnets to bias the magnetic switch.

The others possibilities could be to use MEMS because they have very low losses and also they affect the antenna very less. The MEMS switches can be designed

separately for each application.

Some other application should also be explored where the reconfigurability is not applied yet, like beam forming of reconfigurable antenna, reconfigurable omnidirectional pattern of polarization diversity antenna on switching frequencies etc.

LIST OF PUBLICATIONS

Peer-reviewed International Journals

[**P.1**] **M. S. Khan**, A. Iftikhar, S. Asif, A. -D. Capobianco and B. D. Braaten, "A Compact 4 Elements UWB MIMO antenna with on-demand WLAN rejection," *accepted for publication in the Microwave Optical and Technology Letters.*

[**P.2**] **M. S. Khan**, A. -D. Capobianco, A. Iftikhar, S. Asif and B. D. Braaten, "A Compact Dual Polarized UWB-MIMO Antenna," *accepted for publication in the Microwave Optical and Technology Letters.*

[**P.3**] **M. S. Khan**, A. -D. Capobianco, A. Naqvi, B. Ijaz and B. D. Braaten, "Planar, Compact Ultra-Wideband Polarization Diversity Antenna Array," *accepted for publication in the IET Microwaves, Antennas and Propagation.*

[**P.4**] A. Naqvi, **M. S. Khan** and B. -D. Braaten, "A 1 x 2 Microstrip Array with Reduced Mutual Coupling Achieved with a Cylindrically-Shaped Cloaking-Based Surface," *accepted for publication in the Microwave Optical and Technology Letters.*

[**P.5**] J. W. Hansen, S. Asif, L. Singelmann, **M. S. Khan,** S. Ghosh, T. Gustad, C. Doetkott, B. D. Braaten, and D. L. Ewert, "A Far-Field Radio-Frequency Experimental Procedure to Determine the Alteration of Gene Expression In Vivo," *accepted for review in the SpringerPlus.*

[**P.6**] S. Asif, J. Hansen, **M. S. Khan**, S. Walden, M. O. Jensen, B. D. Braaten and D. L. Ewert, "Design and In Vivo Test of a Battery-less and Fully Wireless Implantable Asynchronous Pacing System," *IEEE Transactions on Biomedical Engineering.* vol. pp, no. 99, Sep, 2015.

[**P.7**] **M. S. Khan**, A. -D. Capobianco, S. Asif, A. Iftikhar, B. Ijaz and B. D. Braaten, "Compact 4×4 UWB-MIMO Antenna with WLAN Band Rejected Operation," *IET Electronic Letters,* vol. 51, no. 14, pp. 1048-1050, July, 2015.

[**P.8**] **M. S. Khan**, A. -D. Capobianco, A. Iftikhar, S. Asif, B. Ijaz and B. D. Braaten, "A Frequency Reconfigurable Series-Fed Microstrip Patch Array with Interconnecting CRLH Transmission Lines," *IEEE Antenna and Wireless Propagation Letters,* vol. PP, no. 99, June, 2015.

[**P.9**] **M. S. Khan**, A. -D. Capobianco, A. Naqvi, M. F. Shafique, B. Ijaz and B. D. Braaten, "Compact Planar UWB MIMO Antenna with On-Demand WLAN Rejection," *IET Electronic Letters,* vol. 51, no. 13, pp. 963-964, June, 2015.

[**P.10**] **M. S. Khan**, A. -D. Capobianco, M. F. Shafique, B. Ijaz and B. D. Braaten, "Isolation Enhancement of a wideband MIMO antenna using Floating Parasitic Elements," *Microwave Optical and Technology Letters,* vol. 57, no. 7, pp. 1677-1682, July, 2015.

[**P.11**] **M. S. Khan**, M. F. Shafique, A. Naqvi, A. Naqvi, A. -D. Capobianco, B. Ijaz and B. D. Braaten, "A Miniaturized Dual-Band Diversity Antenna for WLAN Applications," *IEEE Antenna and Wireless Propagation Letters,* vol. 14, pp.958-961, Jan. 2015.

[**P.12**] A. -D. Capobianco, **M. S. Khan**, M. Caruso and A. Bevilacqua, "3-18 GHz Planar Antenna System for Short Range Radar Imaging," *IET Electronic Lett.,* vol. 50, no. 14, pp.1016-1018, Jul. 2014.

[**P.13**] **M. S. Khan**, M. F. Shafique, A. -D. Capobianco, E. Autizi, I. Shoaib and Imran Ali, "Compact UWB-MIMO Antenna Array with a floating Digitated

Decoupling Structure," *IET Microwaves, Antennas and Propagation,* vol. 8, no.10, pp. 747-753, March, 2014.

[**P.14**] M. Bassi, M. Caruso, **M. S. Khan**, A. Bevilacqua, A. -D. Capobianco and A. Neviani, "An Integrated Microwave Imaging Radar with Planar Antennas for Breast Cancer Detection," *IEEE Trans. on Microwave Theory and Techniques,* vol. 61, no. 5, pp. 2108-2118, Feb. 2013.

Conference Proceedings

[**C.1**] **M. S. Khan**, A. -D. Capobianco, A. Iftikhar, S. Asif, B. Ijaz and B. D. Braaten, "An Electrically Small CPW Fed Frequency Reconfigurable Antenna," *2015 IEEE International Symposium on Antennas and Propagation,* pp. 2391-2392, Jul. 19 - 25, 2015, Vancouver BC, Canada.

[**C.2**] **M. S. Khan**, A. -D. Capobianco, S. Asif, A. Iftikhar, B. D. Braaten, B. Ijaz and M. F. Shafique, "A Small Footprint Ultra-Wideband Multiple-Input Multiple-Output Antenna," *2015 IEEE International Conference on Electro/Information Technology,* May 21 - 23, 2015, Northern Illinois University, DeKalb IL, USA.

[**C.3**] S. Asif, A. Iftikhar, S. Z. Sajal, B. D. Braaten and **M. S. Khan**, "On Using Graphene-Based Conductors as Transmission Lines for Feed Networks in Printed Antenna Arrays," *2015 IEEE International Conference on Electro/Information Technology,* May 21 - 23, 2015, Northern Illinois University, DeKalb IL, USA.

[**C.4**] A. Iftikhar, M. M. Masud, M. N. Rafiq, S. Asif, B. D. Braaten and **M. S. Khan**, "Radiation Performance and Specific Absorption Rate (SAR) Analysis of a Compact Dual Band Balanced Antenna," *2015 IEEE International Conference on Electro/Information Technology,* May 21 - 23, 2015, Northern Illinois University, DeKalb IL, USA.

[**C.5**] **M. S. Khan**, A. -D. Capobianco, S. Asif, A. Iftikhar and B. D. Braaten, "A 4 Element Compact Ultra-Wideband MIMO Antenna Array," *2015 IEEE International Symposium on Antennas and Propagation,* pp. 2305-2306, Jul. 19 - 25, 2015, Vancouver BC, Canada.

[**C.6**] B. D. Braaten, T. Tolstedt, S. Asif, M. J. Schroeder and **M. S. Khan**, "On Using the Electrical Characteristics of Graphene-Based Conductors for Designing a Conformal Monopole on a Transparent Substrate," *2015 IEEE International Symposium on Antennas and Propagation,* pp. 2435-2436, Jul. 19 - 25, 2015, Vancouver BC, Canada.

[**C.7**] S. Asif, A. Iftikhar, B. D. Braaten and **M. S. Khan**, "An Initial Study on Using Carbon Microfiber Transmission Lines in Conformal Array Networks," *2015 IEEE International Symposium on Antennas and Propagation,* pp. 234-235, Jul. 19 - 25, 2015, Vancouver BC, Canada.

[**C.8**] S. Asif, A. Iftikhar, M. N. Rafiq, B. D. Braaten, **M. S. Khan**, D. E. Anagnostou and T. S. Teeslink, "A Compact Multiband Microstrip Patch Antenna with U-Shaped Parasitic Elements," *2015 IEEE International Symposium on Antennas and Propagation,* pp. 617-618, Jul. 19 - 25, 2015, Vancouver BC, Canada

[**C.9**] B. D. Braaten, S. Asif, **M. S. Khan**, J. Hansen and D. L. Ewert, "A Compact Printed Van Atta Array with Zero-Phase CRLH Transmission Lines," *2015 IEEE International Symposium on Antennas and Propagation,* pp. 1856-1857, Jul. 19 - 25, 2015, Vancouver BC, Canada.

[**C.10**] **M. S. Khan**. M. F. Shafique, A. -D. Capobianco, E. Autizi and I. Shoaib, "Compact UWB-MIMO Antenna Array with a Novel Decoupling Structure," *IEEE International Bhurban Conference on Applied Science and Technology (IBCAST),* pp. 347-350, Jan. 2013.

BIBLIOGRAPHY

[1] A. A. Yassin and R. A. Saeed, "Reconfigurable dual band antenna for 2.4 GHz and 3.5 GHz using single PIN diode," *Internation Conf. on Computing, Electrical and Electronis Engineering,* pp.63-66, 2013.

[2] L. Ge and K-M. Luk, "Frequency-Reconfigurable low profile circular monopolar patch antenna," *IEEE Transaction on Antennas and Propag.,* vol. 62, no. 7, pp. 3443-3449 , 2014.

[3] S. C. Basaran and K. Sertel, "Dual-band frequency reconfigurable monopole antenna for WLAN applications," *Microwave and optical tecn. Lett.,* vol. 57, no. 1, pp.55-58, 2014.

[4] Y. Pan, K. Liu and Z. Hou, "A novel printed microstrip antenna with frequency reconfigurable characteristics for bluetooth/WLAN/WIMAX applications," *Microwave and optical tecn. Lett.,* vol. 55, no. 6, pp. 1341-1345, 2013.

[5] D. Peroulis, K. Sarabandi and L. P. B. Katehi, "Design of Reconfigurable Slot Antennas," *IEEE Transaction on Antennas and Propag.,* vol. 53, no. 2, pp. 645-654, 2005.

[6] D. H. Schaubert, F. G. Farrar, S. T. Hayes and A. R. Sindoris, " Frequecy agile polarization diversity microstrip antennas and frequency scanned arrays," U.S. Patent 4367474, 1983.

[7] J. -F. Li, Q. -Xi. Chu, Z. -H. Li and X. -X. Xia, "Compact Dual Band-Notched UWB MIMO Antenna With High Isolation," *IEEE Trans. Antennas Propag.,* vol. 61, no. 9, pp. 4759-4766, 2012.

[8] H. Zhao, F. Zhang, X. Zhang and C. Wang, "A Compact Band-Notched Ultra-Wideband Spatial Diversity Antenna," *PIERS,* vol. 51, pp. 19-26, 2014

[9] A. Najam, Y. Duroc, and S. Tedjni,"UWB-MIMO Antenna with Novel Stub Structure," *PIERS,* vol. 19, pp. 245-257, 2011.

[10] J. - M. Lee, K. -B. Kim, H. -K. Ryu, and J. -M Woo, "A compact Ultra-wideband MIMO Antenna with WLAN Band-Rejected Operation for Mobile Devices," *IEEE Antennas and Wireless Propag. Letters,* vol. 11, pp. 990-993, 2012.

[11] N. K. Kiem, H. N. B. Phuong and D. N. Chein, "Design of Compact 4 x 4 UWB-MIMO antenna with WLAN band rejection," *International Journal of Antennas and Proapag.,* vol. 2014, pp. 1-11, 2014.

[12] H. Huang, Y. Liu, S. S. Zhang and S. X. Gong, ''Compact Polarization Diversity Ultrawideband MIMO antenna with triple band-notched characteristics," *Microw. and Optical techn. Lett.,* vol. 57, no. 4, pp. 946-953, 2015.

[13] H. K. Yoon, Y. J. Yoon, H. Kim and C. H. Lee, "Flexible ultra-wideband polarisation diversity antenna with band-notch function," *IET Microw. Antennas Propag.,* vol. 5, no. 12, pp. 1463-1470, 2011.

[14] P. Gao, S. He, X. Wei, Z. Xu, N. Wang and Y. Zheng, "Compact Printed UWB diversity Slot Antenna with 5.5 GHz band-notched characteristics," *IEEE Antenna wireless propag. Lett.,* vol. 13, pp. 376-379, 2014.

[15] B. P. Chacko, G. Augustin and T. A. Denidni, "Uniplanar Slot antenna for Ultrawideband polarization-diversity applcations," *IEEE Antenna wireless propag. Lett.,* vol. 12, no. 10, pp. 88-91, 2013.

[16] A. P. Saghati, M. Azarmanesh and R. Zaker, "A novel switchable single- and multifrequency triple slot antenna for 2.4 GHz bluetooth, 3.5 GHz Wimax, and 5.8 GHz WLAN," *IEEE Antenna wireless propag. Lett.,* vol. 9, pp. 534-537, 2010.

[17] D. E. Anagnostou and A. A. Gheethan, "A coplanar reconfigurable folded slot antenna without bias netwrok for WLAN applications," *IEEE Antenna wireless propag. Lett.,* vol. 8, pp. 1057-1060, 2009.

[18] T. Kaiser, F. Zheng and E. Dimitrov, "An Overview of Ultra-Wide-Band Systems with MIMO," *Proceedings of the IEEE,* vol. 97, no. 2, pp. 285-312, 2009.

[19] R. G. Vaughan and J. B. Andersen, "Antenna diversity in mobile communications," *IEEE Trans. Veh. Tech.,* vol. 36, no. 4, pp. 149-172, 1987.

[20] H. -X. Xu, G.-M. Wang and M. -Q. Qi, "A minaturized triple-band metamaterial antenna with radiation pattern selectivity and polarization diversity," *PIERS,* vol. 137, pp. 275-292, 2013.

[21] Fed. Commun. Comm., "First report and order, revision of part 15 of the commissions rule regarding ultra wideband transmission systems," FCC 02-48, Apr. 22, 2002.

[22] D. E. Anagnostou, M. T. Chryssomallis, B. D. Braaten, J. L. Ebel and N. Sepulveda, "Reconfigurable UWB antenna with RF-MEMS for on-demand WLAN Rejection," *IEEE Trans. Antennas Propag.,* vol. 62, no. 2, pp. 602-608, 2014.

[23] C. C. Lin, P. Jin and R. W. Ziolkowski, "Single, dual and tri-band-notched ultrawide band antennas using capacitively loaded resonators," *IEEE Trans. Ant. Propag.,* vol. 60, no. 1, pp. 102-109, 2012.

[24] F. Zhu, S. Gao, A. T. Ho, R. A. A-Alhameed, C. H. See, T. W. C. Brown, J. Li, G. Wei and J. Xu, "Multiple Band-Notched UWB Antenna With Band Rejected Elements Integrated in the Feed Line," *IEEE Trans. Ant. Propag.,* vol. 61, no. 8, pp. 3952-3960, 2014.

[25] C. X. Mao and Q. X. Chu, "Compact coradiator UWB-MIMO antenna with dual polarization," *IEEE Trans. Ant. Propag.,* vol. 62, no. 9, pp. 4474-4480, 2014.

[26] P. L. O'Donovan and A. W. Rudge, "Adaptive control of a flexible linear array," *Electron. Lett.,* vol. 9, no. 6, pp. 121-122, 1973.

[27] E. Lier, M. Zemlyansky, D. Purdy and D. Farina, "Phased array calibration and characterization based on orthogonal coding: Theory and experimental validation," *in Proc. IEEE Int. Symp. Phased Array Syst. Technol. (Array),* pp. 271-278, 2010.

[28] T. J. Seidel, W. S. T. Rowe and K. Ghorbani, "Passive compensation of beam shift in a bending array," *Prog. Electromagn. Research,* vol. 29, pp. 41-53, 2012.

[29] B. D. Braaten, S. Roy, S. Nariyal, M. A. Aziz, N. F. Chamberlain, I. Irfanullah, M. T. Reich and D. E. Anagnostou,"A Self-Adapting Flexible (SELFLEX) Antenna Array for Changing Conformal Surface Applications," *IEEE Trans. Antennas Propag.,* vol. 61, no. 2, pp. 655-665, 2013.

[30] Constantine A. Balanis, *Antenna Theory: Analysis and Design,* Harper and Row, Publishers, New York, 1982.

[31] V. Veselago, "The electrodynamic of sunstance with simultaneously negative values of ϵ and μ," *Soviet Physics Uspekhi,* vol. 10, no. 4, pp. 509-514, 1968.

[32] B. Ijaz, "Metamaterial-inspired reconfigurable series-fed arrays," Ph.D. dissertation, Electr. and Comut. Eng.Dept. North Dakota State Uni. (NDSU), Fargo, ND, 2014.

[33] B. Ijaz, S. Roy, M. M. Masud, A. Iftikhar, S. Nariyal, I. Ullah, K. Asirvatham, B. Booth and B. D. Braaten, "A Series-fed Microstrip Patch Array with Interconnecting CRLH Transmission Lines for WLAN Applications," *Proceedings of the 7th European Conference on Antennas and Propagation (EuCAP 2013),* pp. 2088-2091, Gothenburg, Sweden.

[34] Skyworks Inc. [Online]. Available: www.skyworksinc.com

[35] Mini-circuits [Online]. Available: www.minicircuits.com

[36] Ansys, Inc., Ansoft HFSS, ver. 15.0 [Online]. Available: www.ansoft.com.

[37] M. Qaraqe, Q. H. Abbasi, A. Alomainy and E. Serpendin, " Experimental Evaluation of MIMO Capacity for Ultrawideband Body-Centric Wireless Propagation Channels," *IEEE Antennas and Wireless Propag. Letters,* vol. 13, pp. 495-498, 2014.

[38] A. I. Najam, Y. Duroc and S. Tedjini, "Multiple-Input Multiple-Ouput Antenna for Ultra Wideband Communications," *Intech Publishing,* Ch. 10, 2012.

[39] M. Koohestani, A. A. Moreira and A. K. Skrivervik, "A Novel Compact CPW-Fed Polarization Diversity Ultrawideband Antenna," *IEEE Ant. and Wireless Propaga. Lett.,* vol. 13, 2014.

[40] M. Koohestani and M. Golpour, "U-shaped microstrip patch antenna with novel parasitic tuning stubs for ultra wideband applications," *IET Microw., Ant. and Propag.,* vol. 4, no. 7, pp. 938-946, 2010.

[41] S. Zhang, B. K. Lau, A. Sunesson, and S. He, "Closely-Packed UWB MIMO/Diversity antenna withe different patterns and polarizations for USB dongle application," *IEEE Trans. Antennas Propag.,* vol. 60, no. 9, pp. 4372-4380, 2012.

[42] K. Rosengren and P. -S. Kildal, "Radiation efficieny, correlation, diversity gain and capacity of a six monopole antenna array for a MIMO system: Theory, simulation and measurement in reverberation chamber," *IEEE Proc. Microw. Ant. and Propag.,* vol. 152, no. 1, pp. 7-16, 2005.

[43] M.S. Khan, M. F. Shafique, A.D. Capobianco, E. Autizi and I. Shoaib, "Compact UWB-MIMO antenna array with a novel decoupling structure," *Proceeding of 10th Intl. Bhurban Conf. on Applied Sciences and tech.,* pp. 347-350, 2013.

[44] J. Thaysen, and K.B. Jakobsen, "Envelope correlation in (N, N) MIMO antenna array from scattering parameters," *Microw. Opt. Technol. Lett.,* vol. 48, no. 5, pp. 832-834, 2006.

[45] P. J. Callus, "Conformal load-bearing antenna structure for australian defense force aircraft," *DSTO Platforms Sciences Laboratory,* Victoria Australia, 2007.

[46] S. E. Morris, Y. Bayram, L. Zhang, Z. Wang, M. Shtein and J. L. Volakis,"High-strength, metalized fibers for conformal load bearing antenna applicaitions," *IEEE Trans. on Antennas Propag.,* vol. 59, no. 9, pp. 3458-3462, 2011.

[47] M. Klemm and G. Troester, "Textile UWB antennas for wireless body area networks," *IEEE Trans. Antennas Propag.,* vol. 54, no. 11, pp. 3192-3197, 2006.

[48] T. F. Kennedy, P. W. Fink, A. W. Chu, N. J. Champagne, G. Y. Lin and M. A. Khayat, "Body-Worn E-Textile Antennas: The Good, the Low- Mass, and the Conformal," *IEEE Trans. on Ant. Propag.,* vol. 57, no. 4, pp. 910-918, 2009.

[49] P. Salonen, Y. Rahmat-Samii, M. Schaffrath and M. Kivikoski, "Effect of textile materials on wearable antenna performance: A case study of GPS antennas," *in Proc. IEEE Antennas Propag. Soc. Int. Symp.,* vol. 1, pp. 459-462, 2004.

[50] D. Psychoudakis, G. Y. Lee, C.-C. Chen and J. L. Volakis, "Estimating diversity for body-worn antennas," *3rd European Conference on Antennas and Propagation (EuCAP),* pp. 704-708, 2009, Berlin Germany.

[51] Y. Byram, Y. Zhou, B. S. Shim, S. Xu, J. Zhu, N. A. Kotov and J. L. Volakis, "E-textile conductors and polymer composites for conformal lightweight antennas," *IEEE Trans. on Antennas Propag.,* vol. 56, no. 8, pp. 2732-2736, 2010.

[52] Z. Wang, L. Zhang, Y. Bayram and J. L. Volakis, "Multilayer printing of embroidered RF circuits on polymer composites," *Proc. IEEE Antennas Propag. Soc. Int. Symp. Dig.,* pp. 278-281, 2011, Spokane WA.

[53] H. Schippers, P. Knott, T. Deloues, P. Lacomme and M. R. Scherbarth, "Vibrating antennas and compensation techniques research in NATO/RTO/SET 087/ RTG 50," *IEEE Aerospace Conference,* pp. 1-13, 2007.

[54] P. Knott, "Deformation and vibration of conformal antenna arrays and compensation techniques," *Meeting proc. RTO-MP-AVT-141,* paper 19, pp. 1-12, 2006.

[55] H. Schippers, J. Verpoorte, P. Jorna, A. Hulzinga, A. Meijerink, C. Roeloffzen, R. G. Heideman, A. Leinse and M. Wintels, "Conformal phased array with beam forming on airborne satellite communication," *International ITG Workshop on Smart Antennas,* pp. 343-350, 2008.

[56] R. C. Hansen,*Phased Array Antennas.* John Wiley and Sons, Inc., New York, NY, 1998.

[57] R. L. Haupt, *Antenna Arrays: A Computational Approach,* John Wiley and Sons, Ltd., Hoboken, New Jersey, pp. 287-315, 2010.

[58] L. Josefsson and P. Persson, *Conformal Array Antenna Theory and Design,* John Wiley and Sons, Ltd., Hoboken, New Jersey, 2006.

[59] P. Jorna, H. Schippers and J. Verpoorte, "Beam synthesis for conformal array antennas with efficient tapering," *Proc. of 5th Europ. Workshop on Conformal Antennas,* Bristol, 2007.

[60] B. D. Braaten, I. Ullah, S. Nariyal, A. Naqvi, M. Iskander and D. E. Anagnostou, "Scanning Characteristics of a Self-Adapting Phased-Array Antenna

on a Wedge-Shaped Conformal Surface," *Proc. IEEE Antennas Propag. Soc. Int. Symp. Dig.,* pp. 1056-1057, 2013, Orlando FL.

[61] K. Wincza and S. Gruszczynski, "Influnce of curvature radius on radiation patterns in multibeam conformal antenna," *in Proc. 36th Eur. Microw. Conf.,* pp. 1410-1413, 2006.

[62] H. Schippers, G. Spalluto and G. Vos, "Radiation analysis of conformal phased array antennas on distorted structures," *12th International Conference on Antennas and Propagation (ICAP 2003)*, pp. 160-163, 2003.

[63] E. Kiely, G. Washington and J. Bernhard, "Design and development of smart microstrip patch antennas," *Smart Mater. Struct.,* vol. 7, no. 6, pp. 792-800, 1998.

[64] J. Huang, "Bandwidth study of microstrip reflectarray and a novel phased reflectarray concept," *Proc. of the IEEE Int. Symp. on antennas and propag., Newport Beach, CA,* pp. 582-585, 1995.

[65] J. -L. Guo and J. -Y. Li, "Pattern synthesis of conformal array antenna in the presence of platform using differential evolution algorithm," *IEEE Trans. on Antennas Propag.,* vol. 57, no. 9, pp. 2615-2621, 2009.

[66] E. Lier, D. Purdy and G. Kautz, US Patent 6163296, "Calibration and integrated beam control / conditioning system for phased-array antennas," Dec. 19, 2000.

[67] E. Lier, D. Purdy, J. Ashe and G. Kautz, "An On-Board Integrated Beam Conditioning System for Active Phased Array Satellite Antennas," *2000 IEEE Intern. Conf. on Phased Array Systems and Technol.,* Dana Point, CA, pp. 509-512, 2000.

[68] D. Purdy, J. Ashe and E. Lier, US Patent: 2002/0171583 A1, "System and Method for Efficiently Characterizing the Elements in an Array Antenna," Nov. 21, 2002.

[69] Y. Wu, K. F. Warnick and C. Jin, "Design study of an L-band phaed array feed for wide-field surveys and vibration compensation on FAST," *IEEE Trans. Antennas Propag.,* vol. 61, no. 6, pp. 3026-3033, 2013.

[70] I. Chiba, K. Hariu, S. Sato and S. Mano, "A projection method providing low sidelobe pattern in conformal array antennas," *Proc. IEEE Antennas Propag. Soc. Int. Symp. Dig.,* pp. 130-133, 1989.

[71] S. Yang, C. Zhang, H. K. Pan, A. E. Fathy and V. K. Nair, "Frequency-Reconfigurable Antenna for Multiradio Wireless Platforms," *IEEE Micro. Mag.,* pp. 66-83, 2009.

[72] D. E. Anagnostou, Z. Guizhen, M. T. Chryssomallis, J. C. Lyke, G. E. Ponchak, J. Papapolymerou and C. G. Christodoulou, "Design, fabircation, and measurements of an RF-MEMS-based self-similar reconfigurable antenna," *IEEE Trans. Antennas Propag.,* vol. 54, no. 2, pp. 422-432, 2006.

[73] Y. Tawk, J. Costantine, K. Avery and C. G. Christodoulou, "Implementing a cognitive radio front-end using rotatable controlled reconfigurable antennas," *IEEE Trans. Antennas Propag.,* vol. 59, no. 5, pp. 1773-1778, 2011.

[74] Y. Tawk, J. Costantine, S. Hemmady, G. Balakrishnan, K. Avery and C. G. Christodoulou, "Demonstration of a cognitive radio front end using an optically pumped reconfigurable antenna system (OPRAS)," *IEEE Trans. Antennas Propag.,* vol. 30, no. 2, pp. 1075-1083, 2012.

[75] [D. Rodrigo, L. Jofre and B. A. Cetiner, "Circular beam-steering reconfigurable antenna with liquid metal parasitics," *IEEE Trans. Antennas Propag.,* vol. 60, no. 4, pp. 1796-1802, 2012.

[76] G. H. Huff, J. Feng, S. Zhang, G. Cung and J. T. Bernhard, "Directional Reconfigurable Antennas on Laptop Computers: Simulation, Measurement and Evaluation of Candidate Integration Positions," *IEEE Trans. Ant. and Propag.,* vol. 52, no. 12, pp. 3220-3227, 2004.

[77] Hittite Microwave Corporation, [online] www.hittite.com.

[78] Spectra Symbol, [online] www.spectrasymbol.com.

[79] Rogers Corporation, [online] www.rogerscorp.com.

[80] S. Yang, C. Zhang, H. K. Pan, A. E. Fathy and V. K. Nair, "Frequency reconfigurable antenna for multiradio wireless platforms," *IEEE Microw. Mag.,* vol. 10, no. 1, pp. 66-83, 2009.

[81] C. W. Jung, M. Lee, G. P. Li, and F. De Flaviis, "Reconfigurable scanbeam single-arm spiral antenna integrated with RF-MEMS switches," *IEEE Trans. Antennas Propag.,* vol. 54, no. 2, pp. 455-463, 2006.

[82] S. Shelley, J. Costantine, C. G. Christodoulou, D. E. Anagnostou, and J. C. Lyke, "FPGA-controlled switch-reconfigured antenna," *IEEE Antennas Wireless Propag. Lett.,* vol. 9, pp. 355-358, 2010.

[83] C. J. Panagamuwa, A. Chauraya, and J. C. Vardaxoglou, "Frequency and beam reconfigurable antenna using photoconductive switches," *IEEE Trans. Antennas Propag.,* vol. 54, no. 2, pp. 449-454, 2006.

[84] Y. Tawk, A. R. Albrecht, S. Hemmady, G. Balakrishnan, and C. G. Christodoulou, "Optically pumped frequency reconfigurable antenna design," *IEEE Antennas Wireless Propag. Lett.,* vol. 9, pp. 280-283, 2010.

[85] M. M. Alam, M. M. R. Sonchoy and M. O. Goni, "Design and performance analysis of microstrip array antenna," *Progress in Electromagnetics Research Symposium Proceedings,* Moscow, Russia, pp. 1837-1842, 2009.

[86] A. Lai, T. Itoh and C. Caloz, "Composite Right/Left-Handed Transmission Line Matematerials," *IEEE Microwave magazine,* vol. 5, no. 3, pp. 34-50, 2004.

[87] T. Jang, S. -H. Hwang, Y. -S. Bang, J. -M. Kim, Y. -K. Kim, C. -W. Beak and S. Lim, "Switchable composite right/left handed (S-CRLH) transmission line using MEMS switches," *IEEE Microw. Wireless Compon. Lett.,* vol. 19, no. 12, pp. 804-806, 2009.

[88] G. Monti, R. De Paolis and L. Tarricone, "Design of a 3-state reconfigurable CRLH transmission line based on MEMS switches," *Progress in Electro. research 95,* vol. 95, pp. 283-297, 2009.

[89] B. D. Braaten, S. Roy, I. Ullah, S. Nariyal, B. Ijaz, M. M. Masud, S. A. Naqvi and A. Iftikhar, "A cascaded reconfigurable RH/CRLH-Zero-Phase Microstrip transmission line unit cell," *proceedings of the IEEE international conference on wireless info. tech. and syst. (ICWITS),* Maui, Hawaii, pp. 1-4, 2012.

[90] M. Hashemi, N.Yuan and T. Itoh, "Dual-Band Composite Rigth Left-Handed Matematerial concept." *IEEE Microw. Wireless compon. Lett.,* vol. 22, no. 5, pp. 248-250, 2008.

[91] Z. Zhang and S. Xu, "A novel parellel-series feeding network of microstip patch arrays with composite right/left-handed transmission line for millimeter wave

applications," *International Journal of Infrared and Millimeter waves,* vol. 26, no. 9, pp. 1329-1341, 2005.

[92] M. A. Antoniades and G.V. Eleftheriades, "A metamaterial series-fed linear dipole array with reduced beam squinting," *Proc. IEEE International Symposium on Antennas and Propagation,* Albuquerque, NM, pp. 4125-4128, 2006.

[93] T. Yuan, N. Yuan and L. Li, "A novel Series-Fed Taper Antenna Array design," *IEEE Antennas and Propag. Letters,* vol. 7, pp.362-365, 2008.

[94] W. L. Stutzman and G. A. Thiele, *Antenna Theory and Design,* 2nd ed., John Wiley and Sons, Inc., New York, NY, 1998.